1-1-2002

Investigation of the structure of cold-drawn high-density polyethylene using solid-state NMR.

Daniel M. Mowery
University of Massachusetts Amherst

INVESTIGATION OF THE STRUCTURE OF COLD-DRAWN HIGH-DENSITY POLYETHYLENE USING SOLID-STATE NMR

A Dissertation Presented

by

DANIEL M. MOWERY

Submitted to the Graduate School of the
University of Massachusetts Amherst in partial fulfillment
of the requirements for the degree of

DOCTOR OF PHILOSOPHY

September 2002

Polymer Science and Engineering

INVESTIGATION OF THE STRUCTURE OF COLD-DRAWN HIGH-DENSITY POLYETHYLENE USING SOLID-STATE NMR

A Dissertation Presented

by

DANIEL M. MOWERY

Approved as to style and content by:

Klaus Schmidt-Rohr, Chair

E. Bryan Coughlin, Member

H. Henning Winter, Member

Thomas J. McCarthy, Department Head
Polymer Science & Engineering

To my parents, to Logan and to Tara

ACKNOWLEDGMENTS

On a professional level, many people have been of tremendous assistance to me in completing the research and work of this dissertation but none more than my advisor, Professor Klaus Schmidt-Rohr. He is by far the most brilliant person I have ever worked with to date. Studying with him was an incredible scientific experience. I thank Klaus for his patience and efforts during my tenure as his graduate student. It was difficult at times for both us, especially because of the long-distance relationship we had to manage. (Klaus had moved to Ames, Iowa, as a professor at Iowa State University in early 2000.) But I learned much from him, not only about NMR but also the qualities needed to excel as a scientist.

Great thanks are also extended to the members of my dissertation committee, Professors Bryan Coughlin and Henning Winter. Bryan warmly invited me to participate in his research group functions after Klaus' departure and the 'evaporation' of the Schmidt-Rohr group at UMass. He always showed an interest in my research and in a way helped keep me motivated in my graduate work. Henning regularly gave a cheery 'hello' when I saw him in the halls of Conte and offered valuable comments to my research.

I also give special 'professional' thanks to Ms. Eileen Besse and Dr. Charlie Dickinson. Eileen is not only a superior program coordinator (could any of us grad students in PS&E make it without her?), but she is also a wonderful and caring person. Charlie provided invaluable assistance with the spectrometer. Whenever software or hardware problems crept up, you could always count on Charlie to help you out of a jam. Plus, he continually showed a genuine interest in my research.

Fond memories and lasting thanks go hand-in-hand with recollections of the friends and colleagues I met during my years as a graduate student at UMass. Noteworthy mention should be given to Dr. Doug Harris, Professor Tito Bonagamba (and his wonderful family), Mr. Joe McNamara, Dr. Robin McKiernan, Dr. Nicole Karttunen-Cerasoli, and Ms. Taline Inguilizian for their friendship and support. Also, thanks to the members of the research groups I have worked with in Polymer Science & Engineering: the Schmidt-Rohr group (1999-2000), the Coughlin group (2000-2001), the Lesser group (1999-2000), and the Farris group (1998).

Thanks to Ms. Amy Heintz for assistance with Raman scattering experiments and to Professor Alan Lesser for advice with mechanical testing. I also express sincere gratitude to MRSEC and the Sloan Foundation for funding my graduate research.

On a personal level, I am forever indebted to my parents for their ever-present love and support, not only in the pursuit of my Ph.D. but for my entire life. They never gave up on me, even I when I was ready to give up on myself, and they always encouraged me to strive for what's right and what's best. I will love them always.

Heart-felt thanks go to my brothers and my sisters-in-law for their love and concern. Thanks also to my best friend, Dr. Joe Metz. We have grown up together since the seventh grade, not only in our education, but in our maturity and our friendship as well. And blessed thanks to my late grandmother, Mrs. Louise Ashbrook, who passed away in June 2002, for her love and kindness to me. And thanks also to my baby nephew Logan, who was born in June 2001. His strength is a powerful inspiration for me.

I so very grateful to the newest love in my life, my girlfriend Tara. I met her in the final year of my studies, but she has become the best of friends and the dearest of my

angels. She was there at the beginning and the end of my dissertation writing, always encouraging and helping me along the way. Although this dissertation is complete, I know our life adventures together are just starting.

And finally, last but certainly not least, I want to thank and praise my Lord. He is the rock and fire of my existence. I know that only through His everlasting love and knowledge am I able to accomplish feats such as these in my life.

ABSTRACT

INVESTIGATION OF THE STRUCTURE OF

COLD-DRAWN HIGH-DENSITY POLYETHYLENE

USING SOLID-STATE NMR

SEPTEMBER 2002

DANIEL M. MOWERY, B.S., UNIVERSITY OF CINCINNATI

M.S., UNIVERSITY OF MASSACHUSETTS AMHERST

Ph.D., UNIVERSITY OF MASSACHUSETTS AMHERST

Directed by: Professor Klaus Schmidt-Rohr

In this dissertation, the cold-drawing response of a commercial high-density polyethylene (HDPE) resin has been studied using solid-state nuclear magnetic resonance (NMR) spectroscopy and variety of other complementary techniques. Melt-crystallized, isotropic samples of the HDPE have been drawn to various extensions at ambient temperature (21°C) and at a relatively slow strain rate (0.0013 s^{-1}).

Using solid-state NMR, the first unambiguous evidence for a major morphological component intermediate to the crystalline and amorphous domains in the cold-drawn HDPE microstructure has been found. Employing an 'inverse ^{13}C T_1 filter' and other filtering techniques, signals from the various components have been selected and compared. The intermediate component comprises chains of all-trans conformation but with significant disorder in packing. The chains show fast, intermediate-amplitude motions about their axes and are generally aligned with the draw direction, but with a greater distribution of orientation angles relative to crystalline phase.

A quantitative ^{13}C NMR procedure has been utilized in the analysis of morphological component composition during cold drawing. In the undeformed material, the NMR-derived composition shows excellent agreement with other common techniques. The mass fraction of the intermediate component has been measured by NMR to be as high as 35% in the cold-drawn HDPE, greater than the contributions from the amorphous domains and monoclinic crystals. The intermediate component content dramatically increases by 240% just after necking, along with a doubling in the monoclinic crystals. At the same time, decreases of about 25% in the total crystalline and amorphous phases occur. A general re-ordering in the microstructure takes place during neck propagation and strain hardening. The total crystallinity rises by about 8%, with a corresponding decrease in the monoclinic crystals (50%) and amorphous material (30%).

Based on ^{1}H spin diffusion data, a microstructural model of cold-drawn HDPE is offered. The spin diffusion data identify the intermediate component with tie-molecule bundles that connect small 'mosaic block' crystallites (ca. 10–15 nm side dimension) along the draw direction. The bundles consist of about 30 chains and are estimated to be about 2.5 nm in diameter and 3 nm in length.

TABLE OF CONTENTS

LIST OF TABLES

LIST OF FIGURES

Figure

Figure

Page

CHAPTER 1

INTRODUCTION

1.1 Motivation of the Dissertation

Since the dawn of the modern industrial age, materials science has matured into an important and diverse branch of the physical sciences. As commerce and technology continue to grow, the need for highly specialized, advanced materials also increases. At the same time, ever-expanding markets require materials to be manufactured in great volume and at low cost, while maintaining optimum properties. In the last century, the development of synthetic polymeric materials has arisen in the wake of these demands.

Polyolefins are by far the largest-selling class of synthetic polymers in today's market. Because of their low production costs, processing ease, and versatility, polyolefins account for almost half of the $60 billion in synthetic polymers sold each year in the United States.[1] Polyethylene (PE) is chief among the polyolefins. It is one of the world's most important commercially produced polymers. The applications of this common semi-crystalline thermoplastic are found in a multitude of facets in everyday life. Polyethylene grades exhibit excellent deformability in the solid state, with appreciable stiffness and durability. Yet these materials are lightweight, which gives them a great advantage in product engineering. Depending on the molecular size and architecture of the individual grades, polyethylene can be shaped into highly anisotropic states. One example is the uniaxial drawing of polyethylene. Some grades, such as ultra-high molecular weight polyethylene (UHMWPE), can be ultradrawn into fibers that demonstrate incredible strengths.

The cold drawing of high-density polyethylene (HDPE) has been selected as the subject of this dissertation. High-density polyethylene is a PE grade constituting linear molecular chains that form a significant crystalline fraction. It is readily available, and numerous test samples can be made for a variety of experiments. In 2002 it is projected that over 20 million tons of HDPE will be consumed globally[2] in many forms, from plastic cups and chemical bottles to children's toys. The performance and lifetime of the HDPE material fashioned into these products is of great interest. These properties can be characterized through research of the solid-state deformation behavior. The mechanisms of material deformation are important in the processing, handling, and durability of products fabricated from the material.

'Cold drawing' is a simple deformation process in which a material sample is uniaxially strained at ambient temperatures. Analytical methods designed to elucidate details of solid-state deformation can be more efficiently developed when examining simple cases of deformation first. (As the old saying goes, 'in order to run, you need first to walk.') These methods can later be applied and modified to more complex deformation processes, like fiber strengthening, blown film production, and the estimation of service lifetimes. For example, the creep of micron-sized craze fibrils located at a growing crack tip has been recognized as a major mechanism in the slow crack growth in polyethylenes. This fibril creep has been modeled with the creep performance of macroscopic, cold-drawn PE samples.[3-6] If light is shed on the microstructure of cold-drawn polyethylene, then the creep response of such materials may be better explained in terms of the material morphology and molecular dynamics.

Such an understanding may be useful in the development of polyethylene resins with superior stress crack resistance.

Solid-state nuclear magnetic resonance (NMR) spectroscopy is an important and rapidly evolving technique in polymer science.[7,8] Experiments using solid-state NMR have shown its remarkable power in probing the structure and dynamics of molecules and microstructural components comprising polymeric materials. By discerning the nature of polymer solids on a nanoscopic level, materials scientists may correlate these findings with corresponding macroscopic properties, as in the case of the PE creep and crack growth studies. The discovery of structure-property relationships for material systems like polyethylene[9,10] is key to unlocking the secrets of materials physics.

1.2 Overview of the Dissertation

The solid-state deformation of semi-crystalline synthetic polymers such as polyethylene has been investigated for many years.[11-15] As mentioned above, drawing is a simple type of deformation whose general behavior is well known.[12,13,15-18] However, many questions into the relationships between molecular and microstructural characteristics and macroscopic properties during the drawing process remain unanswered. In particular, the non-crystalline components have been difficult to characterize with traditional scattering and thermal-analysis techniques.

In this dissertation, the cold-drawing response of a commercial, injection molding grade HDPE resin (DOW HD-12450N) has been examined. Samples of the HDPE have been drawn to various extensions at room temperature and at a relatively slow strain rate so as to analyze the distinct stages of the cold-drawing process. Solid-state NMR

experiments were used to characterize the morphology and molecular aspects of the changing material bulk during cold drawing. Other techniques, such as differential scanning calorimetry (DSC) and Raman scattering, complemented NMR data.

Several solid-state NMR experimental methods have been developed or modified to investigate the component microstructure of the cold-drawn HDPE. An 'inverse ^{13}C T_1 filter'[19] has been introduced to discriminate microstructural domains based on their distinctive ^{13}C T_1 relaxation times, which are influenced by chain mobility. This method has been used in the dissertation work with many other modern NMR experiments to show differences in the morphological phases, to identify a major intermediate component in cold-drawn HDPE, and to present a more conclusive picture of the plastically deformed microstructure. The quantitative ^{13}C NMR procedure of Hu and Schmidt-Rohr[20] has been employed and expanded to reveal several interesting changes in the component composition during drawing. Proton spin diffusion and ^{13}C spin exchange experiments were conducted to give information about the proximities of different morphological components on the nanometer scale.

1.3 References

1. *Designer plastics*, in *The Economist Technology Quarterly*. Dec 8, 2001. p. 26-28.

2. Sinclair, K.B. *Macromolecular Symposia*, 2001. **173**: p. 237-261.

3. Lagaron, J.M.; Dixon, N.M.; Reed, W.; Pastor, J.M.; Kip, B.J. *Polymer*, 1999. **40**: p. 2569-2586.

4. Lagarón, J.M.; Dixon, N.M.; Gerrard, D.L.; Reed, W.; Kip, B.J. *Macromolecules*, 1998. **31**(17): p. 5845-5852.

5. O'Connell, P.A.; Bonner, M.J.; Duckett, R.A.; Ward, I.M. *Polymer*, 1995. **36**(12): p. 2355.

6. Cawood, M.J.; Channell, A.D.; Capaccio, G. *Polymer*, 1993. **34**: p. 423-425.

7. Schmidt-Rohr, K.; Spiess, H.W. *Multidimensional Solid-State NMR and Polymers*. 1994, San Diego: Academic Press, Inc.

8. Komoroski, R.A., ed. *High Resolution NMR Spectroscopy of Synthetic Polymers in Bulk*. Methods in Stereochemical Analysis, ed. Marchand, A.P. Vol. 7. 1986, VCH Publishers, Inc.: Deerfield Beach, Florida, USA.

9. Mandelkern, L.; Peacock, A.J. *Studies in Physical and Theoretical Chemistry*, 1988. **54**: p. 201-227.

10. Popli, R.; Mandelkern, L. *Journal of Polymer Science: Part B: Polymer Physics*, 1987. **25**: p. 441-483.

11. Lin, L.; Argon, A.S. *Journal of Materials Science*, 1994. **29**: p. 294-323.

12. Peterlin, A. *Colloid & Polymer Science*, 1987. **265**(5): p. 357-382.

13. Peterlin, A. *Colloid and Polymer Science*, 1975. **253**(10): p. 809-823.

14. Bowden, P.B.; Young, R.J. *Journal of Materials Science*, 1974. **9**: p. 2034-2051.

15. Peterlin, A. *Journal of Materials Science*, 1971. **6**: p. 490-508.

16. Hu, W.-G.; Schmidt-Rohr, K. *Acta Polymerica*, 1999. **50**: p. 271-285.

17. Strobl, G. *The Physics of Polymers*. 2nd ed. 1997, Berlin: Springer-Verlag.

18. Ward, I.M.; Hadley, D.W. *An Introduction to the Mechanical Properties of Solid Polymers*. 1993, New York: John Wiley & Sons, Inc.

19. Mowery, D.; Schmidt-Rohr, K. *Polymeric Materials: Science and Engineering*, 2001. **85**: p. 35-36.

20. Hu, W.-G.; Schmidt-Rohr, K. *Polymer*, 2000. **41**: p. 2979-2987.

CHAPTER 2

SOLID-STATE NMR AS A TOOL TO CHARACTERIZE SEMI-CRYSTALLINE POLYMERS

2.1 Introduction

Semi-crystalline polymer solids such as polyethylene show a diverse array of morphological phases.[1-5] These phases contrast not only on the micron size-scale, but on the nanometer size-scale as well. Solid-state NMR demonstrates a powerful capability in probing the segmental and supramolecular regimes of semi-crystalline polymers from various aspects, such as molecular structure, mobility, orientation, packing, and nanometer-scale domain size. NMR can significantly contribute to a sound understanding of the molecular and morphological landscape, which is quite advantageous in the development and control of structure-property relationships for semi-crystalline polymers. Hence, solid-state NMR lends itself as a highly beneficial analytical tool in the science of such materials.

High-resolution NMR spectroscopy has long been used in the analytical and synthetic chemistry of materials[6,7], predominantly when these materials are in the liquid state or dissolved in liquid solution. The physics of NMR in itself is considerably involved, and extensive treatments by Ernst et al.[8] and Abragam[7] are recommended for consultation in this matter. Only in the last quarter century has high-resolution NMR been effectively employed in the study of solids, particularly organic polymers.[9,10] Such research endeavors call for the development and advancement of multidimensional methods to elucidate details in molecular structure and dynamics not obtained with the simplest approaches commonly used in liquid-state and solution-state NMR. An

experimental method is tailored to specifically analyze a particular feature, or features, of the molecular state, e.g. the correlation of polymer chain segment mobility with spatial arrangement of the chain.

Many such methods have been and continue to be formulated in the characterization of semi-crystalline polymer solids. For extensive information concerning the methods, advantages and physics of solid-state NMR in the research of organic polymers, the interested reader should refer to the text by Schmidt-Rohr and Spiess.[9] Also, several researchers have written literature reviews regarding the examination of polyethylene and other semi-crystalline polymers by solid-state NMR.[11-13]

In this chapter, experimental solid-state NMR methods employed in the research presented in subsequent chapters are briefly described. Their relevance in the characterization of semi-crystalline polymer materials, specifically high-density polyethylene, is explained. Methods discussed include ^{1}H wideline measurement, static ^{13}C NMR, magic-angle spinning, spectral filtering by ^{13}C T_1 relaxation, 2D wideline separation, ^{1}H $T_{1\rho}$ measurement, ^{1}H spin diffusion, and 2D ^{13}C exchange.

2.2 ^{1}H Wideline Measurement

Hydrogen (^{1}H) has a spin-½ nucleus detectable by NMR spectroscopy. ^{1}H NMR is sometimes called 'proton NMR' because the ^{1}H nucleus contains only a single proton with no neutrons. ^{1}H nuclei occur in a large natural abundance (99.98%) in organic polymers like polyethylene. Hence, standard solid-state ^{1}H NMR spectra are readily available for most polymers by elementary acquisition methods. The simplest of such

experimental schemes is detection after a single applied 90°-excitation pulse per scan. For polymer solids rich in ^{1}H, a proton dipolar 'wideline' spectrum is obtained by this scheme.

The dipolar coupling of a large number of ^{1}H nuclear spins results in a multitude of lines in the ^{1}H spectrum. The number of lines for a single configuration and orientation of the coupling increases exponentially with the number of coupled spins, even when most spin-spin interactions are ignored. In a real polymer sample, with a large distribution of configurations and orientations of the ^{1}H-^{1}H couplings, a broad, featureless 'line' appears in the ^{1}H spectrum. The width of this wideline pattern reflects the strength of the average ^{1}H-^{1}H dipolar coupling. For typical polymer solids, the full-width-at-half-maximum (fwhm) is about $2\pi \times 40$ kHz. This width is much greater than ^{1}H chemical shifts (discussed briefly in the next section) appearing in spectra acquired with the magnetic field strengths of modern spectrometers. Hence, ^{1}H-^{1}H dipolar couplings generally dominate in single-pulse ^{1}H experiments.[9]

Fast molecular motions reduce the dipolar coupling by averaging effects, thereby narrowing the ^{1}H wideline pattern. In the isotropic limit, where the motions are very fast and without preferred directions, the dipolar couplings are diminished to zero, resulting in a narrow peak in the ^{1}H spectrum. Such averaging occurs naturally for molecules in solution or in the liquid state. Reduction in the ^{1}H line width ensuing from increased large-amplitude mobility in molecular segments has long been used in the study of solid organic polymers. For instance, Wilson and Pake[14] first noted the composite nature of the ^{1}H wideline patterns of low density polyethylene and polytetrafluoroethylene. Significant motional contrast exists between molecular chains in the rigid crystalline

phase and the more mobile amorphous phase in a typical semi-crystalline polymer above the glass transition temperature. Consequently, at least two components appear in the ^{1}H wideline pattern of semi-crystalline polymers: a broad component originating from the crystalline fractions and a narrow component produced by the amorphous domains.

2.3 ^{13}C Static NMR

The chemical shift of the spin resonance frequency is one of the most important features in the application of NMR spectroscopy to materials characterization. Chemical shifts provide extremely insightful information into the structural and motional aspects of molecules and are extensively used by chemists today in the determination of atomic arrangements and bonding in molecules. The chemical shift of a nuclear spin depends on the electronic environment about the spin. Electrons shield the nuclear spin from the externally applied, static magnetic field, referred to by NMR spectroscopists as the $\mathbf{B}_o$ field. The degree of shielding is influenced by the specific electronic configuration around the spin and is reflected in the chemical shift of the spin resonance in the resulting NMR spectrum.

In a solid material sample, the various NMR interactions are rigidly fixed in space relative to analogous interactions in liquid and gaseous samples. Hence, the orientation of these NMR interactions with respect to the applied magnetic field becomes important in solid-state NMR. The chemical shift of a nuclear spin is no exception. The chemical shift of a specific nucleus is represented as a symmetric 3×3 tensor; the resonance frequency of the nucleus is dependent on the relative orientation of the tensor's principal axes to the magnetic field. If a multitude of these nuclei with similar electronic

environments exist in a solid sample, and the sample is held fixed with respect to $\mathbf{B}_o$, the resulting spectrum forms a pattern indicative of the chemical shift anisotropy (CSA) of the nuclei. The frequencies in the spectral pattern are dependent on the orientations of the molecular segments to which the nuclei are part.[9]

In ^{13}C static NMR, samples with carbon-13 nuclei (^{13}C) are analyzed while the samples are held stationary with respect to $\mathbf{B}_o$. ^{13}C nuclear spins, like ^{1}H, are a spin-½ nucleus detectable by NMR spectroscopy. However, ^{13}C nuclei are not naturally abundant (only 1.108%). ^{13}C-^{1}H nuclear interactions are effectively removed via high-power decoupling. The ^{13}C CSA patterns of the samples can thus be measured. For ^{13}C sites, the orientations of the chemical shift tensor (i.e. the principal axes system) are often dominated by the local electronic structure around the site.[9] Therefore, ^{13}C static NMR can be employed in deriving segmental orientation distributions of carbon-rich molecules, using the physical orientation of the sample with respect to the $\mathbf{B}_o$ field as a directional reference. Motions of these segments can also partially average out the ^{13}C chemical shift anisotropy, which again will be reflected in the spectral pattern. For semi-crystalline polymer solids, ^{13}C static NMR can provide useful information on chain orientation in a sample and small-scale molecular motions about some axis in the chain geometry.

Veeman[15] has written a review of ^{13}C chemical shift anisotropy. For studies and applications of the ^{13}C CSA in organic polymers, the book by Schmidt-Rohr and Spiess[9] is recommended.

2.4 Magic-Angle Spinning

As with ^{1}H-^{1}H couplings, fast molecular motions tend to reduce chemical shift anisotropy by averaging the chemical shift tensor. In the isotropic limit, which occurs naturally in liquid and solution-state analyses, only the isotropic chemical shifts are detectable. The relative frequencies of these shifts are a quantitative indication of the electronic and structural environment surrounding the nuclear spins being examined. As a result, isotropic chemical shifts are a powerful aspect of NMR utilized by chemists to reveal molecular structure, bonding and composition. Characteristic ^{13}C and ^{1}H isotropic chemical shifts for many molecular moieties useful in the study of organic polymers can be found in the literature.[6]

In polymer solids, molecules are more rigid and constrained. Additional inter- and intramolecular interactions affect isotropic chemical shifts. Frequency shifts are sensitive to changes in the molecular conformation.[16,17] The best known among such phenomena is the γ-gauche effect[17] observed in the methylene groups of aliphatic structures via ^{13}C NMR. A substituent group in the γ position to an observed ^{13}C nucleus causes an upfield chemical shift of about 2–5 ppm when the substituent group is in a gauche arrangement with the ^{13}C nucleus. Such effects are of great advantage in the research of semi-crystalline polymer solids like polyethylene. For instance, Earl and VanderHart[18] noted that the methylene resonances of the amorphous phase in polyethylene ^{13}C spectra occurred about 2 ppm upfield from the corresponding crystalline signals due to the γ-gauche effect. Molecular segments in the amorphous domains undergo fast transitions between trans and gauche conformations, whereas the chains in the crystallites remain in all-trans arrangements.

Packing differences in polymer chains can also be seen in isotropic chemical shifts. Various crystalline lattice packings of n-alkanes[19] and polyethylene[20] influence the chemical shift frequencies. In polyethylene, planes of all-trans chains in the crystalline domains can be packed perpendicular (orthorhombic structure[21]) or parallel (monoclinic structure[22]). The monoclinic lattice induces a downfield shift in the methylene ^{13}C resonance by approximately 1.3 ppm relative to the orthorhombic crystalline signal. VanderHart and Khoury[20] used this shift to quantitatively determine the fractions of orthorhombic and monoclinic crystals in polyethylene samples.

To obtain isotropic chemical shifts in the ^{13}C NMR of solids, a procedure called magic-angle spinning (MAS) is employed.[9,23] Artificially-induced averaging of the chemical shift tensor to the isotropic limit is achieved by fast macroscopic sample spinning in the presence of $\mathbf{B}_0$. MAS of the sample is performed around an axis that makes the 'magic angle' $\theta_m = 54.74^\circ$ with respect to the $\mathbf{B}_0$ field. This angle is the value of θ such that the second Legendre polynomial $\frac{1}{2}(3\cos^2\theta - 1)$ is equal to zero. The magic angle is half the tetrahedral angle (109.5°) or the angle between the diagonal of a cube and any of the cube's edges. Spinning at the magic angle averages out all anisotropic interactions that can be described by second-order tensors (like CSA), as long as the sample rotation frequency exceeds the strength of the largest spin interaction. MAS, when used in conjunction with high-power decoupling, is an extremely beneficial experimental method in the ^{13}C NMR of semi-crystalline polymers.

2.5 Spectral Filtering by ^{13}C T_1 Relaxation

Molecular motions that cause fluctuations in nuclear spin interactions generate nuclear magnetic relaxation in materials. Characteristic time constants of these relaxation phenomena are called relaxation times. Ever since the discovery of NMR in bulk matter, relaxation times have held an important role in the physics of NMR. Relaxation times are sensitive to the spectral density of molecular motions with rates near the characteristic frequency $\omega_r = \gamma B_r$, where γ is the magnetogyric ratio of the specific nuclear spin being considered, and B_r is the strength of the relevant applied magnetic field. When the rate of molecular motion is approximately the same as the characteristic frequency, a maximum in the relaxation rate is reached, corresponding to a minimum in the relaxation time.[9]

The longitudinal relaxation time in the laboratory frame is referred to as the T_1 relaxation time. T_1 relaxation is sensitive to molecular motions with a frequency near $\gamma B_o/2\pi$, which is generally on the order of 10^1–10^2 MHz in modern spectrometers. In organic solids, ^{13}C T_1 relaxation is intrinsically brought about by modulations in the ^{13}C-^1H dipolar coupling or ^{13}C CSA. These modulations originate from fast molecular dynamics.[9] However, ^{13}C T_1 relaxation is not always a local phenomenon arising from molecular activity in relatively close proximity to the ^{13}C site. In polyethylene crystals, for instance, it has been proved that ^{13}C T_1 relaxation is dependent on the diffusion of chains from the amorphous domains into the crystallites.[24]

As with other experimental methods discussed above, the ^{13}C T_1 relaxation time (or $T_{1,C}$) can discriminate between the morphological phases in a typical semi-crystalline polymer solid based on contrasts in molecular mobility. Due to fast intrinsic molecular motions, the $T_{1,C}$ of the amorphous phase in polyethylenes is generally < 1 s, whereas the

$T_{1,C}$ of the crystals is commonly 10^2–10^3 s.[13,25,26] Based on this large difference in $T_{1,C}$ values between the phases, ^{13}C NMR signals of mobile phases with short $T_{1,C}$ can be filtered out by applying the ^{13}C T_1 filter pulse sequence of Torchia.[27] An 'inverse $T_{1,C}$ filter'[28] has been recently introduced to acquire ^{13}C spectra of domains with small and intermediate $T_{1,C}$ constants and will be discussed further in Chapter 4. These ^{13}C T_1 filtering procedures can be used in conjunction with many of the other experimental approaches mentioned in this chapter.

2.6 2D Wideline Separation

As discussed in Section 2.2, ^1H wideline NMR spectroscopy has long been utilized in the qualitative characterization of molecular mobility in semi-crystalline polymer solids. However, 1D ^1H wideline patterns are a superposition of the broad and narrow 'lines' originating from the various phases and structural units in the polymer matrix, and this superposition may not easily be decomposed into pure line shapes representative of the specific matrix fractions. A novel version of the 2D heteronuclear correlation experiment, achieving ^1H wideline separation (WISE), has been developed to address this issue.[29] ^1H wideline shapes, used as a qualitative measure of large-amplitude molecular motions, are separated in the second spectral dimension by ^{13}C isotropic chemical shifts when the experiment is performed under MAS conditions. Hence, 2D WISE spectra allow for the correlation of molecular mobility and structure in organic solids.

2.7 ^{1}H $T_{1\rho}$ Measurement

Another important NMR relaxation time often used in the characterization of semi-crystalline polymers is the longitudinal relaxation time in the rotating frame, denoted as $T_{1\rho}$. For a particular nuclear spin, $T_{1\rho}$ is measured when the magnetization of that spin is 'locked' along a transverse magnetic field $\mathbf{B_1}$. The strength of $\mathbf{B_1}$ is typically about three orders of magnitude less than the strength of the corresponding static field $\mathbf{B_0}$. As a result, $T_{1\rho}$ probes spectral densities near a characteristic frequency of $\gamma B_1/2\pi$, which is generally about 10^2 kHz in modern spectrometers. Compared to T_1 relaxation, $T_{1\rho}$ relaxation is influenced by much slower molecular motions.[9]

In organic solids like polyethylene, the ^{1}H $T_{1\rho}$ (or $T_{1\rho,H}$) detects the modulation of ^{1}H-^{1}H dipolar couplings. The sensitivity of $T_{1\rho,H}$ to molecular mobility can be utilized in the study of semi-crystalline polymers. Hu et al.[30] directly determined a dependence of the $T_{1\rho,H}$ on the correlation time of 180° chain-flip motions in polyethylene crystallites. These particular chain motions play a significant role in the dynamic-mechanical α_c relaxation[31-33] in polyethylene, which is related to important material properties such as ultradrawability.[34] $T_{1\rho,H}$ has also been used as a measure of crystalline thickness magnitudes and distributions in polyethylenes.[35,36]

2.8 ^{1}H Spin Diffusion

In solid-state NMR spectroscopy, spin diffusion involves the spatial transfer of longitudinal magnetization, also known as z-magnetization, between dipolar-coupled spins. The term 'spin diffusion' is actually a misnomer, for the process involves the diffusion of polarization between homonuclear spins, not the diffusion of the nuclear

spins themselves. The characteristics and efficiency of spin diffusion depend on the dipolar couplings and the distances between coupled spins. The process of spin diffusion can be measured through appropriate pulse sequences, such as the classic approach of Goldman and Shen.[37]

For organic solids rich in protons, the diffusion of ^{1}H magnetization occurs quite rapidly in the dense matrix of strong ^{1}H-^{1}H dipolar couplings. ^{1}H spin diffusion is therefore sufficiently described by continuum models of diffusion. The time dependence of the diffusion process in non-equilibrium distributions of z-magnetization can be exploited in the characterization of multi-domain systems, such as the morphologies of semi-crystalline polymers and block copolymers. A gradient in z-magnetization between morphological domains is established by selection of the ^{1}H magnetization specific to one domain. Taking advantage of the existing contrasts in molecular mobility between the domains, the selection of the ^{1}H magnetization can be based on the differences in decay of the transverse ^{1}H magnetization. In a given time period referred to as the mixing time, during which no radio-frequency irradiation is applied to the nuclear spin under analysis, the magnetization in the system is allowed to proceed towards an equilibrium distribution. Hence, systems with small domains will undergo faster magnetization equilibration than systems with large domains. As a result, the sizes of domains can be quantified up to lengths of 100 nm.[9,38] Also, the proximity of domains can be determined by observing the path of magnetization diffusion. Hence, ^{1}H spin diffusion provides an extremely effective means of modeling the phase morphologies of semi-crystalline polymers.[9]

2.9 2D ^{13}C Exchange

Two-dimensional exchange NMR is a powerful experimental method in the analysis of slow dynamic processes occurring on time scales of up to several seconds.[8,9] This type of NMR spectroscopy correlates the frequencies of molecular segments before and after a mixing time. Data appear in the form of a 2D spectrum. Segments that remain unchanged during the mixing time will show signals on the diagonal of the spectrum. Segments that undergo some dynamic process will change frequencies in the mixing time; they will yield signals in off-diagonal positions.

2D ^{13}C exchange experiments have been used to detect solid-state chain diffusion between the crystalline and amorphous regions of polyethylene samples.[24] In regards to polyethylene characterization, 2D ^{13}C exchange can detect the proximity of morphological phases along the chain axis, in contrast to ^{1}H spin diffusion, which shows proximity along any direction.

2.10 References

1. Strobl, G. *The Physics of Polymers*. 2nd ed. 1997, Berlin: Springer-Verlag.

2. Mandelkern, L. *Accounts of Chemical Research*, 1990. **23**(11): p. 380-386.

3. Fischer, E.W. *Polymer Journal*, 1985. **17**(1): p. 307-320.

4. Flory, P.J.; Yoon, D.Y. *Nature*, 1978. **272**: p. 226-229.

5. Flory, P.J. *Journal of Chemical Physics*, 1949. **17**(3): p. 223-240.

6. Bovey, F.A.; Jelinski, L.; Mirau, P.A. *Nuclear Magnetic Resonance Spectroscopy*. 2nd ed. 1988, San Diego: Academic Press, Inc.

7. Abragam, A. *The Principles of Nuclear Magnetism*. The International Series of Monographs on Physics. 1961, New York: Oxford University Press Inc.

8. Ernst, R.R.; Bodenhausen, G.; Wokaun, A. *Principles of Nuclear Magnetic Resonance in One and Two Dimensions*. The International Series of Monographs on Chemistry. 1987, New York: Oxford University Press Inc.

9. Schmidt-Rohr, K.; Spiess, H.W. *Multidimensional Solid-State NMR and Polymers*. 1994, San Diego: Academic Press, Inc.

10. Komoroski, R.A., ed. *High Resolution NMR Spectroscopy of Synthetic Polymers in Bulk*. Methods in Stereochemical Analysis, ed. Marchand, A.P. Vol. 7. 1986, VCH Publishers, Inc.: Deerfield Beach, Florida, USA.

11. Yamanobe, T. *Structure and Dynamics of Crystalline and Noncrystalline Phases in Polymers*, in *Solid State NMR of Polymers*, Ando, I.; Asakura, T., Editors. 1998, Elsevier Science B.V.: Amsterdam. p. 267-305.

12. Aoki, A.; Asakura, T. *Polyolefins*, in *Solid State NMR of Polymers*, Ando, I.; Asakura, T., Editors. 1998, Elsevier Science B.V.: Amsterdam. p. 415-444.

13. Axelson, D.E. *Carbon-13 Solid-State NMR of Semicrystalline Polymers*, in *High Resolution NMR Spectroscopy of Synthetic Polymers in Bulk*, Komoroski, R.A., Editor. 1986, VCH Publishers, Inc.: Deerfield Beach, Florida, USA. p. 157-226.

14. Wilson, C.W.; Pake, G.E. *Journal of Chemical Physics*, 1957. **27**(1): p. 115-122.

15. Veeman, W.S. *Progress in NMR Spectroscopy*, 1984. **16**: p. 193-235.

16. Tonelli, A.E. *Journal of Molecular Structure*, 1995. **355**: p. 105-119.

17. Tonelli, A.E.; Schilling, F.C. *Accounts of Chemical Research*, 1981. **14**: p. 233-238.

18. Earl, W.L.; VanderHart, D.L. *Macromolecules*, 1979. **12**(4): p. 762-767.

19. VanderHart, D.L. *Journal of Magnetic Resonance*, 1981. **44**: p. 117-125.

20. VanderHart, D.L.; Khoury, F. *Polymer*, 1984. **25**: p. 1589-1599.

21. Bunn, C.W. *Transactions of the Faraday Society*, 1939. **35**: p. 482-491.

22. Seto, T.; Hara, T.; Tanaka, K. *Japanese Journal of Applied Physics*, 1968. **7**(1): p. 31-42.

23. Schaefer, J.; Stejskal, E.O.; Buchdahl, R. *Macromolecules*, 1975. **8**(3): p. 291-296.

24. Schmidt-Rohr, K.; Spiess, H.W. *Macromolecules*, 1991. **24**(19): p. 5288-5293.

25. Kitamaru, R.; Horii, F.; Murayama, K. *Macromolecules*, 1986. **19**(3): p. 636-643.

26. Axelson, D.E.; Mandelkern, L.; Popli, R.; Mathieu, P. *Journal of Polymer Science: Polymer Physics Edition*, 1983. **21**: p. 2319-2335.

27. Torchia, D.A. *Journal of Magnetic Resonance*, 1978. **30**: p. 613-616.

28. Mowery, D.; Schmidt-Rohr, K. *Polymeric Materials: Science and Engineering*, 2001. **85**: p. 35-36.

29. Schmidt-Rohr, K.; Clauss, J.; Spiess, H.W. *Macromolecules*, 1992. **25**(12): p. 3273-3277.

30. Hu, W.-G.; Boeffel, C.; Schmidt-Rohr, K. *Macromolecules*, 1999. **32**(5): p. 1611-1619.

31. Boyd, R.H. *Polymer*, 1985. **26**(8): p. 1123-1133.

32. Boyd, R.H. *Polymer*, 1985. **26**(3): p. 323-347.

33. McCrum, N.G.; Read, B.E.; Williams, G. *Anelastic and Dielectric Effects in Polymeric Solids*. 1967, New York: Dover Publications, Inc.

34. Hu, W.-G.; Schmidt-Rohr, K. *Acta Polymerica*, 1999. **50**: p. 271-285.

35. Gelfer, M.; Beyer, F.; Gido, S.P.; Alamo, R.; Schmidt-Rohr, K. *Macromolecules*, submitted.

36. Gelfer, M.Y.; Schmidt-Rohr, K. *Polymeric Materials: Science and Engineering*, 1999. **80**: p. 380-381.

37. Goldman, M.; Shen, L. *Physical Review*, 1966. **144**(1): p. 321-331.

38. Clauss, J.; Schmidt-Rohr, K.; Spiess, H.W. *Acta Polymerica*, 1993. **44**: p. 1-17.

CHAPTER 3

INITIAL DISCUSSION OF THE COLD DRAWING OF HDPE

3.1 Introduction

The study of solid-state deformation is a prominent aspect of materials science and engineering. To characterize and understand the response of a material to various conditions of deformation is vital in the development of stronger, longer-lasting materials for product-based implementation. As mentioned in Chapter 1, polyethylene represents one of the most important and widely used engineering polymeric materials in use today. Studies of polyethylene deformation can be found in great volume in the literature. Detailed reviews have been published on the subject of solid-state deformation of semi-crystalline polymers and, in particular, polyethylene.[1-5]

Types of deformation are defined by a large set of variables, including orientation of applied stress and strain, temperature, sample environment, and intrinsic material properties. Numerous texts such as works by Dieter[6] and Ward[7] have been written about the engineering mechanics of solid-state deformation. For reasons stated in Chapter 1, deformation by cold drawing has been chosen for examination in this dissertation. 'Cold drawing' entails the uniaxial deformation of a solid material sample under ambient conditions, i.e. room temperature in most cases. In this chapter, an initial discussion of the response of a high-density polyethylene (HDPE) material to cold drawing is presented. During the course of the discussion, observations and hypotheses in the literature are summarized.

3.2 Experimental

3.2.1 Material Description

Dow Chemical's HD-12450N, a commercial injection-molding grade HDPE resin, was selected as the primary material of study in this dissertation. This particular grade is a copolymer of ethylene and an α-olefin, although the comonomer concentration and small-chain branching content are relatively very small. As a result, DOW HD-12450N is classified as a high-density (HD) polyethylene grade, with an ambient density of 0.952 g/cm^3.

For the research experiments presented in this dissertation, a polyethylene grade with overall linear molecular structure, comparatively high density, and moderate stiffness was preferred. Sufficient amounts of the material were required, so a commercially produced resin was appropriate and convenient. The HDPE resin was received from Dow Chemical in the form of pellets modified with suitable antioxidants; in this form the material could be readily processed into sample sheets. In contrast to the majority of commercial HDPE resins, HD-12450N grade is synthesized with a narrow molecular weight distribution (polydispersity index PDI ~ 2.5), which reduces the potentially undesirable complications of multiple chain lengths in these studies.

Finally, the attainment of a moderately high draw ratio at break ($\lambda_B > 10$) was wanted. According to Popli and Mandelkern[8], the draw ratio at break for conventional linear polyethylenes increases with decreasing molecular weight. DOW HD-12450N has a relatively low molecular weight ($M_n \sim 3 \times 10^4$ g/mol), as reflected in its melt flow index MI ~ 12 dg/min. Such a molecular weight is necessary for the injection-molding process for which the grade was fabricated.

3.2.2 Sample Preparation and Testing

Compression-molded test sheets (1.97 ± 0.04 mm thick) of the HDPE were prepared from the pellets according to ASTM Standard Practice D 1928-90 Procedure C. A molding pressure of approximately 4.3 MPa was used. A cooling rate of 15 ± 4°C/min was maintained.

Standard dumbbell-shaped test specimens were punched from the molded sample sheets. The specimen shape and dimensions conformed to the Type V design outlined in ASTM Standard Test Method D 638. A schematic of this test sample during various stages of cold drawing is presented in Figure 3.1.

Using an Instron Model 1123 screw-driven tensile tester, specimens were drawn at 2 mm/min under uniaxial tension. All drawing was done at room temperature (21 ± 1°C). With the Type V design, the specimens had an initial length of 25.4 mm between the tensile tester sample grips. Because of the dramatically heterogeneous straining that occurs in a typical HDPE sample during cold drawing, this length was chosen as the specimen gauge length L_o. Hence, absolute extensions and speeds are normalized by L_o to determine drawing (or so-called 'engineering') strains and strain rates. Therefore, the drawing strain rate for deformed samples in this dissertation was 0.0013 s^{-1}. Drawing (or engineering) stresses were calculated by normalizing the recorded tensile load forces F with the initial cross-sectional areas A_o of the test specimens.

A drawing speed of 0.0013 s^{-1} is relatively slow for typical HDPE materials. Application of this strain rate increased the range of extension during deformation, which was important in better separating the distinct regions of cold drawing for analysis.

These regions in extension domain will be elaborated on in the next section. Test specimens were pulled to fracture and to various pre-selected extensional changes ΔL before fracture, as shown in Figure 3.2. The determination of these pre-selected extensional changes will be justified later in the chapter.

Draw ratios λ in the neck were calculated by a conventionally used method. An ink grid of squares 3.2 mm × 3.2 mm in dimension was softly applied to the flat surface of a specimen before deformation. After drawing, the average distance between the lines of the stretched grid in the sample's necked region was measured parallel to the drawing direction. The draw ratio λ is computed by normalizing this measured 'tick' distance by 3.2 mm. As a result, λ represents a so-called 'true' strain[6] in the necked region, due to the heterogeneous straining that takes place in the narrow section of the dumbbell-shaped test specimen during cold drawing. Necked samples with a draw ratio as high as $\lambda > 16$ were obtained.

Before any further characterization, drawn samples were allowed to freely and sufficiently relax and recover at room temperature for at least a week after unloading from the drawing tension. The macroscopic effects of room-temperature strain recovery upon release from a tensile load have been shown to be quite small in highly crystalline polyethylenes.[2,9] Such polyethylenes demonstrate significant storage of plastic strain after deformation due to their crystalline matrix. As a check, a variety of standard solid-state NMR experiments were performed at room temperature on a necked sample of DOW HD-12450N immediately after unloading the sample from tension. No significant changes in the results of these experiments were observed over time, with the exception of the crystalline $T_{1\rho,H}$, which was found to slightly increase and sufficiently equilibrate

in less than two days. Current solid-state NMR hardware configurations make detailed and successful *in-situ* analyses of mechanical testing virtually impossible and quite costly. Hence, the *ex-situ* (or 'post-mortem') analytical approach was used as a reasonable estimation of drawing dynamics in the HDPE material.

3.2.3 Wide-Angle X-Ray Diffraction

As a qualitative measure of the crystalline texture and orientation in samples of the HDPE, wide-angle X-ray diffraction (WAXD) experiments were conducted. Monochromatic X-rays of pinhole-collimated CuK_{α} radiation were used in transmission mode. X-ray reflections were recorded with a GADDS detector manufactured by Bruker (formerly Siemens). Cold-drawn samples were extracted from the centers of the necked region. The incident beam was perpendicular to the neck face.

3.3 Initial Results and Description of the Cold-Drawing Response of the HDPE

The general drawing behavior of semi-crystalline polymer solids is well known.[2,3,5,7,10,11] Based on abundant descriptions and analyses found, as well as the author's personal observation of the deformation process during experimentation, the cold-drawing response of DOW HD-12450N has been classified into several distinct stages of activity in the domain of extension state (Table 3.1). Others[2,3,5,9] have undertaken similar approaches. This systematization of the drawing process will be utilized throughout the dissertation.

Two figures are presented as a guide to the reader in the discussion that follows. A generalized illustration of the HDPE test specimen during cold drawing is depicted in

Figure 3.1. The stages and corresponding specimen appearances are identified on a characteristic plot of stress versus strain. A drawing stress-strain curve of DOW HD-12450N made from one of the testing runs is shown in Figure 3.2. The curve is typical of all specimens deformed in the work of this dissertation. The limits of the cold drawing stages (Table 3.1) are superimposed on the stress-strain data of Figure 3.2.

3.3.1 The Elastic Regime and Initial Yielding

In the cold-drawing process, the isotropic HDPE specimen initially undergoes elastic deformation that is mostly recoverable. Classic Hookean behavior is exhibited in which the resulting stress is linearly proportional to the applied strain by Young's modulus. Gradually, the linear stress-strain curve turns into a maximum. This local maximum in stress has been commonly, but probably incorrectly[9,12] referred to as the material yield point for many years. Deformation beyond this point generally becomes increasingly permanent in character as straining proceeds. The yield point marks the start of the second defined stage of conventional drawing, initial yielding.

The onset points of initial yielding and neck formation (stages 2 and 3, respectively) are synonymous with the so-called 'double yield point' phenomenon which has been extensively examined in the past decade.[13-16] DOW HD-12450N exhibits a double yield point in the fashion observed in these published articles. After the first yield point and during the stage of initial yielding, the narrow section of the HDPE tensile specimen undergoes strain softening, in which the resulting stress decreases while the specimen generally deforms homogeneously. Permanent (plastic) strain also increases[9,16], and localized stress whitening is observed, indicating heightened void

formation. The production of voids in this stage has also been detected with small-angle X-ray scattering (SAXS) experiments.[17-19]

WAXD studies of initial yielding (stage 2) have revealed several interesting changes in the crystalline texture. Two phenomena have been observed at the onset of yielding. First, reflections of the orthorhombic crystals[20] tend toward broad intensity maxima at oblique angles (~30°–45°) from the equator in all quadrants of 2D patterns.[9,13,14,21,22] This reorientation of the crystalline alignment results in a 'tilted' morphology.[21] Second, new reflections identified with the monoclinic crystalline packing[23] are observed at equatorial positions in the 2D patterns.[9,14,17,18,21,22,24] The formation of monoclinic crystalline material in polyethylene drawn to yielding has also been seen in solid-state ^{13}C NMR experiments.[25]

The tilted morphology arises from the general reorientation of the crystalline *c* axis in the spherulitic lamellae. The *c* axis is parallel to the chain direction in polyethylene crystals. Hence, the polyethylene chains align roughly 30–45° to the external tensile force. Researchers[9,13,14] have attributed this preferential tilting to intralamellar slip[1,26] by *c* shear. When a material sample is subjected to a tensile load, the maximum resolved shear stress occurs at 45° to that load. In polyethylene crystals, shear by crystallographic slip is most favorable along the chain direction. As a result, the crystalline chains realign to maximize shear with the least expense of energy. This molecular process gives rise to the terms '*c* slip' or 'chain slip'.[1,4]

Chain slip is carried out in the crystalline lattice by the nucleation, activation, and subsequent motion of screw dislocations oriented along the chain axes. Along with chain slip, other deformation processes such as interlamellar slip, interlamellar separation, and

lamellar stack rotation are speculated to take place.[1,4,18,26] Mechanical studies by various scientists[27-29] also lend evidence to this deformation scenario during initial yielding, and their work explains the dependence of the material yield stress on crystalline thickness[28] and mass fraction[8].

The formation of the monoclinic crystalline form upon yielding originates from the transition of the orthorhombic to the monoclinic lattice structure. This transition is often termed a 'martensitic' transformation[1,4,23], induced by the application of stress into the polymer matrix. Monoclinic crystals in polyethylene have been found to exhibit metastable character[30], converting back to the orthorhombic packing upon relief of residual stresses in the material by treatments such as unloading or annealing.

Deformation in stage 2 of cold drawing generally exhibits a significant portion of recoverable (elastic) strain[9,14,16]. Chain slip may be very small in the crystalline lamellae at the onset of yielding.[9,13] This degree of chain slip is called 'fine' slip[4] and would explain the homogeneity and recoverability of the deformation after the first yield point and before necking. Because of such strain recovery, a sample cold drawn to this stage and tested *ex-situ* would not sufficiently represent the intrinsic deformation dynamics in the material.

3.3.2 Necking

The deformation of the specimen is much more dramatic and significantly heterogeneous during and after the second yield point. At this non-traditional yield point, the polymer specimen begins to narrow significantly in a concave fashion at usually one specific location. ('Non-traditional' is used in describing the second yield point, as the

'traditional' yield point is defined by the local maximum in the drawing stress-strain curve as per a long-standing materials science convention.) A highly oriented, stress-whitened macrostructure known as the 'neck'[3,5] is formed. The resulting stress reaches a local minimum, as the faces of the neck become parallel with the applied strain. This point coincides with stabilization of the newly formed neck and the onset of the fourth stage. The amount of material in the embryonic neck of stage 3 is too small for proper analysis by solid-state NMR.

Once the newly formed neck has stabilized by stage 4, the morphology in the neck has become 'fibrous' in nature. WAXD patterns have proved this fibrous texture by the general reorientation of all detectable crystalline reflections to equatorial positions.[9,14,17,18,21,22,24] These data indicate a realignment of the chain axes to a direction parallel with the applied tensile force. No doubt the load-bearing capability of the chains is strongest in this orientation. Fibrillar microstructures have also been observed by microscopic techniques.[1,3,5,14,22] Experiments using Raman spectroscopy[31,32] have noted a shift in the band associated with the C-C asymmetric stretching mode (~1060 cm^{-1}). The researchers assigned this shift to increased chain orientation[32] and molecular strain[31] in the fibrous neck. Macroscopically, rapid increases in the sample draw ratio have been observed in cold-drawn linear PE upon necking.[29] This sudden extension of the material bulk is explained by the nanoscopic orientations occurring in the fibrillar development.[3,5]

In the necked microstructure, crystalline order is severely diminished relative to the melt-crystallized precursor. Raman scattering experiments[24,33] have detected a decrease in the intensity of bands associated with the well-ordered crystallites. In one of

the studies[24], the mass-percentage orthorhombic crystallinity was calculated to decrease from 60% in the undrawn, isotropic sample to 40% in the cold-drawn, necked sample. Another study[34] showed an increase in non-crystalline all-trans segments upon cold drawing; these segments were found to be metastable and decreased in content with subsequent annealing. Meinel and Peterlin[29] also observed drops in the crystallinity during the necking of a linear polyethylene material. However, the density gradient technique and differential scanning calorimetry (DSC) were used to measure these crystallinity values, and these techniques are prone to error due to voids and other metastable structures in the necked microstructure.

This disordering of the morphology in necked semi-crystalline polymers has been attributed to the formation of small, 'mosaic-block' crystallites. Peterlin[2,3,5,35] has presented a classic model of the necked microstructure. In this model, the small crystalline blocks are sheared from the lamellar stacks of the spherulites and drawn at a microscopic level into highly oriented microfibrils of material. Fibrils in the neck that are visible to the naked eye are composed of bundles of these microfibrillar structures. So-called 'tie molecules' connect the crystallites within an individual fibril and between fibrils. These tie molecules account for the mechanical strength of the necked region along the draw direction.

Two contrasting hypotheses have been made to describe the necking phenomenon. Recently, Hiss et al.[9] have associated the various morphological transitions occurring in the necking process with the mechanism of 'course' slip[4], based in part on earlier studies.[1,4] Unlike fine slip, course slip leads to a heterogeneous deformation in which the spherulitic lamellae disintegrate via crystalline block sliding by *c* shear. The

crystalline lamellar shearing results in the mosaic blocks of Peterlin's model. This view of necking is based on crystallographic plasticity theory[6].

On the other hand, a hypothesis has been proposed by Flory and Yoon[36] in which localized melting and recrystallization of the crystallites explains the dramatic changes that occur during necking. Juska and Harrison[37] also offered this concept for plastic deformation in semi-crystalline polymers. They pointed out that block crystals with small transverse dimensions would theoretically melt at much lower temperatures than lamellar crystals. Using the small-angle neutron scattering (SANS) technique, Sadler and Barham[38] have likened the order of the molecular rearrangements in the polyethylene necking process during 'hot' drawing (draw temperature > 70°C) to those occurring in melting and crystallization. However, they found no such evidence for lower drawing temperatures. Meinel and Peterlin[29] calculated the maximum possible temperatures that could be achieved during adiabatic plastic deformation of polyethylene and found them to be much lower than the material melting point at low drawing temperatures. Peterlin[5] suggested that although true melting does not occur, "high chain mobilisation" may take place by the phase transformation of crystalline chains into a well-aligned "pseudomelt" or liquid crystal-like microstructure due to intense tensile stresses.

3.3.3 Drawing of the Neck

The propagation of the neck (stage 4) following stabilization was referred to by Peterlin[3] as the first distinct region of neck drawing. In the stress-strain curves presented in Figure 3.1 and Figure 3.2, the specimen shows a drawing stress that is almost constant with strain in this stage. The neck draw ratio λ is plotted versus drawing strain in

Figure 3.3. Recall that the draw ratio as determined in these experiments reflects a true strain in the material bulk. From the graph, the draw ratio is observed to increase at a much slower rate in stage 4 in comparison to later stages. As stated by Peterlin[3], the deformation taking place as the neck propagates is very heterogeneous. The neck grows in mass from its origin along the tensile axis of the specimen, transforming unoriented, spherulitic material into the highly oriented, fibrous structure of the neck. However, the neck itself is strained very little, as indicated by the draw ratio data of Figure 3.3. The work of deformation applied by the constant extension rate to the specimen is used primarily in the conversion of spherulitic material into the neck. The area under the drawing stress-strain curve is a measure of this mechanical work. Because of the stress plateau observed in stage 4 deformation (Figure 3.2), the time rate of change of mechanical work being imparted into the propagating neck is roughly linear with time.

Once the transformation of the originally uniform narrow section of the specimen into the necked morphology is complete, the uniaxial drawing of the HDPE reaches the fifth stage, strain hardening. Defined by Peterlin[3] as the second region of neck drawing, strain hardening of the specimen results in a significant rise in drawing stress up to the point of fracture (Figure 3.1 and Figure 3.2) and a significant increase in the draw ratio (Figure 3.3). An analogous trend is observed in area reduction A_r of the neck cross-section (Figure 3.4). The reduction in area is given by the ratio of the instantaneous specimen cross-sectional area A and the initial area A_o. The value of A was determined from the length and width of the neck cross-section measured after unloading. As seen in Figure 3.4, the reduced area decreases at the inverse rate of the draw ratio increase. This corresponds to a conservation of volume in the strain-hardened neck.

A plastic 'flow curve' of the necked material is shown in Figure 3.5. A plastic flow curve plots true stress versus true strain and indicates the nature of plastic deformation in a strained material.[6] Values of true stress were computed by dividing the instantaneous load force F at the specific extension ΔL by the instantaneous cross-sectional area A of the necked sample. The behavior exhibited by DOW HD-12450N during cold drawing of the neck is characteristic of strain-hardening plasticity, where true stress increases with true strain (Figure 3.5). Meinel and Peterlin[29] observed a similar mechanical response in cold-drawn linear polyethylenes.

Textural changes in the necked material during strain hardening have also been seen. Studies employing WAXD[18,21,22] have noted a decrease in the content of monoclinic crystals during neck drawing (stages 4 and 5), possibly due to reordering in the crystals. Long microscopic voids that are parallel to the draw direction have been seen with electron microscopy.[22] These longitudinal voids were located between microfibrils and were found to increase in length with draw ratio. As strain hardening proceeds, residual stresses in the material become very high, and the sample finally fails at one location into several splintering, macroscopic fibers at appreciably slow strain rates. Zhurkov and Kuksenko[39] have attributed this catastrophic failure in drawn polymers to a critical proliferation of microscopic voids or 'submicrocracks', which they observed experimentally with SAXS.

As mentioned in the Experimental section, several test specimens of DOW HD-12450N were drawn to various extensional changes ΔL (Figure 3.2) in order to characterize the cold-drawing process of the HDPE. One extension (98% strain) was selected just after the stabilization of the neck, another (394% strain) at the onset of strain

hardening. Three other extensions (630%, 787%, and 945% strain) were chosen at various points during strain hardening up to fracture. WAXD patterns of the undrawn, melt-erystallized preeursor, along with necked samples of 98% strain and 945% strain, are shown in Figure 3.6. After neeking, the sample develops a highly oriented, fibrillar texture, as indieated by the equatorial positions of the refleetion intensities. Intensity due to the monoelinie erystal (001) refleetion is also observed, in agreement with previous WAXD studies in the literature.

The model proposed by Peterlin[2,3,5] to describe necking and cold drawing is extended to the strain-hardening regime (stage 5) as well. Peterlin aecounted for the simultaneous reduetion in area and draw ratio expansion reeorded in Figure 3.4 with the sliding of fibrils and microfibrils. The shearing of fibrillar boundaries under the applied tensile strain is eonsiderably more favorable than deformation within the microfibrillar bulk. Peterlin explained the strain-hardening behavior of cold-drawn semi-erystalline polymers like polyethylene (Figure 3.5) with the resistanee of the network of interfibrillar tie moleeules to deformation. He suggested that alignment of the tie molecules indueed their ordering or 'erystallization' on the surfaees of pre-existing mosaie bloeks.[5] Sliding of the fibrils results in the increased void formation detected in drawing experiments.[22,39]

3.4 Summary

In this chapter, the maeroseopie eold-drawing behavior of melt-erystallized high-density polyethylene (DOW HD-12450N) has been observed and diseussed. The material exhibited a drawing stress-strain response traditional to highly crystalline polymers at reasonably low strain rates. The so-called 'double yield point' oceurred,

with subsequent necking, giving a highly oriented fibrillar texture confirmed in WAXD patterns. Strain hardening resulted in a significant increase in the true stress and neck draw ratio λ, with reasonably large extensions obtained ($\lambda > 16$) for a cold-drawn polymer.

3.5 Tables and Figures

Table 3.1: Stages of uniaxial cold drawing for DOW HD-12450N (ambient conditions, 0.0013 s^{-1} strain rate). For stress and strain values, 95% confidence limits are given.

Drawing Stage	**Drawing Strain at Onset**	**Drawing Stress at Onset (MPa)**
1. Elastic behavior	0	0
2. Initial yielding	0.087 ± 0.004	21.8 ± 0.2
3. Formation of the neck	0.26 ± 0.01	16.9 ± 0.4
4. Propagation of the neck	0.39 ± 0.02	12.7 ± 0.1
5. Strain hardening	3.52 ± 0.18	14.5 ± 0.3
6. Fracture	10.4 ± 0.4	19.8 ± 1.0

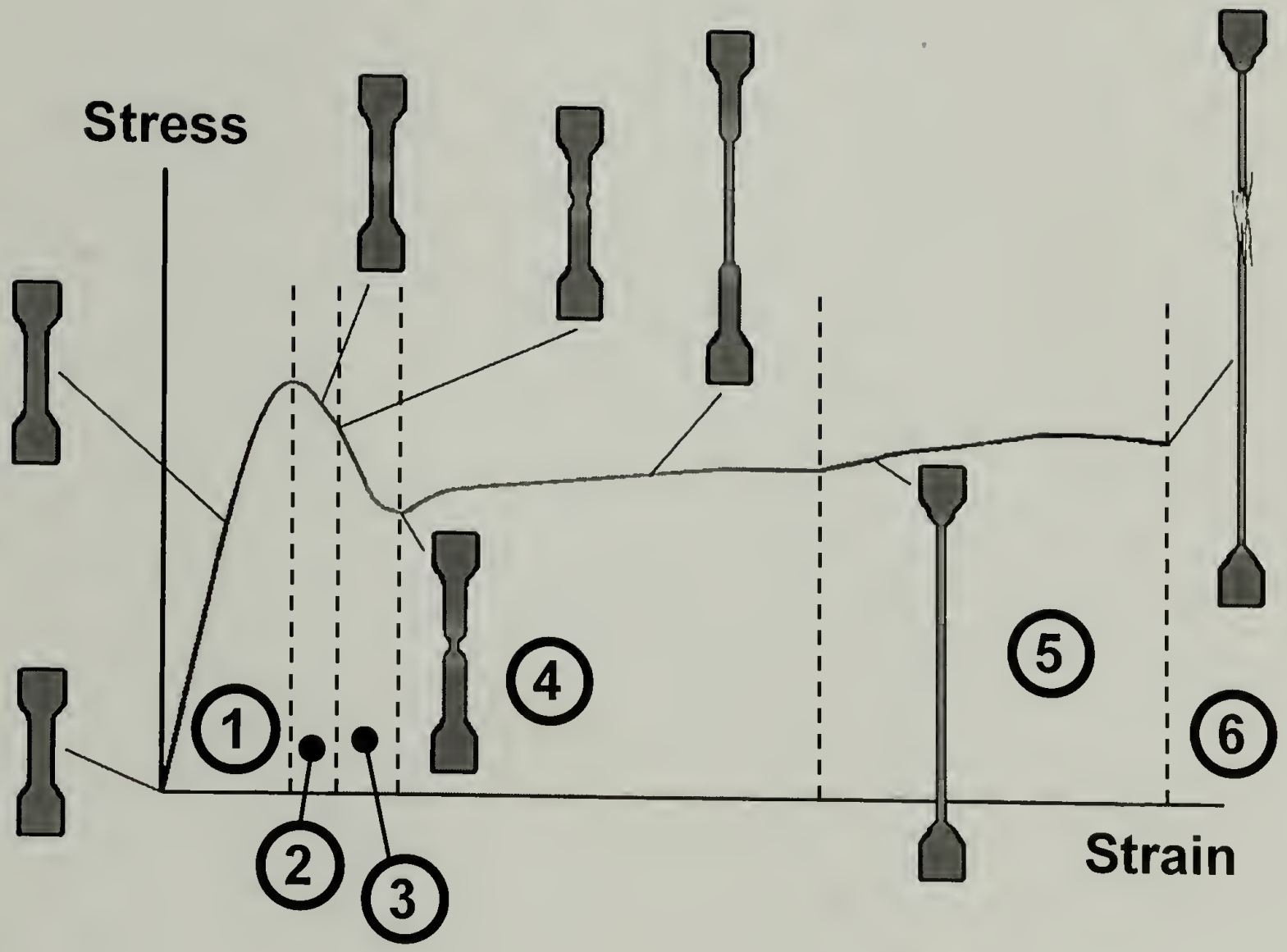

Figure 3.1: Generalized representation of the HDPE test specimen during cold drawing, along with a characteristic stress-strain curve of a significantly crystalline polymer at relatively low strain rates. Stages of drawing described in the text and listed in Table 3.1 are identified by encircled numbers; the numbers correspond to the classification in Table 3.1. The onset points of the drawing stages are marked with dashed vertical lines.

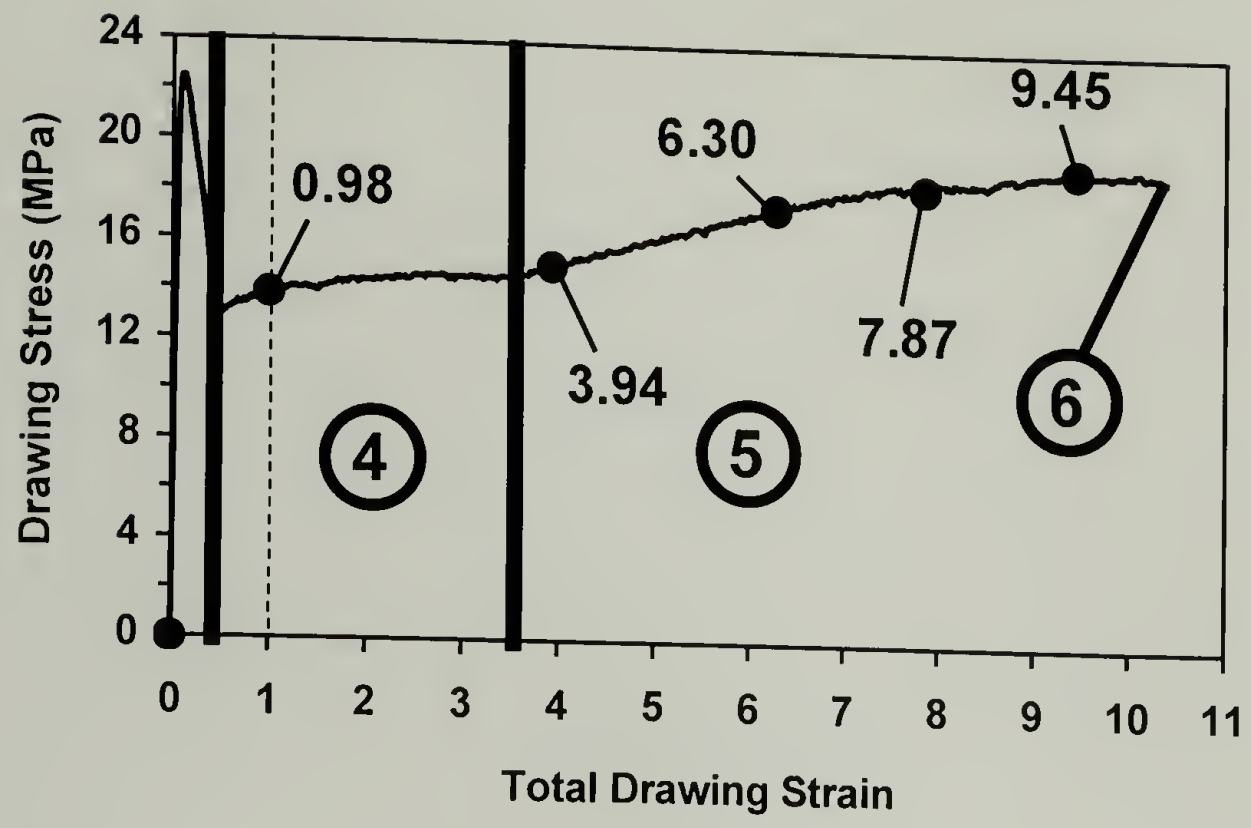

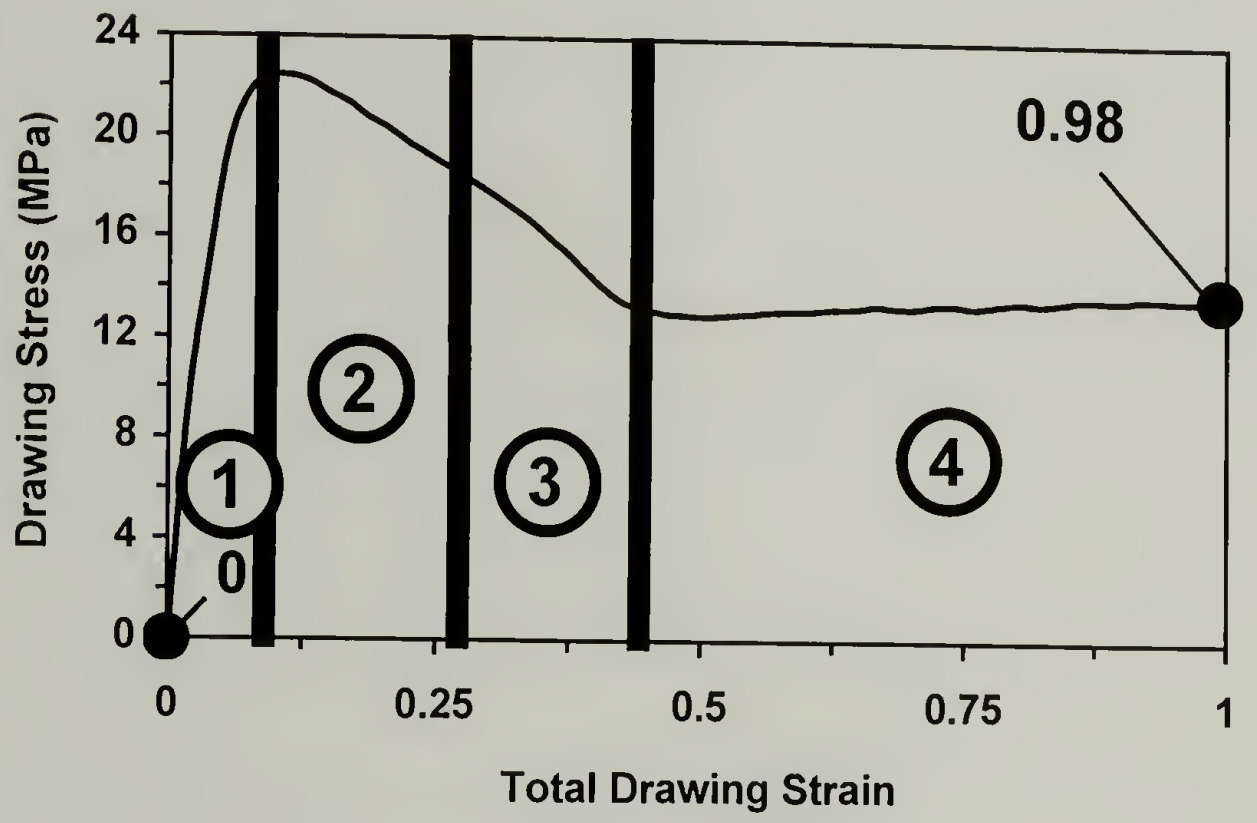

Figure 3.2: Drawing stress-strain curve of DOW HD-12450N subjected to uniaxial cold drawing (ambient conditions, 0.0013 s^{-1} strain rate). The bottom graph details the range of strains up to 100% to show the 'double yield point'. Stages of cold drawing (Table 3.1) are separated by thick vertical lines. Encircled numbers identify the stages on the stress-strain curve as they are listed in Table 3.1 and pictured in Figure 3.1. Extension points characterized in this dissertation are marked (•) and identified by drawing strain values.

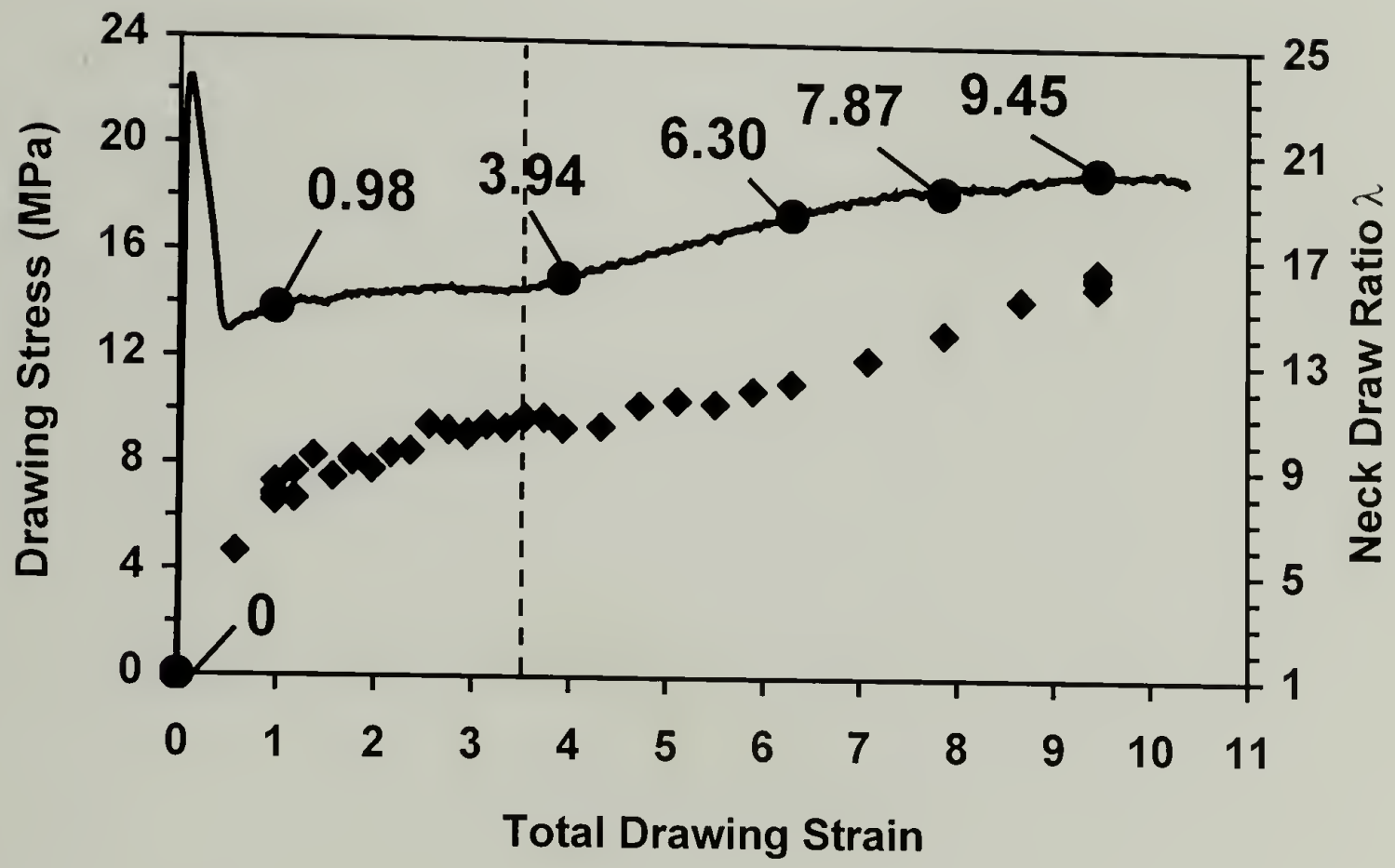

Figure 3.3: Draw ratios in the neck (♦) of the cold-drawn HDPE are plotted versus total drawing strain. The stress-strain response to cold drawing (same as curve shown in Figure 3.2) and points of extension characterized in the dissertation (symbolized as • and identified by total drawing strain) are also given. The dashed vertical line indicates the end of neck propagation (stage 4) and the onset of strain hardening (stage 5).

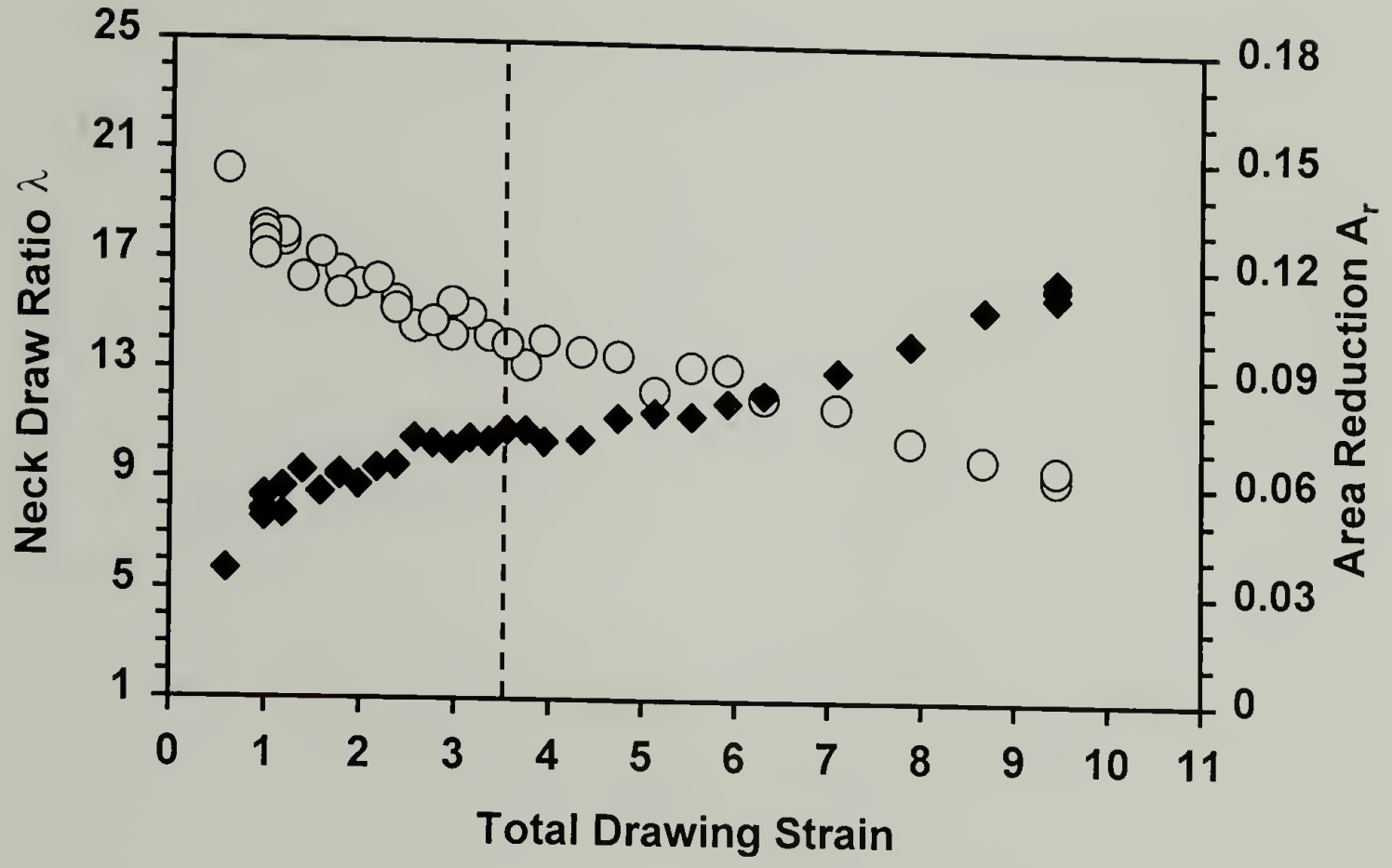

Figure 3.4: Draw ratios (♦) and reduction in area (○) of the cold-drawn HDPE neck plotted versus total drawing strain. The dashed vertical line indicates the end of neck propagation (stage 4) and the onset of strain hardening (stage 5).

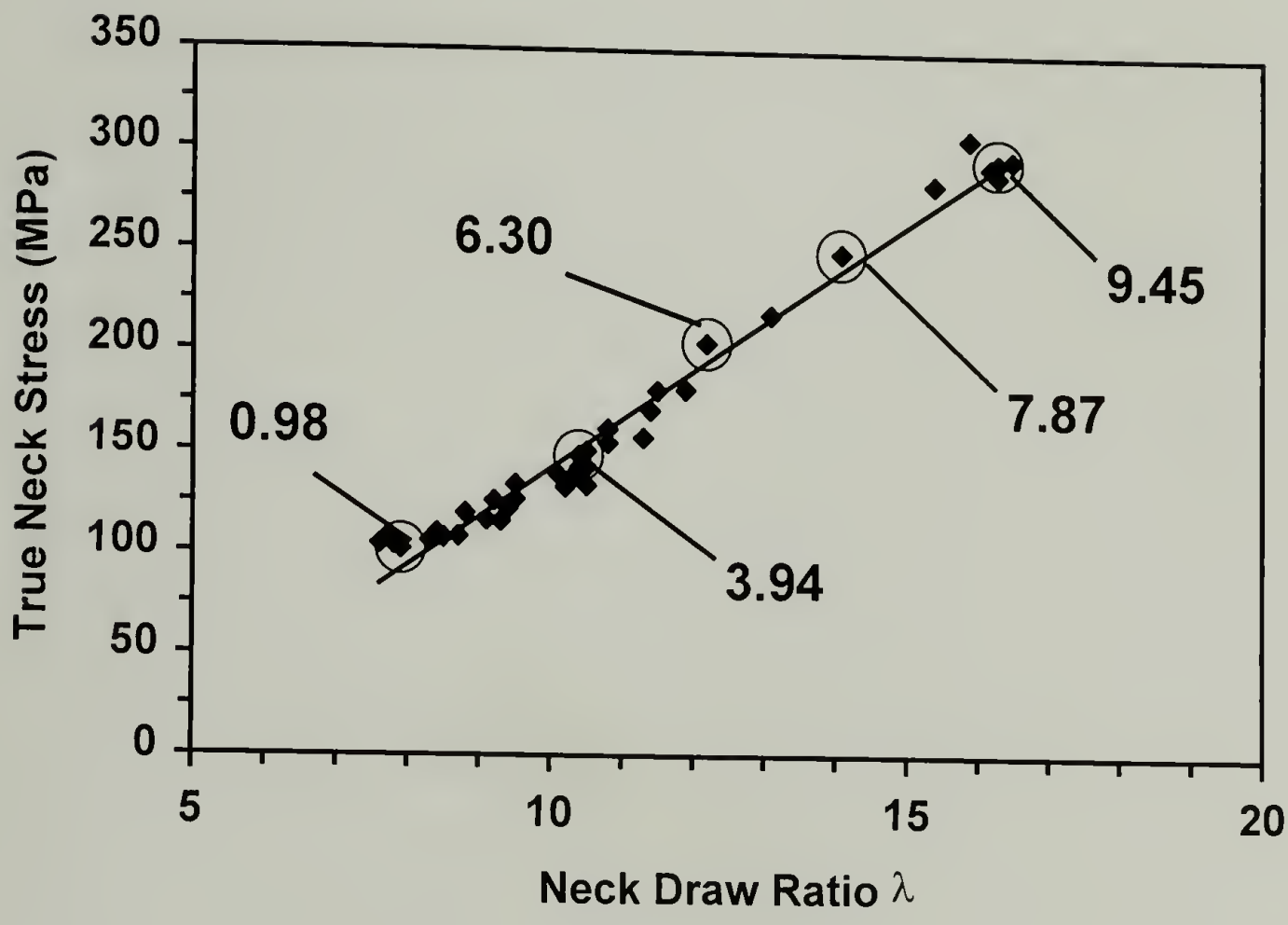

Figure 3.5: A plastic 'flow curve' for necked DOW HD-12450N. The straight line through the data points serves as a guide to the eye. Points of extension analyzed in this dissertation are marked by open circles and identified by drawing strain.

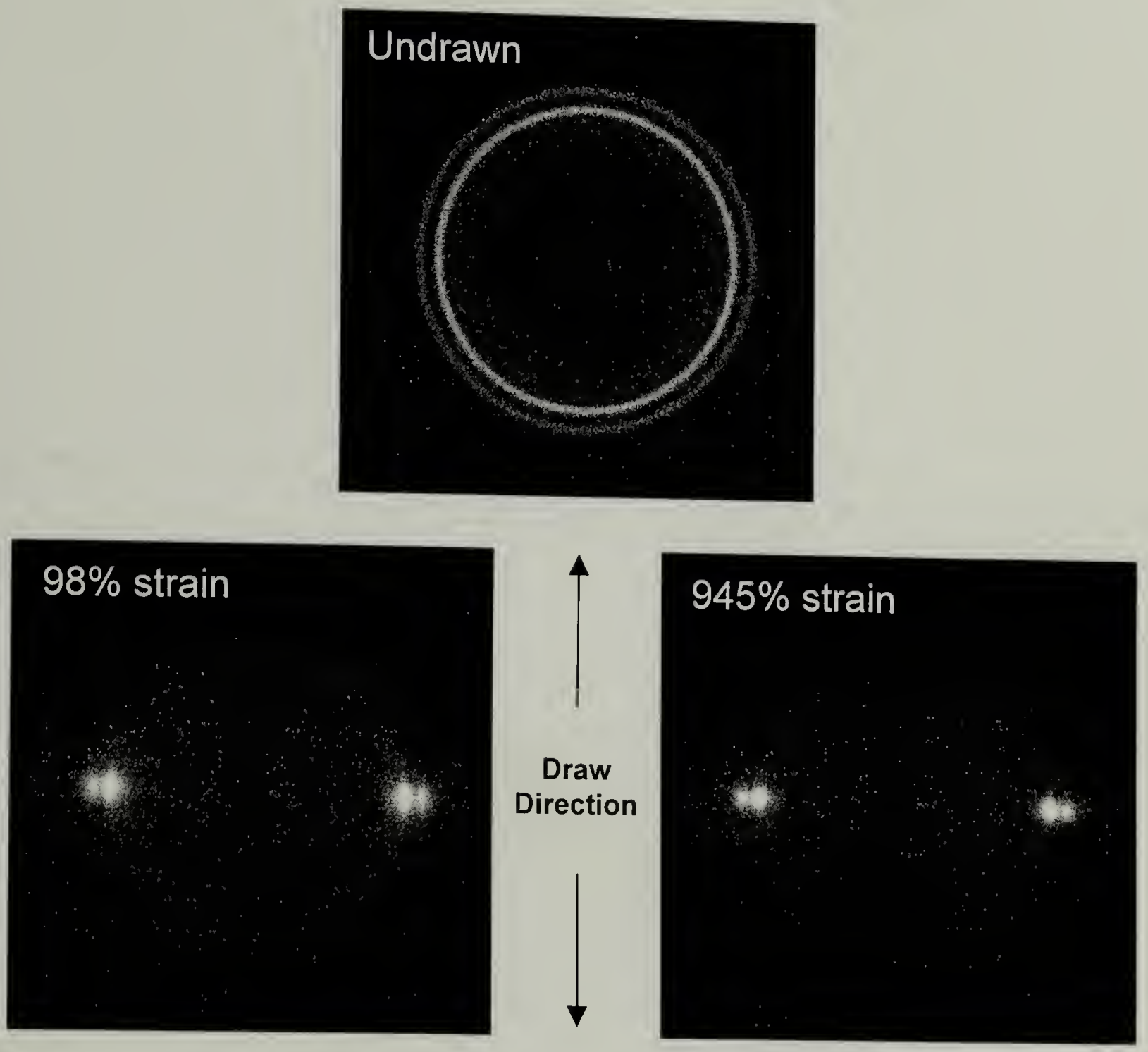

Figure 3.6: WAXD pinhole patterns of the HDPE at various levels of drawing strain. The strong inner and outer intensity maxima observed in the undrawn sample correspond to the (110) and (200) reflections, respectively, of the orthorhombic crystal structure[20]. Upon necking, the intensities conform to equatorial positions, indicative of fibrillar morphology. Also, a weak reflection can be seen inside the (110) angle, identified with the (001) planes of the monoclinic crystal structure[23].

3.6 References

1. Lin, L.; Argon, A.S. *Journal of Materials Science*, 1994. **29**: p. 294-323.

2. Peterlin, A. *Colloid & Polymer Science*, 1987. **265**(5): p. 357-382.

3. Peterlin, A. *Colloid and Polymer Science*, 1975. **253**(10): p. 809-823.

4. Bowden, P.B.; Young, R.J. *Journal of Materials Science*, 1974. **9**: p. 2034-2051.

5. Peterlin, A. *Journal of Materials Science*, 1971. **6**: p. 490-508.

6. Dieter, G.E. *Mechanical Metallurgy*. Third ed. 1986, New York: McGraw-Hill Book Company.

7. Ward, I.M.; Hadley, D.W. *An Introduction to the Mechanical Properties of Solid Polymers*. 1993, New York: John Wiley & Sons, Inc.

8. Popli, R.; Mandelkern, L. *Journal of Polymer Science: Part B: Polymer Physics*, 1987. **25**: p. 441-483.

9. Hiss, R.; Hobeika, S.; Lynn, C.; Strobl, G. *Macromolecules*, 1999. **32**(13): p. 4390-4403.

10. Hu, W.-G.; Schmidt-Rohr, K. *Acta Polymerica*, 1999. **50**: p. 271-285.

11. Strobl, G. *The Physics of Polymers*. 2nd ed. 1997, Berlin: Springer-Verlag.

12. Xiao, C.; Huang, J.; Dafforn, A.; Yee, A. *When Does Plastic Yield Occur?* in *ANTEC*. 1999. New York.

13. Gaucher-Miri, V.; Séguéla, R. *Macromolecules*, 1997. **30**(4): p. 1158-1167.

14. Brooks, N.W.J.; Unwin, A.P.; Duckett, R.A.; Ward, I.M. *Journal of Macromolecular Science -- Physics*, 1995. **B34**(1&2): p. 29-54.

15. Brooks, N.W.J.; Duckett, R.A.; Ward, I.M. *Journal of Rheology*, 1995. **39**(2): p. 425-436.

16. Brooks, N.W.; Duckett, R.A.; Ward, I.M. *Polymer*, 1992. **33**(9): p. 1872-1880.

17. Hughes, D.J.; Mahendrasingam, A.; Oatway, W.B.; Heeley, E.L.; Martin, C.; Fuller, W. *Polymer*, 1997. **38**(26): p. 6427-6430.

18. Butler, M.F.; Donald, A.M.; Bras, W.; Mant, G.R.; Derbyshire, G.E.; Ryan, A.J. *Macromolecules*, 1995. **28**(19): p. 6383-6393.

19. Peterlin, A.; Corneliussen, R. *Journal of Polymer Science: Part A-2*, 1968. **6**: p. 1273-1282.

20. Bunn, C.W. *Transactions of the Faraday Society*, 1939. **35**: p. 482-491.

21. Vickers, M.E.; Fischer, H. *Polymer*, 1995. **36**(13): p. 2667-2670.

22. Steidl, J.; Pelzbauer, Z. *Journal of Polymer Science: Part C*, 1972. **38**: p. 345-356.

23. Seto, T.; Hara, T.; Tanaka, K. *Japanese Journal of Applied Physics*, 1968. **7**(1): p. 31-42.

24. Lagaron, J.M.; Dixon, N.M.; Reed, W.; Pastor, J.M.; Kip, B.J. *Polymer*, 1999. **40**: p. 2569-2586.

25. VanderHart, D.L.; Khoury, F. *Polymer*, 1984. **25**: p. 1589-1599.

26. Keller, A.; Pope, D.P. *Journal of Materials Science*, 1971. **6**: p. 453-478.

27. Brooks, N.W.J.; Duckett, R.A.; Ward, I.M. *Journal of Polymer Science: Part B: Polymer Physics*, 1998. **36**: p. 2177-2189.

28. Darras, O.; Seguela, R. *Journal of Polymer Science: Part B: Polymer Physics*, 1993. **31**: p. 759-766.

29. Meinel, G.; A., P. *Journal of Polymer Science: Part A-2*, 1971. **9**: p. 67-83.

30. Kiho, H.; Peterlin, A.; Geil, P.H. *Journal of Polymer Science: Part B*, 1965. **3**(2): p. 157-160.

31. Lagarón, J.M.; Dixon, N.M.; Gerrard, D.L.; Reed, W.; Kip, B.J. *Macromolecules*, 1998. **31**(17): p. 5845-5852.

32. Rodríguez-Cabello, J.C.; Merino, J.C.; Jawhari, T.; Pastor, J.M. *Polymer*, 1995. **36**(22): p. 4233-4238.

33. Lagarón, J.M.; López-Quintana, S.; Rodriguez-Cabello, J.C.; Merino, J.C.; Pastor, J.M. *Polymer*, 2000. **41**: p. 2999-3010.

34. Rodríguez-Cabello, J.C.; Martín-Monge, J.; Lagarón, J.M.; Pastor, J.M. *Macromolecular Chemistry and Physics*, 1998. **199**(12): p. 2767-2776.

35. Peterlin, A. *Journal of Polymer Science: Part A-2*, 1969. **7**: p. 1151-1163.

36. Flory, P.J.; Yoon, D.Y. *Nature*, 1978. **272**: p. 226-229.

37. Juska, T.; Harrison, I.R. *Polymer Engineering Reviews*, 1982. **2**(1): p. 13-28.

38. Sadler, D.M.; Barham, P.J. *Polymer*, 1990. **31**: p. 36-42.

39. Zhurkov, S.N.; Kuksenko, V.S. *International Journal of Fracture*, 1975. **11**(4): p. 629-639.

CHAPTER 4

IDENTIFICATION OF A MAJOR INTERMEDIATE COMPONENT IN COLD-DRAWN HDPE BY SOLID-STATE NMR

4.1 Introduction

Traditionally, the local morphology of isotropic, melt-crystallized polyethylenes and similar semi-crystalline polymers is described by a two-phase model, which consists of alternating crystalline and amorphous layers, or lamellae.[1-3] However, a third morphological component of intermediate nature has long been suggested.[1,4-6] This 'intermediate' component is generally regarded to be at the interface between crystalline and amorphous domains. For linear, unoriented polyethylenes, the intermediate component has proved difficult to detect directly and reliably and has generally been estimated to comprise less than 20% of the material bulk mass.[4,5,7-18]

Modeling of the phase morphology is not only important in isotropic polymer materials but also in oriented systems. The anisotropic mechanical behavior of oriented semi-crystalline polymers has been explicated and predicted with component models.[19-23] Based on material composite theory, these models comprise elements of distinct mechanical character that are arranged in series or parallel to the axis of orientation. The elements are generally identified with microstructural units in the morphology of the oriented polymer, e.g. stacks of crystalline and amorphous lamellae. A sound qualitative and quantitative knowledge of the component microstructure of oriented semi-crystalline polymers is crucial in effectively developing and applying these models.

Linear polyethylenes can be formed into samples of significant uniaxial orientation by drawing or by fiber spinning processes. These samples can exhibit

remarkable strengths and extensibility along the axis of orientation. To account for this mechanical integrity, various morphological structures have been invoked and incorporated into the classical two-phase model, presenting more intricate representations of the anisotropic morphology of oriented polyethylenes.[22] Such structures include tie molecules[20,24,25] and intercrystalline bridges[26].

'High-strength' polyethylene fibers display Young's moduli about two orders of magnitude greater than traditional melt-crystallized HDPE samples. Through a variety of experimental techniques, studies of high-strength PE fibers have shown the existence of morphological structures distinct from the traditional crystalline and amorphous domains. Using Raman spectroscopy, researchers[27-29] have noted some all-trans chains with molecular strains an order of magnitude greater than other all-trans chains. These highly strained molecules were suggested to account for a large portion of the fibers' load-bearing capability and were quantified up to 40% of the total all-trans content.[28] In combination with X-ray diffraction data, Prasad and Grubb[29] identified these extended, load-bearing chains as non-crystalline material comprising taut tie-molecule structures.

An intermediate component in the morphology of high-strength PE fibers has been suggested in several studies. Fu et al.[30] noted discrepancies while fitting the observed intensities of WAXD patterns with contributions from purely crystalline and amorphous phases. To explain these unaccounted intensities, they introduced an intermediate component consisting of all-trans chains oriented with the fiber axis but poorly packed transverse to the fiber axis. Kwon et al.[31] proposed this intermediate component to have a heat of fusion that contributes to the melting endotherm measured by differential scanning calorimetry (DSC). Analogous studies employing solid-state

NMR[30,32-36] have detected a significant component in high-strength PE fibers composed of mobile, all-trans chains of ^{13}C T_1 intermediate to the crystalline and amorphous domains, although quantification of the component varied depending on the fiber sample and NMR method utilized.

Recent analyses of cold-drawn and necked HDPE samples using Raman scattering[37-39] have revealed all-trans fractions exceeding the measured crystallinity considerably. The increased presence of non-crystalline all-trans chains was attributed to morphological disordering during the necking process. However, distinct spectroscopic peaks of the non-crystalline trans component have not been directly observed in cold-drawn HDPE, and its orientation, conformational order, molecular mobility, and packing still need to be characterized. Even the crystallinity is difficult to determine since the orientational order, the non-equilibrium nature of the necked microstructure, and unknown details of the intricate morphology make interpretations of Raman scattering, DSC, and X-ray scattering measurements difficult.

In this chapter, the spectroscopic characterization of the morphology of cold-drawn, necked HDPE using solid-state NMR is reported. The undrawn, melt-crystallized precursor is used as a reference, to show the effects of cold drawing on the microstructure. A distinct intermediate component is identified and analyzed. By a series of NMR experiments, several of which utilize an 'inverse $T_{1,C}$ filter' that enables selective observation of the signals of the various components, the distinct molecular conformation, mobility, and orientation of this intermediate component is examined.

4.2 Experimental

4.2.1 Sample Preparation

Samples of DOW HD-12450N were used. Compression-molded test sheets were prepared according to the procedure outlined in Section 3.2.2. Samples designated as 'undrawn' in this chapter were extracted directly from the molded sheets.

Standard dumbbell-shaped test specimens were punched from the molded sheets and cold drawn at 2 mm/min (0.0013 s^{-1} drawing strain rate) to an extensional change ΔL of 240 mm (or nominal drawing strain of 945%). Details of the drawing procedure have been given in Section 3.2.2. Necked samples with a draw ratio $\lambda > 16$ were obtained. Samples designated as 'drawn' in this chapter were cut from these necked specimens of 945% drawing strain.

4.2.2 NMR Parameters

Solid-state NMR experiments were conducted using a Bruker DSX 300 spectrometer ($B_o = 7$ T) at a ^{13}C resonance frequency of 75.48 MHz. Measurements were made under both static and magic-angle spinning (MAS) conditions at ambient temperature. For all MAS experiments, 4-mm diameter zirconia rotors with Kel-F caps were used to hold the samples; a 5-kHz spinning speed and decoupling with two-pulse phase modulation (TPPM)[40] at $\gamma B_1/2\pi = 62.5$ kHz were utilized. A ^{13}C 90° pulse length of 4–5.5 μs was employed in ^{13}C direct-polarization (DP) experiments. For standard cross-polarization[41] (CP) measurements, a ^{1}H 90° pulse length of 4 μs and a contact time of 0.5 ms were applied. A 90° pulse length of 3.85 μs was used with ^{1}H wideline measurements.

2D WISE[42] experiments conducted in this study utilized magic-angle spin lock (MASL) on ^1H during CP following the method of Lee and Goldburg[43]. The small crystallite sizes in the drawn HDPE necessitated the suppression of ^1H spin diffusion during the CP contact pulse, which MASL accomplishes via attenuation of the ^1H-^1H dipolar interaction. A ^1H 35° pulse after the t_1 delay in the WISE pulse sequence brings the ^1H magnetization to the magic angle with respect to the $\mathbf{B}_o$ field. ^1H were pulsed off resonance during CP so that the effective field strength at the magic angle would be 62.5 kHz. A shorter CP contact time (0.2 ms) was also used.

Samples of the HDPE were wrapped in Teflon tape for better packing and alignment during ^{13}C NMR measurements. However, for experiments with ^1H detection, no Teflon tape was used, as additives in some Teflon tapes were found to produce undesirable ^1H signals. In most measurements under MAS, the draw directions of pieces from the necked samples were aligned parallel to the long axis of the sample rotor and, hence, the sample coil.

4.2.3 Inverse ^{13}C T_1 Filtering

In order to effectively characterize in detail an intermediate component in the morphology of HDPE, NMR experiments are required that allow the selective observation of the component based predominantly on its distinctive ^{13}C T_1 relaxation time, which was briefly described in Chapter 2. In earlier studies of various forms of polyethylene[10,15,30,33-36], the intermediate $T_{1,C}$ has generally been estimated to differ from the ^{13}C T_1 relaxation times of both the amorphous and crystalline components by at least an order of magnitude. Selective experiments require suppression of both the crystalline

and the amorphous signals, based on these relaxation-time differences. Traditional experiments do not separate resonances either from the crystalline and intermediate components, or the intermediate and amorphous components. Cross polarization suppresses the signals of the highly mobile amorphous components, since they have reduced dipolar couplings and CP efficiencies, but retains both crystalline and intermediate resonances.

Single-pulse excitation of ^{13}C can select the mobile components and could be combined with a ^{13}C T_1 filter to retain only the intermediate component. However, this procedure reduces the sensitivity greatly, due to the loss of CP enhancement and the necessity of long recycle delays (> 5 s) to ensure sufficient relaxation of the magnetization within the intermediate component. In addition, information is not provided with regard to the useful spectral and relaxation properties of ^1H as measured in such experiments as WISE and ^{13}C-detected $T_{1\rho,H}$ experiments that rely on ^1H-^{13}C correlation through cross polarization.

Therefore, an 'inverse $T_{1,C}$ filter' has been introduced.[44] Utilizing this method, it is now possible to selectively observe the signals of short ^{13}C T_1 magnetization with good CP efficiency. The ^1H T_2 and $T_{1\rho H}$ relaxation behavior of the inverse $T_{1,C}$ filtered signals can be easily measured by applying the suitable pulses to ^1H before CP. The basic pulse sequence for the inverse $T_{1,C}$ filter is the same as for a traditional ^{13}C T_1 filter[45] (Figure 4.1). An X-second inverse $T_{1,C}$ filtered spectrum is obtained as the (unscaled) difference between an X-second $T_{1,C}$ filtered spectrum and a reference spectrum obtained with the same pulse program and a very short (1-ms) relaxation delay.

Quantitatively, the spectral intensity after a $T_{1,C}$ filter of duration t_z can be written as the sum of the cross-polarization signals $S_{n,CP}(\omega)$ of the different components, each weighted by $\exp(-t_z/T_{1,n})$, where $T_{1,n}$ is the ^{13}C longitudinal relaxation time of the nth component. The difference signal (ΔS in Figure 4.1) in the inverse $T_{1,C}$ filtered experiment can then be expressed as

$$S_{invfil}(\omega;t_z) = \sum_n \exp(-0/T_{1,n}) \cdot S_{n,CP}(\omega) - \sum_n \exp(-t_z/T_{1,n}) \cdot S_{n,CP}(\omega)$$
$$= \sum_n [1 - \exp(-t_z/T_{1,n})] \cdot S_{n,CP}(\omega). \qquad \text{Eq. 4.1}$$

If the relaxation time is long, $T_{1,n} >> t_z$, the signal of component n is canceled, while the signals of other components with short relaxation times are retained. The inverse $T_{1,C}$ filtered spectrum is like a one-pulse spectrum with a recycle delay of duration t_z, multiplied with the CP efficiency of the specific chemical group.

In an extension of this concept, differences between spectra for two intermediate times t_{za} and t_{zb} can be taken, such that

$$S_{invfil}(\omega;t_{za},t_{zb}) = \sum_n [\exp(-t_{za}/T_{1,n}) - \exp(-t_{zb}/T_{1,n})] \cdot S_{n,CP}(\omega). \qquad \text{Eq. 4.2}$$

This procedure will eliminate the signals of components with short $T_1 << t_{za} < t_{zb}$ as well as long $T_1 >> t_{zb} > t_{za}$, which enables selection and isolation of the signals of components with intermediate $T_{1,C}$ relaxation times. A similar method was employed by Kaji et al.[36] in the acquisition of simple 1D ^{13}C CP/MAS spectra to probe the morphology of high-strength PE fibers.

In contrast to many other difference spectra that have been shown in the literature with the aim of isolating the signal of a specific component, no scaling factors are needed to obtain the inverse $T_{1,C}$ filtered spectra. The filter can also be readily incorporated into WISE, ^{1}H spin diffusion, or ^{13}C-detected $T_{1\rho,H}$ experiments, as demonstrated below and in subsequent chapters.

4.3 Results and Discussion

4.3.1 NMR Characterization of the Undrawn and Drawn HDPE

Various 1D NMR experiments were conducted on the drawn HDPE sample. The undrawn, melt-pressed precursor was examined as a reference. Standard solid-state NMR experiments were first performed. ^{1}H wideline and ^{13}C CP/MAS spectra of the undrawn and drawn samples are presented in Figure 4.2. Clearly, cold drawing leads to structural changes that are reflected in the spectra. For instance, the ^{1}H spectrum of the undrawn sample (Figure 4.2, a) shows a relatively distinct, motion-narrowed peak that can be assigned to the amorphous material.[17,18,46] The much broader 'line' is identified with the crystalline fractions.

An intermediate component has been inferred from such data in past studies[17,18] by fitting the ^{1}H wideline pattern with mathematical functions based on a three-component model. However, as can be readily seen in the spectrum of Figure 4.2(a), a component of intermediate line width is not clearly discernible. This observation applies even more so to the drawn sample (Figure 4.2, b). In this wideline pattern, the line width contrast even between the crystalline and amorphous components is barely visible. The

^{1}H wideline spectra do reveal qualitatively that molecular mobility in the non-crystalline domains decreases upon cold drawing and necking.

In the ^{13}C CP/MAS spectra (Figure 4.2, c and d), additional intensity appears upon deformation downfield (to the left) of the sharp resonance at 32.8 ppm identified with the orthorhombic crystals[47]. These signals correspond to material comprising all-trans chains, but with different molecular packing than the orthorhombic crystalline lattice.[48] In the spectral region of the gauche-containing amorphous phase, around 28–32 ppm[47], indications of line-shape changes due to cold drawing are also observed. The overall intensity of the amorphous signals decreases relative to the crystalline peak. A slight downfield shift is also detectable. However, a lucid and comprehensive inspection into the nature of microstructural changes induced by cold drawing is very difficult from these standard NMR spectra alone.

More detailed and quantitative information about the polymer morphology can be derived from NMR spectra that are discriminating to specific components in the microstructure. Such selectivity can be achieved by utilizing differences in spin relaxation times. These differences are usually based on contrasts in molecular mobility between the various components. In semi-crystalline polymers far above the glass transition of the amorphous domains, a particularly useful distinction is made according to the ^{13}C longitudinal (T_1) relaxation time. $T_{1,C}$ is shortest for molecular segments moving with rates near the Larmor frequency of ^{13}C, which is 75 MHz at the 7-Tesla B_0 field of the spectrometer used in this study. Segments in the amorphous regions have a short ^{13}C T_1, less than one second, due to high-rate molecular mobility, while the $T_{1,C}$ of the crystallite core exceeds 100 s.[15,49,50] For interfacial domains, intermediate $T_{1,C}$

values are found for a variety of reasons, which prominently include transferred relaxation due to chain diffusion from amorphous to crystalline regions in polyethylene.[51]

The inverse $T_{1,C}$ filter outlined in Section 4.2.3 will be used to select signals from the various components based on different ^{13}C T_1 relaxation times. To apply the inverse $T_{1,C}$ filter, times by which the ^{13}C z-magnetization for each component are sufficiently relaxed must be determined. The morphological components will be identified in 1D MAS spectra by their distinctive ^{13}C isotropic chemical shifts.[47,48,52] To monitor the ^{13}C T_1 relaxation of the components, the experiment of Torchia[45] was conducted for each sample. A similar approach has been taken in several studies[15,35,36,50,53] in the measurement of crystalline $T_{1,C}$ values in polyethylenes. A series of ^{13}C CP/MAS spectra with varying $T_{1,C}$ filter delay time (t_z in Figure 4.1) were acquired for the undrawn and drawn samples. In this way, the signals of a given component will become negligible after a certain relaxation delay.

$T_{1,C}$ filtered spectra of both the undrawn and drawn samples at selected delay times t_z are presented in Figure 4.3. In both the undrawn and drawn samples, the amorphous magnetization sufficiently relaxes by 1 s, as indicated by the disappearance of these signals (~28–32 ppm) in both samples. After 1 s, an all-trans peak at ~34.3 ppm becomes apparent, particularly in the drawn sample. VanderHart and Khoury[52] have identified this resonance with the monoclinic crystalline packing[54]. However, all-trans intensities between the orthorhombic and monoclinic shifts are also detectable in both samples after 1 s, and they are quite significant in the drawn sample. Signals between the orthorhombic and monoclinic crystalline shifts have been attributed to intermediate components in high-strength PE fibers by Kaji et al.[36] These resonances indicate

disordered packing of the planes of all-trans chains. In the undrawn sample, the magnetization of these disordered all-trans signals is well relaxed by 10 s, and only a purely crystalline line shape is produced. However, in the drawn sample, the resonances are still visible after 10 s. By 60 s, the disordered all-trans magnetization is sufficiently relaxed, leaving only the sharp peaks of the orthorhombic and monoclinic crystals. In subsequent chapters, these data will be used to make 'Torchia curves' of the morphological components and to calculate $T_{1,C}$ values.

Based on the results of the Torchia experiments, selective ^{13}C spectra of the microstructural components were obtained. A $T_{1,C}$ filter time t_z = 10 s was applied in the selection of long-$T_{1,C}$ components having very limited 75-MHz segmental motion (Figure 4.4, a and b). Of course, these spectra are dominated by signals from the crystalline domains. In both samples, the monoclinic crystalline resonance is seen at ~34.3 ppm. However, in the drawn sample, the intensity of this resonance is larger due to cold drawing. The formation of the metastable monoclinic crystalline form from the orthorhombic form has been observed in the plastic deformation of polyethylenes and is described as a stress-induced 'martensitic' transformation.[54-56] As described above in the Torchia analyses, the resonances of disordered all-trans packing between the orthorhombic and monoclinic shifts have disappeared in the undrawn sample after t_z = 10 s (Figure 4.4, a), but are still present in the drawn sample (Figure 4.4, b). Hence, more rigid (longer $T_{1,C}$) all-trans segments of disordered packing are produced during cold drawing.

Complementary filtering of the most mobile (short $T_{1,C}$) components is achieved by both simple ^{13}C direct-polarization (DP) MAS with a 0.7-s recycle delay

(Figure 4.4, c and d) and ^{13}C CP/MAS with a 0.7-s inverse $T_{1,C}$ filter applied (Figure 4.4, e and f). The inverse $T_{1,C}$ filtered spectra were obtained by Equation 4.1 using a reference spectrum of $t_z = 1$ ms. The four spectra were all acquired in the same experiment time. Note that the inverse $T_{1,C}$ filter reproduces the line shape of the corresponding DP spectra, except for enhanced CP efficiencies, as observed in the increased intensity of the very mobile, all-trans peak (~33 ppm) in the drawn sample (Figure 4.4, f).

As with the rigid components, cold drawing induces major changes in the highly mobile portions of the HDPE microstructure. The line shape of the amorphous intensities (about 28-32 ppm) seems to broaden and shift slightly downfield, which was also seen in the CP/MAS spectra (Figure 4.2, c and d). A significant all-trans peak near 33 ppm (Figure 4.4, d and f) appears in the drawn sample spectra. The chemical shift is slightly downfield of the orthorhombic crystal resonance. However, in the undrawn sample, only a small shoulder is observed in this spectral region (Figure 4.4, c and e). The line width of this very mobile, all-trans peak is much broader compared to the orthorhombic crystal resonance observed in Figure 4.4(a). This increase in line width indicates local disorder in conformation, or more likely, in chain packing. Various researchers[32,36] have detected similar mobile, all-trans resonances in high-strength PE fibers. They have suggested such resonances to be an 'interphase'[32] or 'intermediate' component[36] in the microstructure, but the actual identity was not clear in both studies. Also, the mobile, all-trans peak seems to encompass frequencies downfield from the orthorhombic peak position up to the monoclinic resonance, as noticed in the 10-s $T_{1,C}$ filtered spectrum of the drawn sample

(Figure 4.4, b). Apparently, both rigid (long $T_{1,C}$) and mobile (short $T_{1,C}$) disordered all-trans segments are formed as a result of cold drawing.

Signals from chain segments in which the magnetization is relaxed after 1 s but long before the rigid crystalline core can be isolated using the extension of the inverse $T_{1,C}$ filter described by Equation 4.2, with t_{za} = 1 s and t_{zb} = 10 s. The resulting spectra originate from segments with ^{13}C T_1 times intermediate to the mobile amorphous and rigid crystalline domains. Spectra obtained via Equation 4.2 as the difference between 1 s and 10 s $T_{1,C}$ filtered signals are presented for both samples in Figure 4.4(g),(h). These spectra indicate that only small intensity contributions from the well-ordered crystalline and gauche-containing amorphous phases are retained.

The spectral line shapes of the intermediate $T_{1,C}$ signals (Figure 4.4, g and h) are clearly different from the amorphous (Figure 4.4, c–f) and crystalline (Figure 4.4, a and b) signals. As indicated by the range of chemical shifts (~32–34.4 ppm), chain segments giving these signals in both the undrawn and drawn HDPE samples (Figure 4.4, g and h) have primarily all-trans conformations. However, as noted above when commenting on the disordered, all-trans resonances found in the rigid and mobile components of the drawn sample, the line widths of these intermediate $T_{1,C}$ spectra are significantly larger than the corresponding crystalline spectra (Figure 4.4, a and b). Again, this broadening arises from the disordered packing of planes of all-trans chains. The intensity of the intermediate $T_{1,C}$ drawn-sample spectrum (Figure 4.4, h) is about twice the relative intensity of the undrawn-sample spectrum (Figure 4.4, g), indicating more intermediate $T_{1,C}$ material in the drawn sample.

Because of their intermediate $T_{1,C}$ relaxation times, distinctive MAS spectra, and appreciable intensities, the all-trans chains with disordered packing appear to comprise a distinct morphological component having molecular conformation, packing, and mobility different from the crystalline and amorphous microstructures in both the undrawn and drawn samples. In the case of the undrawn material, the presence of a third 'intermediate' component with all-trans chains of disordered packing and significant mobility agrees with the observations of Strobl and Hagedorn[5] and numerous others[7,10,11,13,15,16]. The intermediate component in undeformed, melt-crystallized polyethylenes has been generally attributed to interfacial regions between the crystalline and amorphous domains. Whether the intermediate component in the drawn sample is interfacial will be discussed in Chapter 6.

4.3.2 Characterization of the Intermediate Component in the Drawn HDPE

In order to further prove that the intermediate component in the cold-drawn HDPE is indeed a distinct microstructural region, it must be demonstrated that its molecular properties are different from those of the crystalline and amorphous domains. Therefore, the amplitude of its segmental mobility and the degree of chain orientation have been subsequently characterized using 2D WISE and ^{13}C static experiments.

4.3.2.1 Mobility Characterization by 2D WISE

The motional amplitude of CH_2 groups along the molecular backbone can be qualitatively estimated using 2D WISE spectroscopy.[42] In combination with the various $T_{1,C}$ filtering methods discussed above, WISE spectra of the morphological components

in the cold-drawn HDPE microstructure can be obtained. As mentioned in the Experimental section (see Section 4.2.2), MASL and a short CP time (0.2 ms) were employed to suppress ^{1}H spin diffusion during cross polarization, which would mix features of the wideline slices of the various components. Also, to eliminate effects of orientation in the necked material, the drawn sample was made 'artificially isotropic' by carefully being cut into pieces about 2.5 mm in length along the draw direction. This size was small enough for the sample pieces to be randomly packed in the 4-mm diameter rotor, but large enough that the presence of stress-induced microstructures like monoclinic crystals were not significantly enhanced due to cutting.

WISE spectra for the crystalline (Figure 4.5, a) and mobile components (Figure 4.5, b) are shown. To the right of the spectra are ^{1}H wideline slices taken at the ^{13}C signal maxima. The wideline spectrum of the orthorhombic crystallites (Figure 4.5, i) at 32.8 ppm is very broad, about 88 kHz fwhm, due to the strong ^{1}H-^{1}H dipolar couplings and only very limited fast motions. Also, the crystalline spectrum reveals two 'horns' separated by a 'well' of intensity reminiscent of a Pake pattern. Such a pattern could possibly be attributed to the ^{1}H-^{13}C heteronuclear dipolar coupling in isolated $^{13}CH_2$ groups. Similar patterns were observed by Nakai and Terao[57] in unlabelled samples of poly(oxymethylene) (POM). Because of the MASL and short CP time, each ^{1}H close to the ^{13}C nucleus is subject to the heteronuclear dipolar coupling of the ^{13}C site. The splitting, or distance between the 'horns', reflects the ^{1}H-^{13}C internuclear distance. The rigidity of the crystalline chains narrows the distribution of these distances and defines the Pake pattern.

Large motional line narrowing is seen in the 10-s inverse $T_{1,C}$ filtered WISE spectrum (Figure 4.5, b). The ^{1}H wideline pattern of the amorphous cross-section (Figure 4.5, iii) at 30.6 ppm has a significantly reduced half width of approximately 30 kHz as a result of high chain mobility. The intermediate component ^{1}H slice (Figure 4.5, ii) at 33 ppm shows a fwhm of about 70 kHz, indicative of intermediate-amplitude fast motions ($> 10^{5}$/s) in the chains. Under the influence of the chain motion, the Pake splitting observed in the crystalline pattern is barely visible in the intermediate component spectrum.

4.3.2.2 Mobility Characterization by ^{13}C Chemical Shift Anisotropy

A quantitative determination of the motional amplitude from WISE line shapes is challenging, due to the multi-spin character of the ^{1}H-^{1}H dipolar interactions. For a quantitative estimate of the motional amplitude, the effects of fast motions on the chemical shift anisotropy of the $^{13}CH_2$ groups are more suitable for examination. Chemical shift anisotropy can be analyzed with experiments without sample rotation, i.e. static NMR. To eliminate effects of sample orientation on the spectral line shape, a macroscopically isotropic sample was prepared from the drawn material, as was done for the WISE experiments. Necked specimens were carefully cut into small flakes of 'soap powder' texture, much finer than the sample used in the WISE experiments, as the artificially increased presence of stress-induced microstructures would not interfere in probing local segment dynamics. These flakes were loosely packed into a 4-mm glass tube that was snuggly fit into the sample coil.

^{13}C static spectra of the undrawn and drawn 'isotropic' samples are shown in Figure 4.6. The spectrum of the undrawn HDPE shows an ideal powder pattern, in particular for the crystalline material (Figure 4.6, c). Calibration of the chemical shifts in ^{13}C static experiments was verified with inspection of the undrawn-sample crystalline spectrum (Figure 4.6, c), in which the chemical shift principal values agreed with those determined by Schmidt-Rohr et al.[58] The crystalline spectrum of the artificially isotropic drawn sample (Figure 4.6, d) exhibits some distortions from the ideal powder pattern, probably from residual macroscopic orientation due to the shape anisotropy of the flakes of fibrillar material used. Variations of the σ_{33} chemical shift principal value (near 10 ppm) with chain packing are not likely to affect the intensity near 20 ppm[48], which is confirmed by the observation that in spectra of the drawn sample, no peak in this range is observed.

The line shapes of the intermediate component spectra for both the undrawn and drawn samples (Figure 4.6, e and f, respectively) excludes rotator-phase, unhindered rotations around the chain axis, which would yield a powder pattern with a peak, not a shoulder, on the downfield (left-hand) side of the spectrum. For fast motions around the chain axis, i.e. around the σ_{33} direction, the difference between the two perpendicular principal values $\underline{\sigma}_{11}$ and $\underline{\sigma}_{22}$ of the motionally averaged chemical shift tensor is reduced. They are related to the rigid-limit values σ_{11}, σ_{22} and the rotation angle ϕ according to[59]

$$\underline{\sigma}_{11} = -\frac{1}{2}\cdot\left(\delta + \left(\sigma_{11} + \sigma_{22}\right)\cdot\left\langle\cos\left(2\phi\right)\right\rangle\right) \qquad \text{Eq. 4.3(a)}$$

$$\underline{\sigma}_{22} = -\frac{1}{2}\cdot\left(\delta - \left(\sigma_{11} - \sigma_{22}\right)\cdot\left\langle\cos\left(2\phi\right)\right\rangle\right) \qquad \text{Eq. 4.3(b)}$$

with $\delta = \sigma_{33} - \sigma_{iso}$. Eq. 4.3(c)

The pointed brackets indicate the averaging of the rotation angle around the chain axis. As a result,

$$\left\langle\cos\left(2\phi\right)\right\rangle = \left(\underline{\sigma}_{11} - \underline{\sigma}_{22}\right)/\left(\sigma_{11} - \sigma_{22}\right) \qquad \text{Eq. 4.4}$$

For small rotation angles, the left-hand-side can be expanded and the root-mean-square (rms) rotation angle $\langle\phi^2\rangle^{1/2}$ (in degrees) can be determined

$$\left\langle\phi^2\right\rangle^{1/2} = \sqrt{2\cdot\left\{1 - \left(\underline{\sigma}_{11} - \underline{\sigma}_{22}\right)/\left(\sigma_{11} - \sigma_{22}\right)\right\}}\cdot 180^\circ/\pi \qquad \text{Eq. 4.5}$$

While the shortened ^{13}C T_1 indicates some molecular mobility of the intermediate component in the drawn sample as selected by the 1 s - 10 s inverse $T_{1,C}$ filter, the spectrum of Figure 4.6(f) shows only limited motional line narrowing. Nevertheless, the powder spectrum is consistent with a reduction in $(\underline{\sigma}_{11}-\underline{\sigma}_{22})/(\sigma_{11}-\sigma_{22})$ by 5% (0.7 ppm), which would correspond to $\langle\phi^2\rangle^{1/2} = 18^\circ$ according to Equation 4.5. This should be compared with the 6° amplitude rotational motion occurring even in the cores of PE crystallites at ambient temperature.[60] Note that chain flips by 180° would leave the chemical shift tensor invariant, but reduce the long-range ^1H-^1H dipolar couplings.[61]

However, the resulting sharpening of the Pake horns in the WISE spectrum (Figure 4.5, ii) is not observed.

4.3.2.3 Degree of Orientation

^{13}C static NMR experiments were also used to characterize the degree of chain orientation in the crystalline, intermediate, and amorphous components of the cold-drawn sample. The draw axes of pieces of the necked specimens were aligned at 0^o, 55^o, and 90^o to the external magnetic field $\mathbf{B_0}$ in order to analyze the molecular orientation distribution in some detail. VanderHart and Khoury[52] have done similar experiments on drawn PE, but without detailed analysis of the intermediate component. Simple CP spectra acquired at the various angles of sample alignment are presented in Figure 4.7.

Selective spectra of the oriented, fibrillar material based on the $T_{1,C}$ filtering schemes used for the MAS and unoriented static experiments are displayed in Figure 4.8. The spectra for the 0^o orientation are easiest to interpret. A sharp peak at the σ_{33} = 10 ppm edge of the spectral range indicates good alignment of the local chain axes, which coincide with the σ_{33} principal axis of the chemical shift tensor, with the $\mathbf{B_0}$ field, and thus with the fiber axis. Such a sharp peak is observed for the rigid components (crystalline and long-$T_{1,C}$ intermediate) and for the intermediate component (Figure 4.8, 0^o-orientation spectra), denoting good alignment of the local chain axes with the draw direction in both components. The amorphous spectra show very poor chain orientation with the draw axis, except for small contributions from the short-$T_{1,C}$ intermediate component.

A spreading of the σ_{33} peak intensity indicates a distribution of chain orientations relative to the B_0 field and draw direction. At the same time, it should be noted that some broadening can also arise from variations in the σ_{33} principal value of the chemical shift tensor with chain packing.[48] The σ_{33} peak in the 0°-orientation intermediate component spectrum of Figure 4.8 is noticeably broader than the corresponding crystal spectrum. Hence, the chain axes in the intermediate component, though generally aligned with the draw direction, have a broader distribution of orientation angles relative to the crystalline material. The disorder in chain alignment seems to coincide with the disorder in chain packing indicated by the 1D ^{13}C MAS spectra of Figure 4.4. Overall comparison of the ^{13}C static spectra in Figure 4.8 also indicates that the mobile, all-trans chains of the intermediate component are aligned with the draw direction, but with appreciable disorder relative to the crystalline chains.

4.4 Summary

Through several one- and two-dimensional solid-state NMR experiments, a morphological component distinct from the crystalline and amorphous domains has been identified in cold-drawn high-density polyethylene. These experiments employed filtering by ^{13}C T_1 relaxation to select the components based on differences in their $T_{1,C}$ relaxation times. From 1D CP/MAS experiments utilizing the inverse $T_{1,C}$ filter, it was found that the signals with intermediate ^{13}C T_1 values in both undrawn and drawn samples showed resonances attributed to predominantly all-trans chain conformations, as seen in the crystalline material. From these experiments alone, it was clear that the intermediate component in both samples was different from the gauche-containing

amorphous phase. However, the line widths of the intermediate component spectra in both samples are much broader than the crystalline peaks, indicating relative disorder in chain packing.

^{13}C static experiments and 2D WISE experiments further proved the distinction between the crystalline and intermediate components in the cold-drawn material based on molecular mobility and orientation. The chains in the intermediate component are undergoing intermediate-amplitude motions, according to the wideline narrowing detected in the inverse $T_{1,C}$ filtered WISE spectrum. ^{13}C NMR experiments without sample spinning reveal the motions to occur mostly around the chain axis; on that basis, the line narrowing converts to rotational amplitudes of about 18°. Chains in the intermediate component are generally aligned with the draw direction, but with a greater distribution of orientation angles relative to crystalline chains. A quantification of this intermediate component and further examination into its nature and identity (i.e. interfacial material, tie molecules, etc.) will be addressed in subsequent chapters.

4.5 Figures

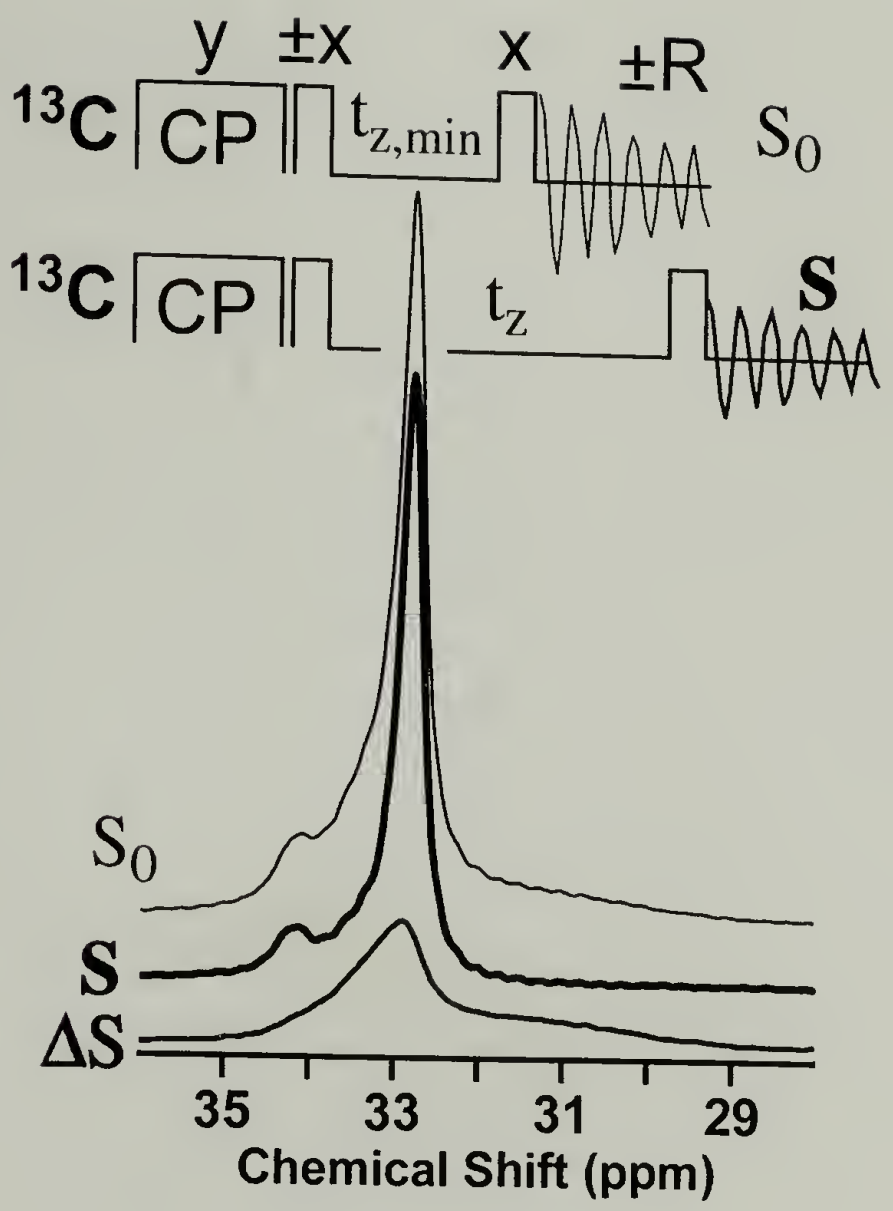

Figure 4.1: Demonstration of the 'inverse $T_{1,C}$ filter' experiment. Utilizing the $T_{1,C}$ filter pulse sequence of Torchia[45], with variable $T_{1,C}$ filter delay time t_z, an X-second inverse $T_{1,C}$ filtered spectrum ($\Delta\mathbf{S}$) is obtained as the unscaled difference between an X-second $T_{1,C}$ filtered spectrum ($\mathbf{S}$, where t_z = X) and a reference spectrum ($\mathbf{S_o}$, where $t_{z,min}$ = 1 ms) acquired with the same number of scans. Spectra shown are of the HDPE sample cold drawn to 945% strain.

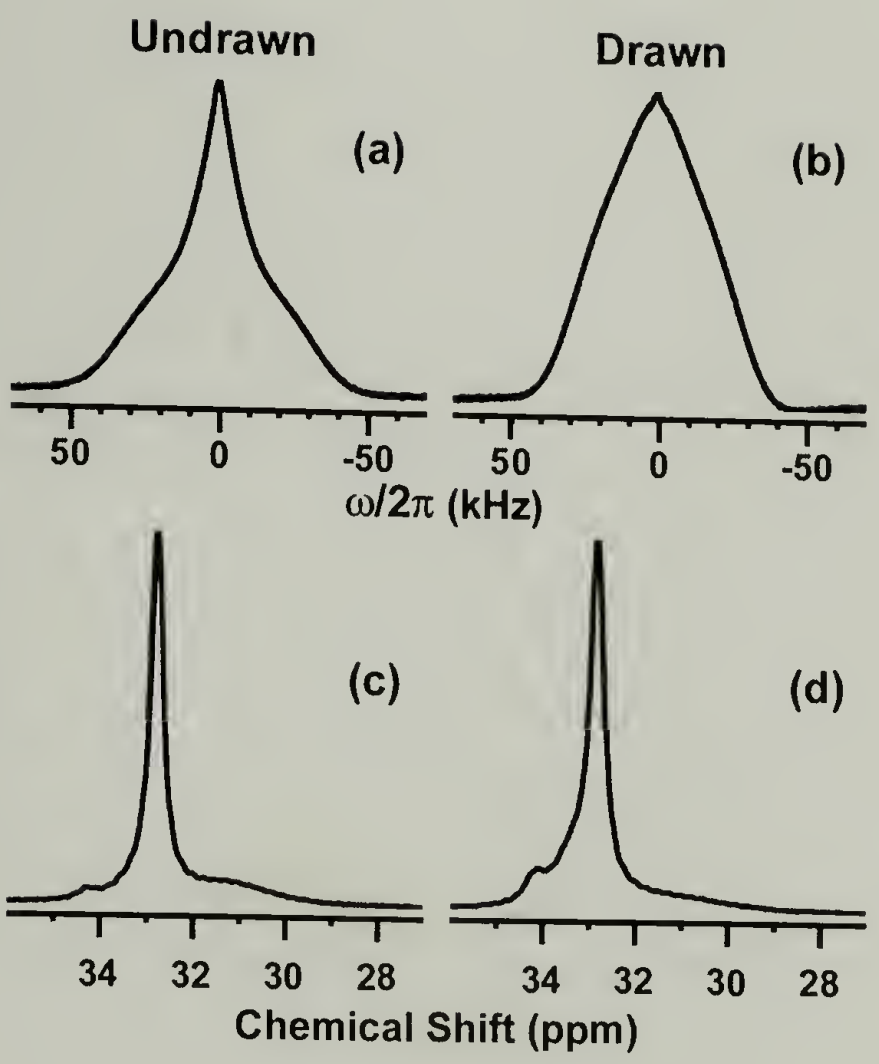

Figure 4.2: Comparison of standard solid-state NMR spectra of the undrawn and drawn samples (left and right columns, respectively). (a), (b) ^{1}H wideline; (c), (d) ^{13}C CP/MAS. The drawn sample was pulled to 945% strain.

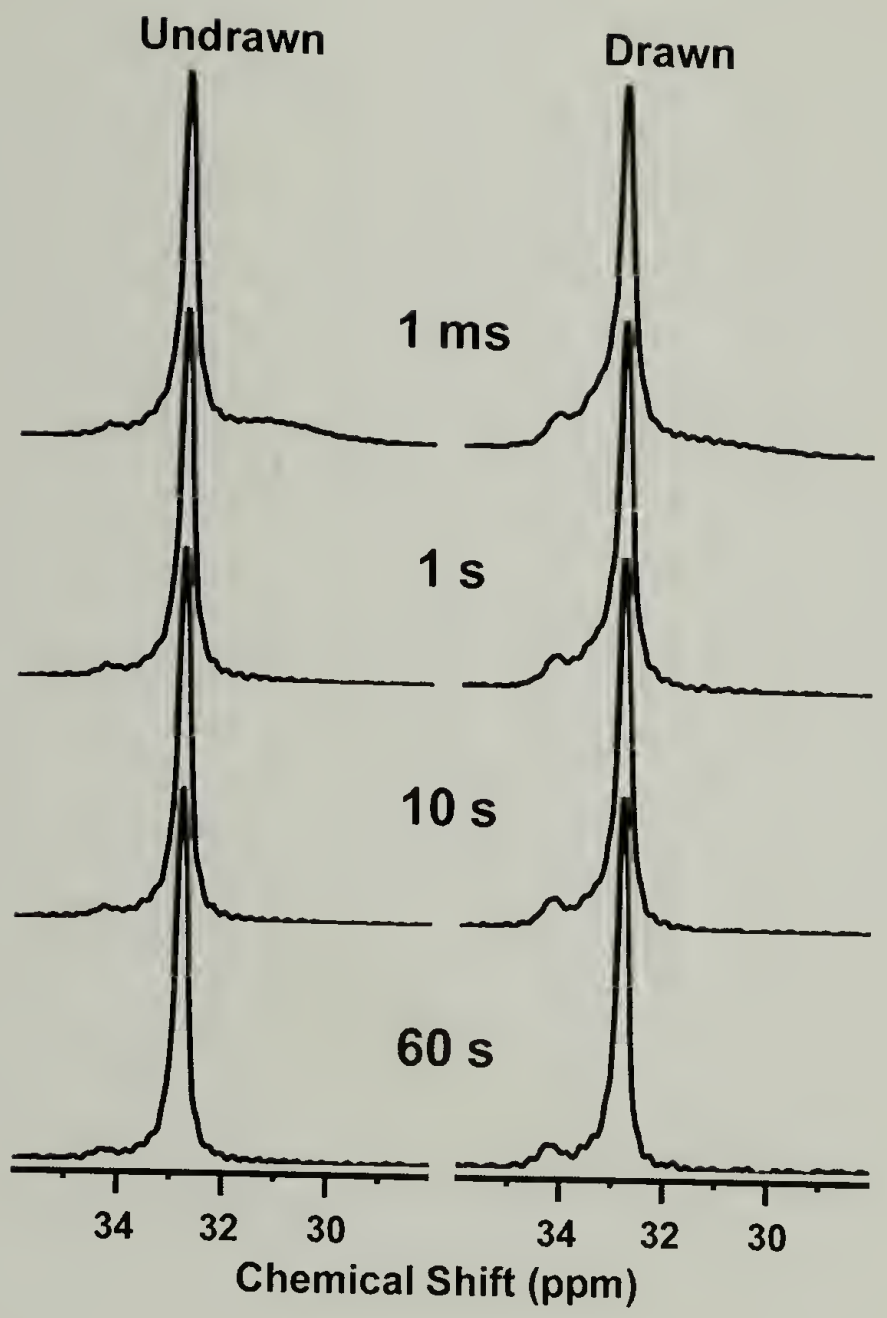

Figure 4.3: ^{13}C CP/MAS $T_{1,C}$ filtered spectra of the undrawn and drawn samples (left and right columns, respectively) at selected $T_{1,C}$ filter delay times, as indicated. Spectra are scaled so that the intensities of the orthorhombic crystalline peaks (32.8 ppm) are the same.

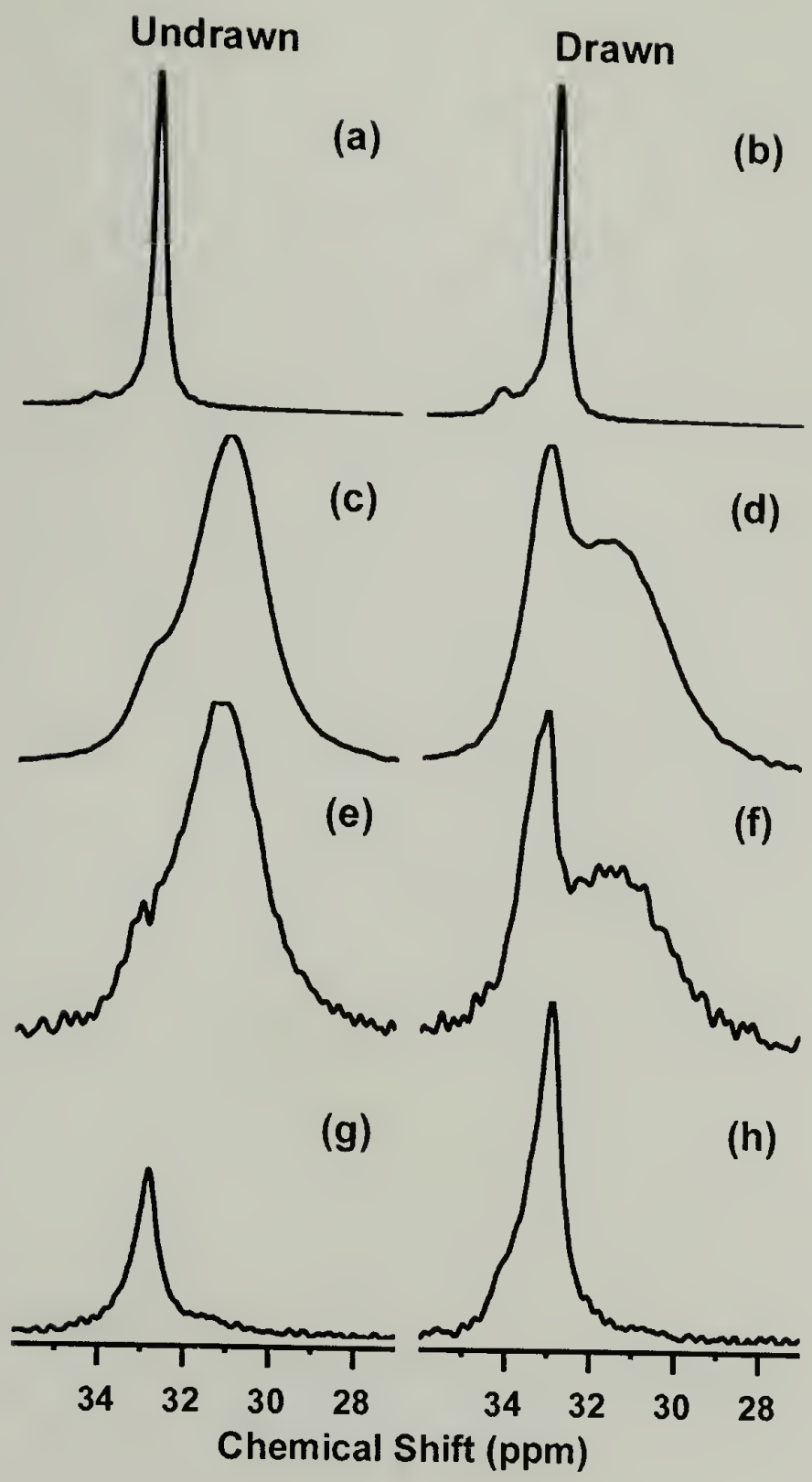

Figure 4.4: Comparison of selective spectra based on the ^{13}C T_1 of the undrawn and drawn samples (left and right columns, respectively). (a), (b) ^{13}C CP/MAS 10-s $T_{1,C}$ filtered spectra (rigid components); (c), (d) ^{13}C DP/MAS with 0.7-s recycle delay (very mobile components); (e), (f) ^{13}C CP/MAS 0.7-s inverse $T_{1,C}$ filtered spectra taken with the same experiment time as (c) and (d) (very mobile components); (g), (h) difference spectra between ^{13}C CP/MAS 1-s and 10-s $T_{1,C}$ filtered spectra (intermediate component).

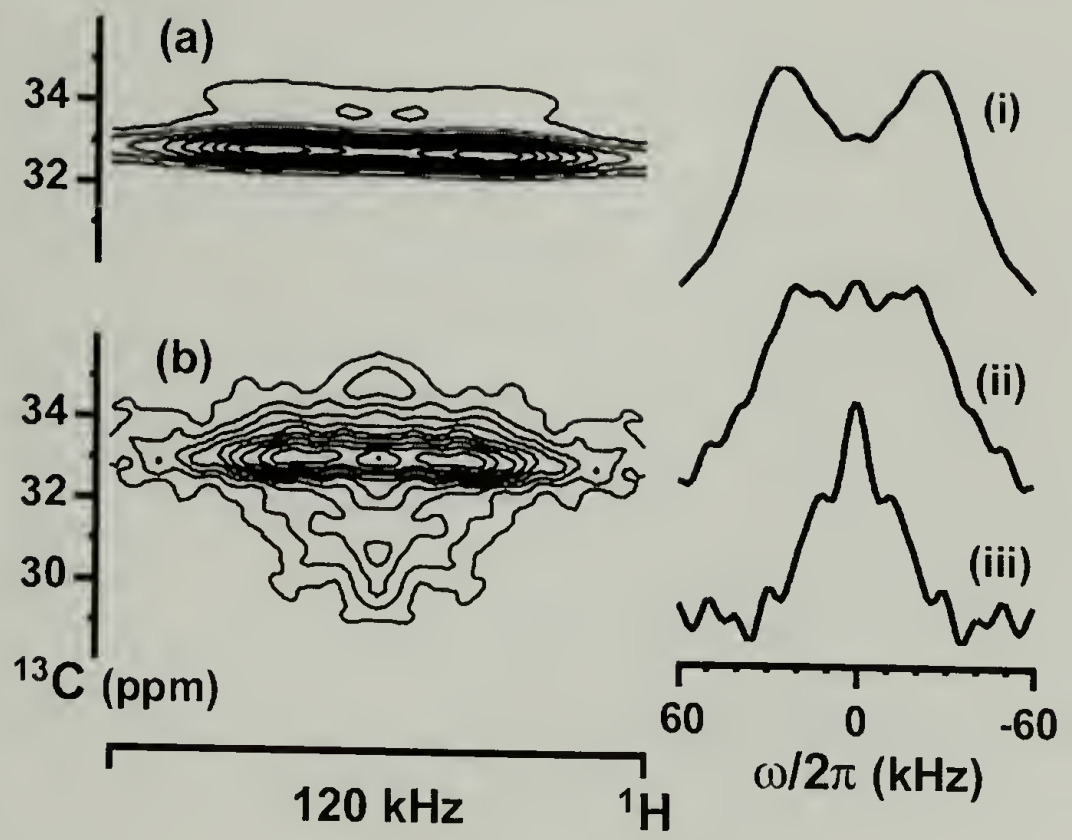

Figure 4.5: WISE spectra (MASL CP, 0.2-ms contact pulse to suppress ^{1}H spin diffusion) of the HDPE sample cold drawn to 945% strain and made macroscopically isotropic in the rotor (a) with 10-s $T_{1,C}$ filter (crystalline) and (b) with 10-s inverse $T_{1,C}$ filter (amorphous and intermediate). Contour lines are spaced at equal intervals, the interval being 10% of the maximum spectral intensity. ^{1}H wide line spectra obtained as cross sections at the orthorhombic crystalline (i), intermediate (ii), and amorphous (iii) ^{13}C signal maxima are displayed on the right.

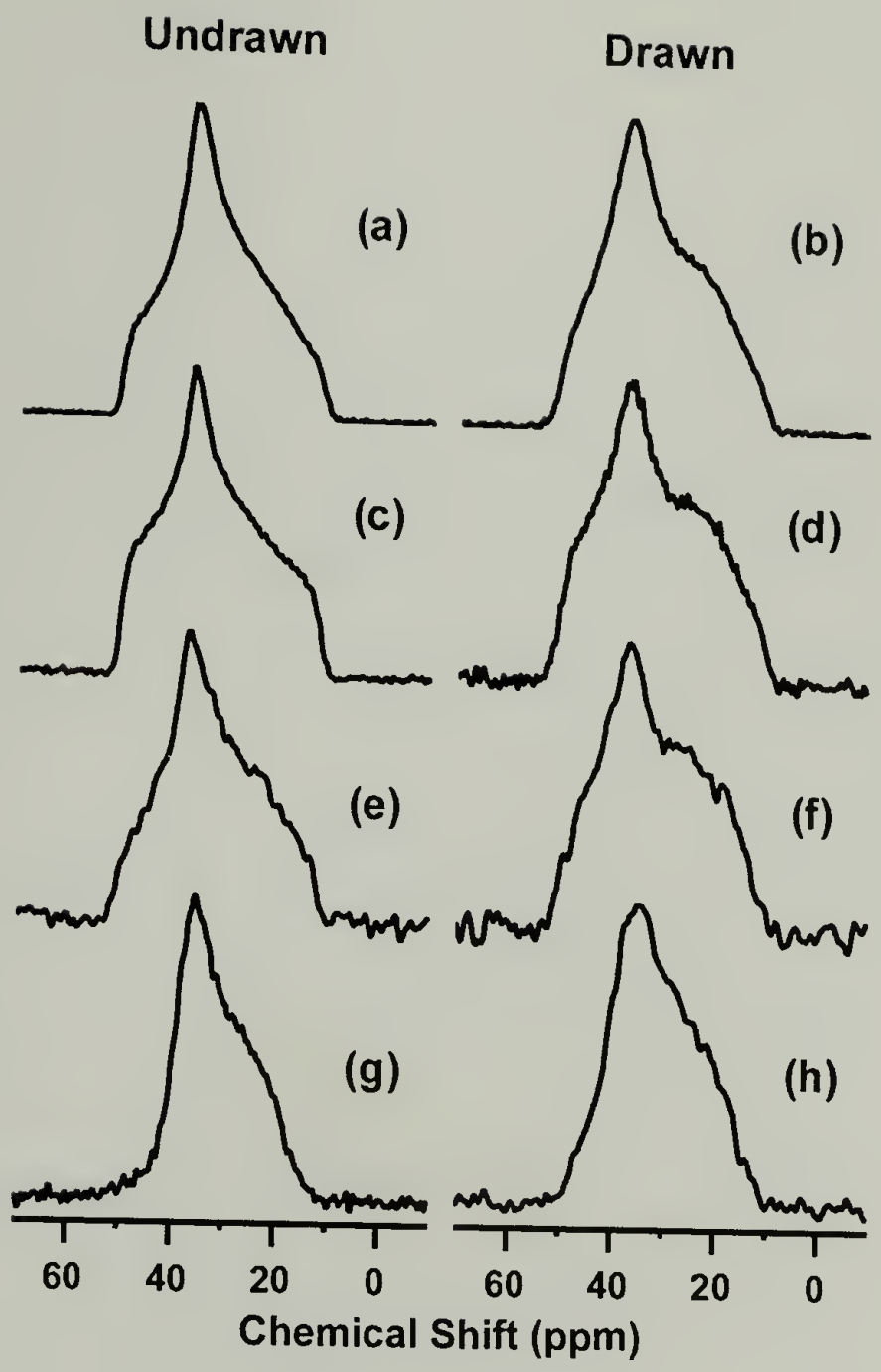

Figure 4.6: ^{13}C CP static spectra of the undrawn and drawn (945% strain) samples unoriented with respect to the $\mathbf{B}_0$ field. (a), (b) CP spectra; (c), (d) 10-s $T_{1,C}$ filtered spectra (crystalline and long $T_{1,C}$ intermediate); (e), (f) difference spectra between 1-s and 10-s $T_{1,C}$ filtered spectra (intermediate); (g), (h) 0.7-s inverse $T_{1,C}$ filtered spectra (amorphous and short $T_{1,C}$ intermediate).

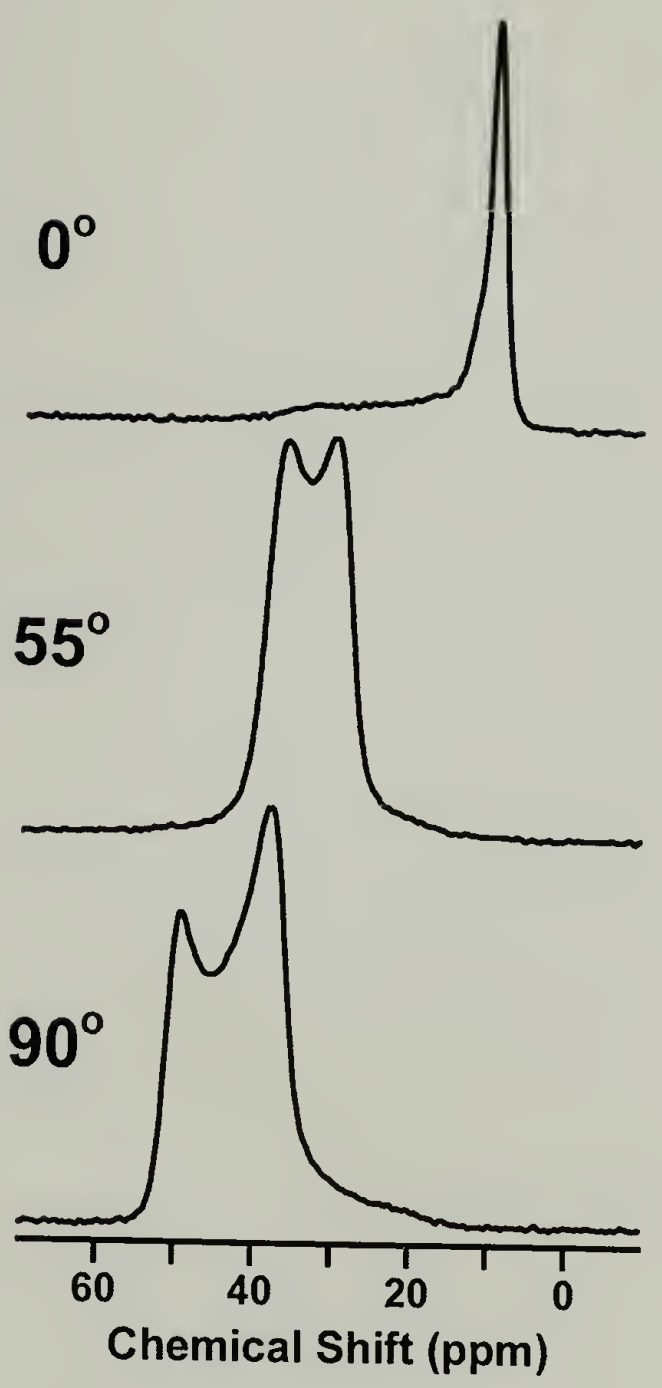

Figure 4.7: ^{13}C CP static spectra of the sample drawn to 945% strain with draw axis oriented at various indicated angles with respect to the $\mathbf{B}_0$ field.

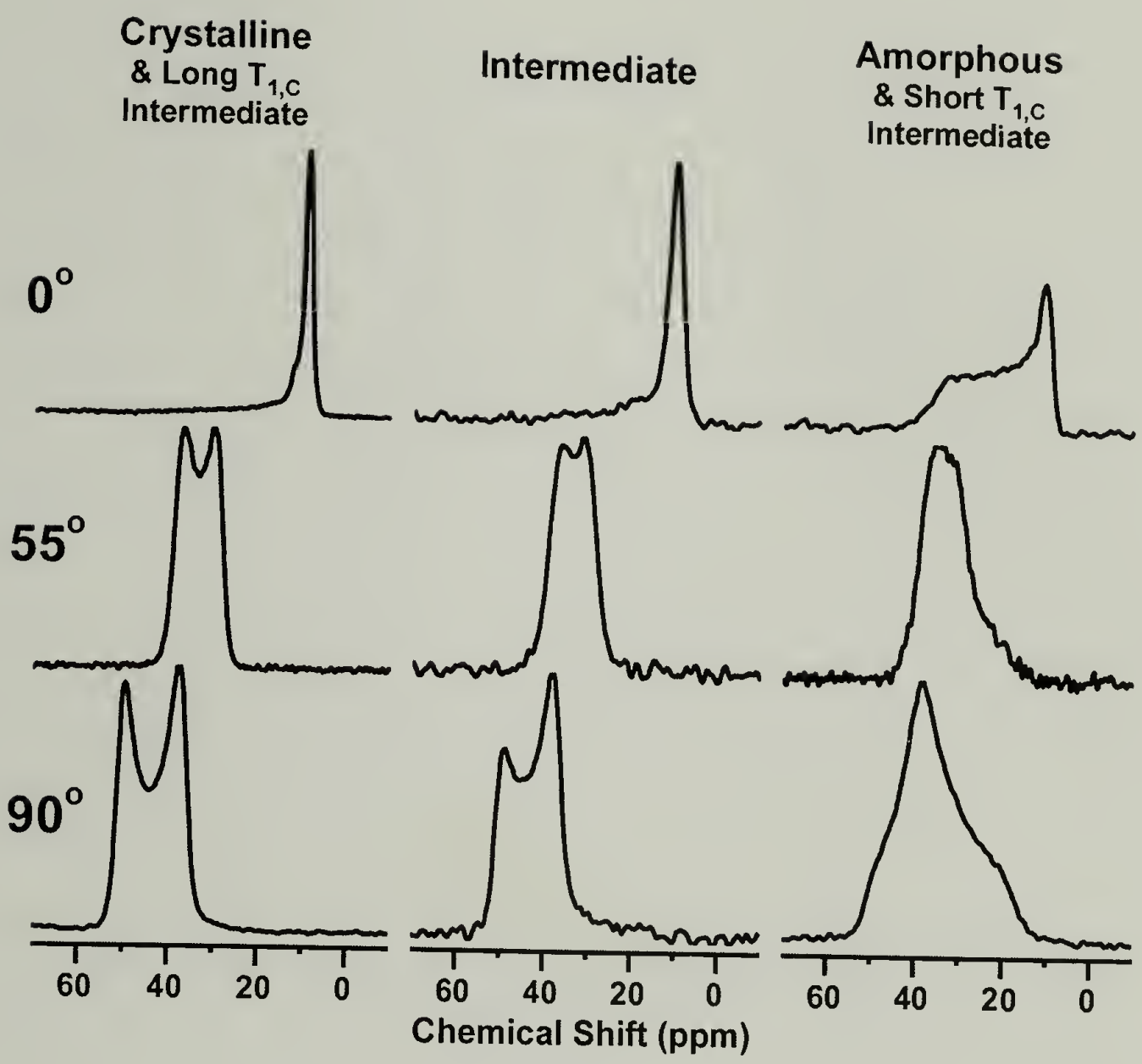

Figure 4.8: Selective ^{13}C CP static spectra of the drawn sample (945% strain) with draw axis oriented at various indicated angles with respect to the $\mathbf{B_0}$ field. Crystalline and long $T_{1,C}$ intermediate components (10-s $T_{1,C}$ filtered spectra); intermediate component (difference between 1-s and 10-s $T_{1,C}$ filtered spectra); amorphous and short $T_{1,C}$ intermediate components (0.7-s inverse $T_{1,C}$ filtered spectra).

4.6 References

1. Mandelkern, L. *Accounts of Chemical Research*, 1990. **23**(11): p. 380-386.
2. Fischer, E.W. *Polymer Journal*, 1985. **17**(1): p. 307-320.
3. Flory, P.J.; Yoon, D.Y. *Nature*, 1978. **272**: p. 226-229.
4. Mandelkern, L. *Polymer Journal*, 1985. **17**(1): p. 337-350.
5. Strobl, G.R.; Hagedorn, W. *Journal of Polymer Science: Polymer Physics Edition*, 1978. **16**: p. 1181-1193.
6. Flory, P.J. *Journal of Chemical Physics*, 1949. **17**(3): p. 223-240.
7. Baker, A.M.E.; Windle, A.H. *Polymer*, 2001. **42**: p. 667-680.
8. Mandelkern, L.; Alamo, R.G. *Macromolecules*, 1995. **28**(8): p. 2988-2989.
9. Naylor, C.C.; Meier, R.J.; Kip, B.J.; Williams, K.P.J.; Mason, S.M.; Conroy, N.; Gerrard, D.L. *Macromolecules*, 1995. **28**(8): p. 2969-2978.
10. Cheng, J.; Fone, M.; Reddy, V.N.; Schwartz, K.B.; Fisher, H.B.; Wunderlich, B. *Journal of Polymer Science: Part B: Polymer Physics*, 1994. **32**(2683-2693).
11. Mutter, R.; Stille, W.; Strobl, G. *Journal of Polymer Science: Part B: Polymer Physics*, 1993. **31**: p. 99-105.
12. Rull, F.; Prieto, A.C.; Casado, J.M.; Sobron, F.; Edwards, H.G.M. *Journal of Raman Spectroscopy*, 1993. **24**: p. 545-550.
13. Shen, C.; Peacock, A.J.; Alamo, R.G.; Vickers, T.J.; Mandelkern, L.; Mann, C.K. *Applied Spectroscopy*, 1992. **46**(8): p. 1226-1230.
14. Mandelkern, L.; Peacock, A.J. *Studies in Physical and Theoretical Chemistry*, 1988. **54**: p. 201-227.
15. Kitamaru, R.; Horii, F.; Murayama, K. *Macromolecules*, 1986. **19**(3): p. 636-643.
16. Glotin, M.; Mandelkern, L. *Colloid & Polymer Science*, 1982. **260**(2): p. 182-192.
17. Kitamaru, R.; Horii, F. *Advances in Polymer Science*, 1978. **26**: p. 138-178.

18. Smith, J.B.; Manuel, A.J.; Ward, I.M. *Polymer*, 1975. **16**: p. 57-65.

19. Ward, I.M.; Hadley, D.W. *An Introduction to the Mechanical Properties of Solid Polymers*. 1993, New York: John Wiley & Sons, Inc.

20. Peterlin, A. *Colloid & Polymer Science*, 1987. **265**(5): p. 357-382.

21. Ward, I.M., ed. *Developments in oriented polymers -- 2*. Developments. 1987, Elsevier Applied Science Publishers Ltd: Barking, Essex, England.

22. Ward, I.M., ed. *Developments in oriented polymers -- 1*. Developments. 1982, Applied Science Publishers Ltd: Barking, Essex, England.

23. Takayanagi, M.; Imada, K.; Kajiyama, T. *Journal of Polymer Science: Part C*, 1966. **15**: p. 263-281.

24. Peterlin, A. *Colloid and Polymer Science*, 1975. **253**(10): p. 809-823.

25. Peterlin, A. *Journal of Materials Science*, 1971. **6**: p. 490-508.

26. Gibson, A.G.; Davies, G.R.; Ward, I.M. *Polymer*, 1978. **19**: p. 683-693.

27. Moonen, J.A.H.M.; Roovers, W.A.C.; Meier, R.J.; Kip, B.J. *Journal of Polymer Science: Part B: Polymer Physics*, 1992. **30**: p. 361-372.

28. Kip, B.J.; van Eijk, M.C.P.; Meier, R.J. *Journal of Polymer Science: Part B: Polymer Physics*, 1991. **29**: p. 99-108.

29. Prasad, K.; Grubb, D.T. *Journal of Polymer Science: Part B: Polymer Physics*, 1989. **27**: p. 381-403.

30. Fu, Y.; Chen, W.; Pyda, M.; Londono, D.; Annis, B.; Boller, A.; Habenschuss, A.; Cheng, J.; Wunderlich, B. *Journal of Macromolecular Science -- Physics*, 1996. **B35**(1): p. 37-87.

31. Kwon, Y.K.; Boller, A.; Pyda, M.; Wunderlich, B. *Polymer*, 2000. **41**: p. 6237-6249.

32. Hu, W.-G.; Schmidt-Rohr, K. *Polymer*, 2000. **41**: p. 2979-2987.

33. Cheng, J.; Fone, M.; Fu, Y.; Chen, W. *Journal of Thermal Analysis*, 1996. **47**: p. 673-683.

34. Chen, W.; Fu, Y.; Wunderlich, B.; Cheng, J. *Journal of Polymer Science: Part B: Polymer Physics*, 1994. **32**: p. 2661-2666.

35. Kaji, A.; Yamanaka, A.; Murano, M. *Polymer Journal*, 1990. **22**(10): p. 893-900.

36. Kaji, A.; Ohta, Y.; Yasuda, H.; Murano, M. *Polymer Journal*, 1990. **22**(6): p. 455-462.

37. Lagarón, J.M.; López-Quintana, S.; Rodriguez-Cabello, J.C.; Merino, J.C.; Pastor, J.M. *Polymer*, 2000. **41**: p. 2999-3010.

38. Lagaron, J.M.; Dixon, N.M.; Reed, W.; Pastor, J.M.; Kip, B.J. *Polymer*, 1999. **40**: p. 2569-2586.

39. Rodríguez-Cabello, J.C.; Martín-Monge, J.; Lagarón, J.M.; Pastor, J.M. *Macromolecular Chemistry and Physics*, 1998. **199**(12): p. 2767-2776.

40. Bennett, A.E.; Rienstra, C.M.; Auger, M.; Lakshmi, K.V.; Griffin, R.G. *Journal of Chemical Physics*, 1995. **103**(16): p. 6951-6958.

41. Hartmann, S.R.; Hahn, E.L. *Physical Review*, 1962. **128**(5): p. 2042-2053.

42. Schmidt-Rohr, K.; Clauss, J.; Spiess, H.W. *Macromolecules*, 1992. **25**(12): p. 3273-3277.

43. Lee, M.; Goldburg, W.I. *Physical Review*, 1965. **140**(4A): p. A1261-A1271.

44. Mowery, D.; Schmidt-Rohr, K. *Polymeric Materials: Science and Engineering*, 2001. **85**: p. 35-36.

45. Torchia, D.A. *Journal of Magnetic Resonance*, 1978. **30**: p. 613-616.

46. Wilson, C.W.; Pake, G.E. *Journal of Chemical Physics*, 1957. **27**(1): p. 115-122.

47. Earl, W.L.; VanderHart, D.L. *Macromolecules*, 1979. **12**(4): p. 762-767.

48. VanderHart, D.L. *Journal of Magnetic Resonance*, 1981. **44**: p. 117-125.

49. Axelson, D.E. *Carbon-13 Solid-State NMR of Semicrystalline Polymers*, in *High Resolution NMR Spectroscopy of Synthetic Polymers in Bulk*, Komoroski, R.A., Editor. 1986, VCH Publishers, Inc.: Deerfield Beach, Florida, USA. p. 157-226.

50. Axelson, D.E.; Mandelkern, L.; Popli, R.; Mathieu, P. *Journal of Polymer Science: Polymer Physics Edition*, 1983. **21**: p. 2319-2335.

51. Schmidt-Rohr, K.; Spiess, H.W. *Macromolecules*, 1991. **24**(19): p. 5288-5293.

52. VanderHart, D.L.; Khoury, F. *Polymer*, 1984. **25**: p. 1589-1599.

53. Kuwabara, K.; Kaji, H.; Horii, F.; Bassett, D.C.; Olley, R.H. *Macromolecules*, 1997. **30**(24): p. 7516-7521.

54. Seto, T.; Hara, T.; Tanaka, K. *Japanese Journal of Applied Physics*, 1968. **7**(1): p. 31-42.

55. Lin, L.; Argon, A.S. *Journal of Materials Science*, 1994. **29**: p. 294-323.

56. Bowden, P.B.; Young, R.J. *Journal of Materials Science*, 1974. **9**: p. 2034-2051.

57. Nakai, T.; Terao, T. *Magnetic Resonance in Chemistry*, 1992. **30**(1): p. 42-44.

58. Schmidt-Rohr, K.; Wilhelm, M.; Johansson, A.; Spiess, H.W. *Magnetic Resonance in Chemistry*, 1993. **31**: p. 352-356.

59. Schmidt-Rohr, K.; Spiess, H.W. *Multidimensional Solid-State NMR and Polymers*. 1994, San Diego: Academic Press, Inc.

60. Hentschel, D.; Sillescu, H.; Spiess, H.W. *Makromol. Chemie*, 1979. **180**: p. 241-249.

61. Hu, W.-G.; Boeffel, C.; Schmidt-Rohr, K. *Macromolecules*, 1999. **32**(5): p. 1611-1619.

CHAPTER 5

ANALYSIS AND QUANTIFICATION OF THE HDPE COMPONENT MICROSTRUCTURE DURING COLD DRAWING

5.1 Introduction

Microstructural and molecular variables such as crystalline lamellar thickness, molecular weight, and short-chain branching can influence the cold-drawing behavior of polyethylenes.[1,2] Of course, these variables are reflected in the component morphology, composition, and properties.[1,3,4] Quantification and analysis of the phase structure is an essential part in ascertaining structure-property relationships and modeling anisotropic mechanical behavior in oriented polymer systems.

Current experimental methods for quantifying the component make-up in polyethylene can be affected by the orientation and complex morphology of the cold-drawn form. For example, molecular orientation must be accounted for in Raman scattering measurements of the component fractions in drawn polyethylene.[5] Estimates of the crystallinity in fibrous PE samples by the density-gradient technique are prone to error due to voids and cracks in the microstructure.[6] Annealing effects such as crystal thickening, solid-state phase transformations, and molecular relaxation can possibly occur in the characterization of drawn samples by differential scanning calorimetry (DSC).

Researchers have also employed solid-state NMR to quantify the fractions of microstructural components in polyethylene, but primarily in the undeformed state. Phase amounts were determined from ^{1}H wideline spectra by ambiguous deconvolution procedures in which the spectral line shapes were fitted with complex functions based on

a multi-component model.[7-9]. In their ^{1}H wideline study, Smith et al.[9] examined isotropic and cold-drawn samples of linear PE and found the 'intermediate' component to decrease in spectral intensity with increasing draw ratio. In the approach of Axelson et al.[10], the slow-decaying (long-time) portion of ^{13}C T_1 relaxation curves associated with the crystalline material was extrapolated to zero delay time and divided by the total intensity at zero time to estimate crystallinity values. However, it has been shown that chain diffusion in the crystallites affects the exponentiality of the relaxation curve[11], making this method unreliable.

VanderHart and Khoury[12] used ^{13}C cross polarization (CP) with MAS and dipolar decoupling to characterize the component microstructure in undrawn and drawn polyethylene samples. In this study, the determination of the orthorhombic to monoclinic crystal ratio was very successful. Differences in CP efficiencies between the crystalline and non-crystalline components were accounted for with estimations of the CP enhancement factors. However, these factors introduce further error into phase content determination. Also, no component intermediate to the crystalline and amorphous domains was considered.

Later studies have also used ^{13}C NMR with MAS to measure component composition in polyethylenes. Cheng et al.[13] presented a quantitative analysis of the intermediate phase in isotropic HDPE samples prepared under a variety of conditions. However, their work exhibited severe technical mistakes in NMR experimentation. Research performed by Kitamaru et al.[14] and Kuwabara et al.[15] produced excellent ^{13}C spectra of various polyethylenes. But in order to derive relative concentrations of the morphological components, both groups employed an ambiguous peak-fitting procedure

using single Lorentzian curves with specified chemical shifts and line widths representing each of the distinctive components. However, several of these Lorentzian peaks were not justified by clear evidence of signal maxima.

Recently, a method has been introduced by Hu and Schmidt-Rohr[16] utilizing a set of ^{13}C DP/MAS and CP/MAS experiments in the characterization of high-strength PE fibers. In this chapter, a ^{13}C NMR quantitative procedure based on this method is outlined. It is used to determine the morphological component composition in cold-drawn polyethylene. Examining the undeformed, melt-crystallized HDPE precursor, phase content results obtained by the NMR procedure are compared with values acquired with two other common techniques, Raman scattering and DSC. The accuracy of the NMR method is thus demonstrated.

In this chapter, the cold-drawing process of the HDPE material initially described in Chapter 3 is also investigated with a variety of 1D NMR experiments. First, NMR spectra of the HDPE at the various extensional changes discussed in Chapter 3 are compared to reveal transitions in chain packing and conformation. The selective filtering methods referred to in Chapter 4 were utilized in many of the spectral series. Next, changes in the component composition are observed via the ^{13}C NMR quantitative procedure mentioned above. Finally, the cold-drawing response of the HDPE is discussed based on the NMR data.

5.2 Experimental

5.2.1 Sample Preparation

Samples of DOW HD-12450N were prepared in the same manner followed in Chapter 4 experiments. Details of these preparation and testing procedures were given in Chapter 3. As in Chapter 4, samples referred to as 'undrawn' or 'undeformed' in this chapter were obtained from melt-crystallized, compression-molded test sheets. 'Drawn' samples were cut from the necked regions of dumbbell-shaped test specimens pulled at 2 mm/min (0.0013 s^{-1} drawing strain rate) under uniaxial tension to various extensional changes ΔL. All mechanical testing was conducted under ambient conditions.

5.2.2 NMR Parameters

Solid-state NMR experiments in this chapter were carried out using the same equipment, settings, and sample preparation techniques described in Section 4.2.2.

5.2.3 Non-NMR Determination of Component Composition

5.2.3.1 Differential Scanning Calorimetry

DSC measurements were performed to quantify crystallinity in undrawn samples of the HDPE. A TA Instruments Model 2910 DSC was employed. First heats were analyzed at 10°C/min using a sample mass of 5–10 mg. A heat of fusion for the perfect PE crystal of 293 J/g was used in calculating mass-percent crystallinity values from the measured sample heats of fusion.[17]

5.2.3.2 Raman Scattering

FT-Raman scattering measurements were made to determine mass percentages of the crystalline, amorphous, and intermediate components in undrawn HDPE samples following the method of Strobl and Hagedorn[18]. Crystallinity was computed using the band at 1416 cm^{-1} and the amorphous content from the 1303 cm^{-1} band. A Bruker FRA 106 instrument equipped with a Nd:YAG (1.064 μm) laser at 250 mW was used in this work; the spectral resolution was 4 cm^{-1}. Spectral curve fitting and calculations were done with PE-GRAMS/2000 software. Based on the recommendations of Rull et al.[19], all bands were freely fit by the software with mixtures of Gaussian and Lorentzian functions. Only the position of the low, broad band at 1270 cm^{-1} was fixed.

5.3 Results

5.3.1 1D NMR Spectra of the HDPE during Cold Drawing

Several types of 1D NMR experiments were conducted in Chapter 4 on samples of the undrawn, melt-crystallized HDPE precursor and the HDPE cold drawn and necked to a strain of 945%. Many of these NMR experiments utilized selective filtering methods that were discussed in detail in the chapter. Expanding on these data, several series of 1D NMR spectra were acquired at the various extensions mentioned in Chapter 3. The observation of trends in the spectral series can give information about changes in chain packing and conformation during the cold-drawing process.

A series of ^{1}H wideline spectra acquired at the different levels of drawing strain is presented in Figure 5.1. As noted in Chapter 4, the contrast of mobility between the rigid and mobile components decreases significantly after necking, as indicated by the

difference in line widths. An interesting observation is made in the detection of a very small peak of narrow line width in the cold-drawn sample spectra. This line was identified by Hu and Schmidt-Rohr[16] with a highly mobile, second amorphous phase that was introduced into the morphology of high-strength PE fibers by the fiber-forming process. They suggested the phase to be chains extending into voids. Note in Figure 5.1 how the peak of the highly mobile component grows in intensity with drawing strain. If indeed the signal originates from chains at void surfaces, then the increasing intensity of the highly mobile component line would result from either a rise in the void population or in the size of existing voids. This picture is consistent with the findings of others using microscopy[20] and SAXS[21].

An analysis of ^{13}C CP/MAS spectra of samples drawn to different strains (Figure 5.2) shows several significant changes. The intensity of the amorphous signals (< 32 ppm) clearly decreases after necking. The height of the monoclinic crystal peak at ~34.3 ppm grows significantly just after necking (98% strain) then decreases as the neck is drawn. As observed in Chapter 4, intermediate component resonances between the orthorhombic (32.8 ppm) and monoclinic crystal frequencies also dramatically increase after necking. These intermediate, all-trans resonances give rise to an apparent broadening of the orthorhombic crystal resonance. Such changes in the rigid components are better seen in the 10-s $T_{1,C}$ filtered spectra shown in Figure 5.3. Again, note the slight increase with drawing strain in the long-$T_{1,C}$ intermediate component signals between the orthorhombic and monoclinic crystal resonances. The sharp growth of the monoclinic crystal resonance just after necking, and its subsequent decrease with neck drawing, is more evident in Figure 5.3.

The mobile components of the HDPE microstructure can also be selectively examined with 1D NMR spectra. In Figure 5.4, a series of 10-s ^{13}C DP/MAS spectra at the different extensions of cold drawing are given. The broad, all-trans resonance at ~33 ppm has been identified with the poorly packed, all-trans chains comprising the intermediate component (Chapter 4). After necking, the intensity of these intermediate signals rises dramatically relative to the upfield amorphous resonances.

Also, the broad amorphous signals seem to shift downfield (to the left) after necking (Figure 5.4). This would indicate a decrease in the gauche-to-trans ratio in the amorphous domains. However, the increased intermediate component intensities underlying the downfield amorphous signals could be introducing this shift. Based on the findings of the 2D WISE experiments in Chapter 4, the amorphous signals can be reasonably separated from the these intermediate signals by the application of a 'dipolar filter'[22] on ^{1}H before cross polarization. The dipolar filter involves a multiple pulse sequence that selects the magnetization in domains where the ^{1}H-^{1}H dipolar couplings are weak. The filter pulse sequence is repeated several times (twelve in experiments conducted in this chapter) to improve the selection. The dipolar filter has been used to select magnetization in ^{1}H spin diffusion studies. In this work, magic-angle spinlock (MASL) was employed during cross polarization in conjunction with the dipolar filter to suppress ^{1}H spin diffusion during CP. MASL was briefly described in Chapter 4.

In Figure 5.5 only very mobile signals are selected with dipolar filtered CP/MAS spectra. The peak of the amorphous intensities consistently remains at about 31 ppm, which strongly suggests that underlying intermediate component signals induce the amorphous downfield shift observed in Figure 5.4. Very mobile stretched chains produce

the all-trans resonances at 33 ppm in Figure 5.5. Because their signals survive the dipolar filter, these chains may be individual molecules dispersed in the amorphous domains. They may also be located at the interface between the intermediate and amorphous components in the HDPE microstructure. Figure 5.5 reveals the content of these very short-$T_{1,C}$ molecules to increase with drawing strain during cold drawing.

Finally, a series of ^{13}C MAS spectra selecting the intermediate component signals were obtained (Figure 5.6). The spectra were acquired using the inverse $T_{1,C}$ filter discussed in Chapter 4. The peak of the intermediate component intensities is located at ~32.9 ppm in the undrawn sample and shifts about 0.1 ppm downfield (to the left) during cold drawing. This shift arises from a general disordering in the chain packing. Also, the spectral shoulder at about 34 ppm rises after necking, coinciding with the increase in the monoclinic crystals detected in Figure 5.2 and Figure 5.3. It is possible that bundles of all-trans chains comprising the intermediate component are anchored in crystallites. Hence, the ordered packing of these chains in the crystallites partially influences their packing in the intermediate component.

5.3.2 Morphological Component Quantification by NMR

5.3.2.1 Discussion of the Basic Procedure

As demonstrated in Chapter 4 and in Section 5.3.1 above, isotropic chemical shifts and ^{13}C T_1 relaxation can readily distinguish microstructural components in polyethylenes. For these reasons, ^{13}C MAS NMR was employed in the analysis of component composition in the HDPE material. However, mobility contrasts between the components and their effects on spectroscopic measurements must be considered.

Determination of amorphous-to-crystalline mass ratios by cross polarization experiments is prone to error due to differences in the CP efficiencies. Therefore, direct-polarization (DP) ^{13}C spectra have been used for quantitative measurements of the relative mass fractions of mobile and rigid components.

Although ^{13}C DP/MAS eliminates the issue of variant CP efficiencies, it also poses two more experimental problems. First, the resonances of the crystalline and amorphous phases overlap in an unfiltered spectrum. Second, full $T_{1,C}$ relaxation of the components during the recycle delay is required to achieve representative spectra of the components. The crystalline phase in polyethylene can have extremely long $T_{1,C}$ times, which are typically on the order of 10^2–10^3 s.[10,14,23] Also, the amorphous-to-crystalline mass ratio is small in polyethylenes of high density. As a result, acquiring a fully relaxed spectrum of the HDPE sample with good amorphous signal would entail unreasonably long experiment times.

These problems are overcome by combining ^{13}C DP/MAS spectra with different recycle delays and numbers of scans as outlined in the method of Hu and Schmidt-Rohr[16] in their study of UHMWPE fibers. A short recycle delay (~1 s) yields signals primarily from the very mobile regions in the component microstructure. Longer delays give spectra that are a superposition of the components in which the ^{13}C magnetization has sufficiently relaxed during the delay time. Spectra with short recycle delays are acquired with a large number of scans to measure the mobile signals (i.e. amorphous, short $T_{1,C}$ intermediate) with good sensitivity. Spectra with very long delays are obtained with few scans, shortening the experiment time. The crystalline signals will be dominant in these spectra when analyzing significantly crystalline polymers. Hence, the amorphous-to-

crystalline mass ratio can be reasonably determined by comparing the spectrum with the short recycle delay to the corresponding spectrum with a very long recycle delay. Spectral areas for fully relaxed ^{13}C signals are proportional to the number of ^{13}C sites detected. By normalizing the original integrated intensities with the number of scans, the relative areas of the different spectra can be compared.

An example of this method is presented in Figure 5.7 for an HDPE sample cold drawn to 945% strain. Three spectra with different recycle delays are presented; their intensities have been scaled to account for the number of scans. Thirty-two scans of the fully relaxed signal with a recycle delay of 2000 s are recorded (Figure 5.7, b). While the all-trans peak is clearly seen, the low amorphous signal is not well defined due to the noise and peak overlap. Together with the mobile all-trans signals of the intermediate component, the amorphous phase is observed fully relaxed with a shorter recycle delay of 10 s and many more scans (Figure 5.7, a and b). A 1-s DP spectrum (Figure 5.7, a) also shows the fully relaxed amorphous magnetization, along with very mobile, short $T_{1,C}$ intermediate component resonances.

Suppression of the transient heteronuclear Overhauser effect (NOE), which could enhance the ^{13}C signals particularly during short recycle delays, is required for accurate quantitative measurements. To prevent this enhancement, two recycle delays are employed in all DP experiments run in the component quantification procedure. An initial recycle delay fixed at 10 s is used, to allow for sufficient longitudinal relaxation of ^{1}H magnetization. After the first recycle delay, a train of 90^{o} pulses on ^{13}C is applied to saturate the ^{13}C magnetization. The effective recycle delay of variable length then follows the saturation pulses and precedes the 90^{o}-excitation pulse on ^{13}C.

During a short recycle delay, the magnetization of long $T_{1,C}$ components will partially relax and could contribute to the total intensity and line shape of the DP spectrum. In this quantification procedure, only those signals that are fully relaxed at a given recycle delay are desired. Partially relaxed, long $T_{1,C}$ signals are 'extraneous' and could result in overestimation of the mobile domain content. To estimate the amount of these partially relaxed, long $T_{1,C}$ signals in ^{13}C DP spectra, a ^{13}C T_1 filter[24] is applied after the single-pulse excitation. The filter is used in a pair of experiments of identical effective recycle delay X seconds, with one experiment having an X-second $T_{1,C}$ filter and the other a very short filter delay (1 ms). The 1-ms $T_{1,C}$ filtered experiment produces a reference spectra, in which very little relaxation in any of the components has occurred. The other experiment in the pair detects only those signals that are partially relaxed after the recycle delay; the filter suppresses fully relaxed signals.

This method is depicted with spectra of the cold-drawn sample in Figure 5.8. Note that predominantly all-trans signals remain after the X-second $T_{1,C}$ filter for both recycle delays of X seconds. These signals originate from the longer $T_{1,C}$ components, i.e. crystalline and intermediate domains. The area of the 10-s $T_{1,C}$ filtered 10-s DP spectrum is 15% of its 1-ms $T_{1,C}$ filtered analog, while the area of the 1-s $T_{1,C}$ filtered 1-s DP spectrum is 24% of its reference analog, both significant quantities. Hence, the $T_{1,C}$ filtered DP method is used to estimate correction factors for the areas of DP spectra with short recycle delays so that fully relaxed signals are only considered.

Based on the experiments described above, an algebraic treatment of the morphological component quantification by ^{13}C DP NMR is presented. To determine relative fractions of the crystalline, intermediate, and amorphous domains in the

polyethylene bulk, three effective recycle delays D1 < D2 < D3 are required. Three different DP spectra are acquired using these recycle delays. The first spectrum is run with recycle delay D1 and N1 scans giving a spectral area of A_{D1}, the second with recycle delay D2 and N2 scans giving a spectral area of A_{D2}, and so on. The shortest two delay times are selected so that amorphous signals are sufficiently relaxed in time D1 and intermediate signals in time D2. Correction for partially relaxed signals in a recycle delay of length X is determined with a pair of $T_{1,C}$ filtered DP experiments, both obtained with recycle delay X and the same number of scans. The experiment with $T_{1,C}$ filter of duration X produces a spectrum of area $A_{X,X}$, while the 1-ms $T_{1,C}$ filtered reference experiment gives a spectral area of $A_{X,1ms}$. The corrected area $A_{D1,c}$ of the DP spectrum with recycle delay D1 is computed by

$$A_{D1,c} = A_{D1}\left(1 - \frac{A_{D1,D1}}{A_{D1,1ms}}\right). \qquad \text{Eq. 5.1}$$

Likewise, the corrected area $A_{D2,c}$ of the DP spectrum with recycle delay D2 is computed by

$$A_{D2,c} = A_{D2}\left(1 - \frac{A_{D2,D2}}{A_{D2,1ms}}\right). \qquad \text{Eq. 5.2}$$

The third ^{13}C DP experiment is conducted with a recycle delay D3. The length of D3 is selected in order for crystalline signals to be sufficiently relaxed in that time. However, polyethylene crystallites can exhibit very long ^{13}C T_1 relaxation times[10] that

can affect the choice of a suitable D3 length. For example, if the crystal $T_{1,C}$ is about 1000 s, most of the ^{13}C crystalline signals will be fully relaxed by a recycle delay D3 = 4000 s; this delay time is experimentally reasonable. At the same time, unreasonably long recycle delays (~ 10000 s) may be required for complete relaxation of the ^{13}C magnetization in the crystalline domains.

As discussed in the method of Hu and Schmidt-Rohr[16], a reasonable length for D3 may be chosen by invoking a correction factor that is determined using ^{13}C CP experiments with the $T_{1,C}$ filter[24]. The decay constant of ^{13}C magnetization during the $T_{1,C}$ filter delay equals the time constant for magnetization increasing from zero to equilibrium in the recycle delay of a DP experiment. The amount of unrelaxed crystalline signals after a recycle delay D3 can be quantified by running a pair of $T_{1,C}$ filtered CP experiments with the same number of scans. The first experiment acts as a reference and has a 1-ms $T_{1,C}$ delay time, giving a spectrum of area $A_{CP,1ms}$. The second experiment contains a $T_{1,C}$ delay time of duration D3, yielding a spectrum of area $A_{CP,D3}$. The ratio of these spectral areas indicates the fraction of unrelaxed crystalline signals after a recycle delay D3 in a DP experiment. As a result, the corrected area $A_{D3,c}$ of the DP spectrum of recycle delay D3 is calculated by

$$A_{D3,c} = A_{D3}\left(1+\frac{A_{CP,D3}}{A_{CP,1ms}}\right). \qquad \text{Eq. 5.3}$$

With the corrected spectral areas of the three DP experiments, the morphological component composition can now be quantified. The mass-fraction of amorphous material X_a is determined by

$$X_a = \frac{A_{DI,c} / N_{DI}}{A_{D3,c} / N_{D3}}, \qquad \text{Eq. 5.4}$$

and the crystalline and intermediate fractions X_c and X_i, respectively, are computed by

$$X_c = 1 - \frac{A_{D2,c} / N_{D2}}{A_{D3,c} / N_{D3}} \qquad \text{Eq. 5.5}$$

$$X_i = 1 - X_a - X_c. \qquad \text{Eq. 5.6}$$

5.3.2.2 Analysis of the Undrawn HDPE

Utilizing this quantitative ^{13}C NMR procedure, an analysis of the component composition in HDPE was first performed on the undrawn, melt-crystallized material. The WAXD pattern of an undrawn sample (Figure 3.6) shows good isotropy of the bulk morphology. Hence, NMR results found for the undrawn HDPE can be compared to values derived from other techniques without regard for orientation and plastic deformation effects. To demonstrate the effectiveness of the NMR method, experiments were also conducted with Raman scattering and DSC, both traditional techniques used to determine phase content in polyethylenes. The method of Strobl and Hagedorn[18] was applied in Raman scattering measurements. This method has long been used to quantify the intermediate component in polyethylene.

To use the quantitative NMR procedure, appropriate values for the recycle delays D1, D2, and D3 must be established for the sample analyzed. These values are best determined by observing the ^{13}C T_1 relaxation of the various morphological components in the HDPE material. The ^{13}C T_1 relaxation can be monitored using the CP $T_{1,C}$ filtered experiment of Torchia[24]. This experiment was conducted in Chapter 4 to set filter delay times in the acquisition of inverse $T_{1,C}$ filtered spectra for undrawn and drawn samples (Figure 4.3). Extinction of signals characteristic to the different components indicated sufficient relaxation of the ^{13}C z-magnetization in those components. Plotting the integrated intensities (spectral areas) of the spectra versus the applied $T_{1,C}$ filter delay time yields ^{13}C T_1 relaxation curves, referred to as 'Torchia' curves. Such plots have been used to measure $T_{1,C}$ relaxation times in polyethylenes.[10,14,15,25,26] A decay of the Torchia curve to zero indicates full relaxation of the ^{13}C magnetization.

Obtaining Torchia curves distinct to the crystalline, intermediate, and amorphous phases can be achieved through spectral scaling based on line shapes. The non-crystalline ^{13}C signals that relax after a certain time t_z can be estimated using an extension of the inverse $T_{1,C}$ filter for selecting spectra of intermediate $T_{1,C}$ relaxation times (Equation 4.2). A pair of CP/MAS $T_{1,C}$ filtered spectra are acquired with the same number of scans, as shown for the cold-drawn HDPE sample in Figure 5.9. One spectrum is acquired with a filter delay t_z, while the other is obtained at a filter time when only crystalline signals are present. In the case of the undrawn, melt-crystallized HDPE, this time was found to be 10 s (Figure 4.3). The crystalline spectrum is then manually scaled so that the difference residual between the two spectra has a reasonable line shape (Figure 5.9). 'Reasonable' scaling is defined in this procedure to be when the sharp

orthorhombic crystal peak of the crystalline spectrum at 32.8 ppm shows no considerable trace of overestimation or underestimation in the residual, i.e. a smooth difference.

The residual difference spectrum obtained from this scaling method approximates the non-crystalline ^{13}C signals that survive a specific $T_{1,C}$ filter time t_z. If the amorphous portion of the difference spectrum is taken at chemical shifts less than 32 ppm (the gauche-containing region[27]), then the remainder of the spectral area is a good estimation of the intermediate component signals. The integrated intensity of crystalline signals at filter times where the non-crystalline signals still exist can be computed by multiplying the area of the pure crystalline reference spectrum used in the scaling procedure with the scaling factor applied in determining the non-crystalline residual. Torchia curves of the various morphological components in the undrawn HDPE material are presented in Figure 5.10. The amorphous and intermediate magnetization is sufficiently relaxed in 1 s and 5 s, respectively. Only about 2% of the crystalline signals remain unrelaxed after 4000 s. Hence, values of 1 s, 10 s, and 4000 s were selected for the DP recycle delays D1, D2, and D3, respectively. The Torchia curves derived here for both undrawn and drawn samples will be used in Chapter 6 to calculate $T_{1,C}$ relaxation times.

Component composition results obtained by the quantitative NMR procedure for the undrawn HDPE material are given in Table 5.1, along with corresponding data measured with Raman scattering and DSC. Good agreement between solid-state NMR and the other techniques is shown. The mass fraction of the intermediate component derived from NMR and Raman scattering measurements falls in line with the value predicted by Mandelkern and Peacock[1] based on the molecular weight of the HDPE analyzed.

5.3.2.3 Analysis of the Cold-Drawn HDPE

Torchia curves for the morphological components in the HDPE sample cold drawn to 945% strain are displayed in Figure 5.11. Several significant differences between the undrawn (Figure 5.10) and drawn (Figure 5.11) samples are apparent. The crystalline signals in the drawn sample relax much faster than in the undrawn precursor, indicating crystallites of smaller thickness in the necked material.[10] In the cold-drawn sample near zero filter time (Figure 5.11), the magnitude of the crystalline intensity is only about 50% of the total sample intensity (all components). In comparison, crystalline signals in the undrawn sample are 70% of the total intensity near zero time (Figure 5.10). However, the most important differences are found in the ^{13}C T_1 relaxation behavior and quantity of the intermediate component. The total relative intensity of intermediate component signals in the drawn sample near zero filter time (Figure 5.11) is much larger than in the undrawn sample (Figure 5.10), about four times greater. ^{13}C magnetization in the intermediate component of the cold-drawn material also relaxes considerably slower than in the undeformed material. This behavior is consistent with observations made in the spectra of Figure 4.3, where the all-trans resonances intermediate to the orthorhombic and monoclinic shifts were extinct in the undrawn sample by 10 s, but still present in the drawn sample until 60 s. The amorphous signals in both samples show similar relaxation character, however, and are sufficiently relaxed by 1 s.

From the analysis of the Torchia curves (Figure 5.11), values of D1 = 1 s and D3 = 2000 s were chosen for the quantitative ^{13}C NMR characterization of the cold-drawn HDPE material. A set of $CP/T_{1,C}$ filtered experiments with varying filter time were also performed on the sample cold drawn to 98% strain. This sample is drawn to a

point just after neck stabilization (Chapter 3). The values of D1 and D3 selected above were applicable to the sample strained to 98% as well. Therefore, since the two extremes of the neck-drawing regime (drawing stages 4 and 5 as described in Chapter 3) demonstrated similar ^{13}C relaxation behavior in the morphological components, the time lengths of the D1 and D3 recycle delays cited above were used for all cold-drawn samples in this study. Application of these values in the characterization of all levels of drawing extension assumes a gradual change in component composition and relaxation behavior with strain, demonstrated in part in subsequent data.

If the duration of D2 for drawn samples was selected so that the intermediate component was sufficiently relaxed, a value of 60 s would be appropriate. However, both a 60-s DP experiment and a 60-s DP $T_{1,C}$ filtered pair (one with a 60-s $T_{1,C}$ filter) would have to be run with several scans to achieve acceptable signal-to-noise, which would entail lengthy experiment times. To circumvent this problem, the scaling method used in deriving Torchia curves for the various morphological components is invoked.

Figure 5.11 shows that after 10 s, about one-third of the intermediate component magnetization is unrelaxed in the drawn sample. If D2 were set at 10 s, as in the analysis of the undrawn sample, then the relative amount of intermediate signals which relax after 10 s would have to be quantified. Applying the scaling method, a CP/$T_{1,C}$ filtered spectrum with t_z = 10 s would be acquired, along with a 60-s $T_{1,C}$ filtered spectrum that contains pure crystalline signals, as shown in Figure 5.9. The corresponding residual contains signals from the intermediate component that relax after 10 s, referred to as the long-$T_{1,C}$ or rigid portion of the intermediate component. The CP efficiency differences between the crystalline and long-$T_{1,C}$ intermediate components are assumed to be

negligible. Hence, the fraction of components that $T_{1,C}$ relax after 10 s which is attributed to the long-$T_{1,C}$ intermediate component can be estimated by measuring the ratio of spectral areas between the residual spectrum and the 10-s $T_{1,C}$ filtered spectrum (Figure 5.9).

Therefore, in the algebraic treatment of the component composition quantification, Equation 5.5 would be replaced by

$$X_{rig} = 1 - \frac{A_{D2,c} / N_{D2}}{A_{D3,c} / N_{D3}} \qquad \text{Eq. 5.7}$$

for a cold-drawn sample, where X_{rig} is the bulk mass-fraction of 'rigid' components that $T_{1,C}$ relax after 10 s. X_{rig} is defined by

$$X_{rig} = X_c + X_{i,long} \qquad \text{Eq. 5.8}$$

where $X_{i,long}$ is the bulk fraction of the long-$T_{1,C}$ intermediate component. If the ratio of areas between the residual spectrum and the 10-s $T_{1,C}$ filtered spectrum is R_{long}, then the mass-fraction of the long-$T_{1,C}$ intermediate component is computed by

$$X_{i,long} = R_{long} \cdot X_{rig} \qquad \text{Eq. 5.9}$$

The crystallinity X_c can then be calculated from Equation 5.8.

A similar scenario exists for the very mobile (short $T_{1,C}$) components in the cold-drawn HDPE morphology. Inspection of the 1-s ^{13}C DP spectrum in Figure 5.7(a) shows a peak at ~33 ppm corresponding to very mobile, all-trans resonances of disordered packing. Analysis of the 2D WISE spectra acquired for the drawn sample (Figure 4.5) showed the amplitude of mobility for these very mobile trans segments to be significantly less than chain segments in the amorphous domains, even though the fast $T_{1,C}$ relaxation of both components indicated comparable mobility. It was suggested in Chapter 4 that these short-$T_{1,C}$ all-trans resonances originate from highly mobile portions of the intermediate component. From the spectra in Chapter 4 and those analyzed in Section 5.3.1 above, it was apparent that the intermediate component in the cold-drawn microstructure showed a distribution of $T_{1,C}$ relaxation behavior, no doubt a result of strain-induced disordering. Hence, these short-$T_{1,C}$ intermediate signals should be quantified separate from the amorphous signals.

The dipolar filter discussed above and used in acquiring the spectra of Figure 5.5 was applied in the separation of the amorphous and short-$T_{1,C}$ intermediate signals. A dipolar filtered CP/MAS spectrum of the sample drawn to 945% strain is shown in Figure 5.12. In comparison to the 1-s DP spectrum in Figure 5.7(a), the fraction of signals from the gauche-containing amorphous phase is much greater. However, an all-trans peak at ~33 ppm still appears in the dipolar filtered spectrum, as noted in the analysis of Figure 5.5 above, though much smaller than in the 1-s DP spectrum. These resonances come from stretched chains that show mobility on the order of gauche-conforming chains. Recall that from Figure 5.5, they were observed to increase in

content with drawing strain. Because their contribution to the whole material bulk is small, they will be counted in the amorphous content.

Selection of the short-$T_{1,C}$ intermediate signals is also based on a scaling procedure. For the procedure, a spectrum representative of only those signals that are sufficiently relaxed by 1 s is required. This spectrum is obtained by taking the unscaled difference between the 1-ms $T_{1,C}$ filtered 1-s DP spectrum and the 1-s $T_{1,C}$ filtered 1-s DP spectrum (Figure 5.8, a). The resulting difference is a 'corrected' 1-s DP spectrum, as shown in Figure 5.12. The dipolar filtered CP spectrum is then scaled so that the residual between the corrected 1-s DP spectrum and the dipolar filtered CP spectrum shows a reasonable all-trans line shape with few gauche-conformers (Figure 5.12). The residual spectrum contains signals from the short-$T_{1,C}$ intermediate component. The area ratio between the residual spectrum and the corrected 1-s DP spectrum quantifies that portion of signals relaxed by 1 s that are from the short-$T_{1,C}$ intermediate component.

Hence, for cold-drawn samples of the HDPE, Equation 5.4 is replaced by

$$X_{mob} = \frac{A_{D1,c} / N_{D1}}{A_{D3,c} / N_{D3}}, \qquad \text{Eq. 5.10}$$

where X_{mob} is the bulk mass-fraction of 'mobile' components that $T_{1,C}$ relax by 1 s. Therefore, X_{mob} is given by

$$X_{mob} = X_a + X_{i,short}, \qquad \text{Eq. 5.11}$$

where $X_{i,short}$ is the bulk fraction of the short-$T_{1,C}$ intermediate component. If the ratio of areas between the short-$T_{1,C}$ residual spectrum and the corrected 1-s DP spectrum is R_{short}, then the mass-fraction short-$T_{1,C}$ intermediate component is computed by

$$X_{i,short} = R_{short} \cdot X_{mob} . \qquad \text{Eq. 5.12}$$

The amorphous fraction X_a can then be calculated from Equation 5.11.

The bulk fraction $X_{i,mid}$ of the intermediate component with 'mid-range' $T_{1,C}$ relaxation behavior is defined by

$$X_{i,mid} = 1 - X_{mob} - X_{rig} . \qquad \text{Eq. 5.13}$$

As a result, the total intermediate component mass-fraction X_i in a drawn sample is given by

$$X_i = X_{i,short} + X_{i,mid} + X_{i,long} , \qquad \text{Eq. 5.14}$$

which replaces Equation 5.6.

5.3.2.4 Component Composition during Cold Drawing

Now that suitable procedures for analyzing the component composition in both undrawn and cold-drawn HDPE samples have been established, changes in the component fractions during the cold-drawing process can be measured. The mass-

percentages of the various morphological components identified in the HDPE were quantified at the selected levels of drawing strain discussed in Chapter 3. Results are shown graphically in Figure 5.13. The mass ratio of monoclinic to orthorhombic crystalline material was determined according to VanderHart and Khoury[12] using a 10-s $CP/T_{1,C}$ filtered spectrum for undrawn sample and a 60-s $CP/T_{1,C}$ filtered spectrum for cold-drawn samples.

A dramatic change is observed after necking. Comparing the undrawn sample with the sample drawn to 98% strain, the crystallinity is found to decrease by 25%. At the same time, the total intermediate contribution grows by about 240%, a tremendous increase. The amorphous content diminishes approximately 25%, consistent with the reduction in the amorphous signal intensities in Figure 5.2 and Figure 5.4. Overall, the newly formed and stabilized neck shows an increased population of all-trans chain segments; however, a large portion of these chains have disordered packing. Transformations in the crystalline structure are also seen with necking. The ratio of monoclinic to orthorhombic crystalline material rises by almost 300%, which concurs with the qualitative observations made from Figure 5.2 and Figure 5.3. The increased presence of the monoclinic crystalline form in freshly-necked polyethylene agrees with numerous studies in the literature.[5,12,20,28-33]

During propagation of the stabilized neck (drawing stage 4, as outlined in Chapter 3), the component composition changes little, except for the monoclinic to orthorhombic crystal ratio, which slightly decreases. However, during strain hardening (stage 5) variations in the component composition again take place with increasing strain, but more gradual compared to necking. The overall crystallinity increases about 8%,

with a corresponding reduction in the monoclinic to orthorhombic crystal ratio. The monoclinic crystal content diminishes by almost 50% from just after necking to just before fracture. A decrease in the intensity of WAXD reflections from the monoclinic crystals during neck drawing has been observed in previous studies.[20,31,32] The intermediate fraction increases only slightly during strain hardening. Therefore, the rise in crystallinity occurs primarily at the expense of the amorphous domains, which are reduced in mass by over 30%.

The bulk fractions $X_{i,mid}$, $X_{i,long}$, and $X_{i,short}$ of the 'mid-range' $T_{1,C}$, long-$T_{1,C}$, and short-$T_{1,C}$ intermediate component portions, respectively, are plotted versus total drawing strain in Figure 5.14. The mid-range $T_{1,C}$ intermediate component, representing those parts of the intermediate material that $T_{1,C}$ relaxes between 1 s and 10 s (Figure 5.6), is the largest portion (> 15% of the total bulk). It remains fairly constant within the measurement error after necking. The short-$T_{1,C}$ intermediate fraction has the smallest contribution (< 7% of the total bulk), and its fraction slightly decreases during strain hardening. This reduction in the short-$T_{1,C}$ intermediate component is interesting, when considered in conjunction with the spectra of Figure 5.5. In that spectral series, the very mobile all-trans chains which generated signals surviving the dipolar filter were qualitatively noted to increase in amount with drawing strain. In Section 5.3.2.3, these chains were included in the amorphous phase contribution to the material composition. Apparently, during neck drawing some of the gauche-containing segments of molecules in the amorphous domain or at the amorphous-intermediate component interface are aligned with the draw direction into all-trans conformations. Also, chains in the short-$T_{1,C}$ intermediate component may achieve greater mobility, possibly at the amorphous-

intermediate component interface. The long-$T_{1,C}$ intermediate material shows an increase from about 7% to 12.5% during strain hardening, which was reflected in the observed line width changes in Figure 5.2 and Figure 5.3. Along with the rise in the total crystallinity and decrease in the amorphous domains and monoclinic crystals, the growth of the rigid intermediate component and the proliferation of very mobile all-trans chains indicate an overall ordering in the chain packing and orientation as strain hardening proceeds.

5.4 Discussion and Summary

Several findings have been made with solid-state NMR in the analysis and quantification of the component microstructure during the cold drawing of HDPE. By far, the most important of these findings was in the quantification of the intermediate component in the cold-drawn HDPE. The bulk fraction of the intermediate component was measured by NMR to be as high as 35% in the cold-drawn and necked material, greater than the contributions from the amorphous domains and monoclinic crystals. The intermediate component should definitely be regarded in microstructural modeling of cold-drawn HDPE due to its distinct molecular properties as characterized in Chapter 4.

The roles of the intermediate component and other phases in the HDPE morphology during cold drawing have also been examined. A dramatic surge in the intermediate component content was observed just after necking (a 240% increase in mass content), along with a doubling of the monoclinic crystals. At the same time, decreases of about 25% in the total crystalline and amorphous phases were seen. The mass-percent crystallinity drops from 62% to 46%. Overall, the fraction of the material

bulk with all-trans chains grew about 10%, no doubt related to the highly oriented fibrillar texture (WAXD patterns in Figure 3.6) and increased draw ratio (Figure 3.3 and Figure 3.4) observed in the neck. Using Raman scattering, Rodríguez-Cabello et al.[34] noted a similar increase in the content of all-trans or 'extended chain' segments in a cold-drawn HDPE of similar density. Other studies using Raman scattering[5,35] have also detected decreases in the well-ordered crystalline material in cold-drawn HDPE. One of these studies[5] quantified a drop in the orthorhombic crystallinity upon necking to be 33%, which is similar to the result found here (Figure 5.13, about 37%).

The reduction in the well-ordered crystalline domains and the simultaneous increase in the content of poorly packed all-trans chains indicate a significant disordering of the crystalline structure during necking. Because these NMR experiments were not conducted *in-situ*, statements concerning the occurrence of partial melting and recrystallization in the yielding process cannot be made. But the result of the necking process can be described. A "high chain mobilisation" of crystalline chains similar to the concept suggested by Peterlin[36] does take place, as found in the large content of the intermediate component after necking. However, in Peterlin's hypothesis the mobilized chains were a temporary state that reverted back to the crystalline form once the neck had stabilized. From the results of this chapter, it is seen that the intermediate component is stabile throughout the neck-drawing process. Also, the static ^{13}C NMR experiments in Chapter 4 clearly showed the intermediate component not to be a well-aligned "pseudomelt" or liquid-crystal like microstructure, but rather a solid component of all-trans chains packed in a disordered fashion, but generally aligned with the draw direction. The exact mechanism of this 'chain mobilization' is unknown, but obviously portions of

the crystallites disorder into chains of higher mobility to allow for the massive rearrangements that occur during necking.

A general microstructural re-ordering takes place during neck propagation (drawing stage 4, as outlined in Chapter 3) and strain hardening (stage 5). A rise in total crystallinity of about 8% was seen, with a corresponding decrease in the monoclinic crystals (50%) and amorphous domains (30%). The total intermediate component fraction changed little, but the more rigid portions of the intermediate material did increase slightly, as did the very mobile all-trans chains observed in Figure 5.5. The growth of components with rigid, all-trans segments aligned with the draw direction during strain hardening is indicative of a 'strain-induced crystallization' process. This would in part explain the strain-hardening behavior observed in the plastic 'flow curve' of Figure 3.5 and the increased draw ratio (Figure 3.3 and Figure 3.4). However, the sliding of fibrils and microfibrils as proposed by Peterlin[36-38] may still take place simultaneously.

5.5 Tables and Figures

Table 5.1: Comparison of morphological component quantities in the undrawn, melt-crystallized HDPE material obtained with different analytical techniques. The experimental methods used with each technique are described in the text.

Analytical Technique	**Crystalline (Mass %)**	**Intermediate (Mass %)**	**Amorphous (Mass %)**
Solid-state NMR	62 ± 3	10 ± 3	28 ± 3
Raman scattering	62 ± 2	8 ± 3	30 ± 3
DSC	64 ± 2	—	—

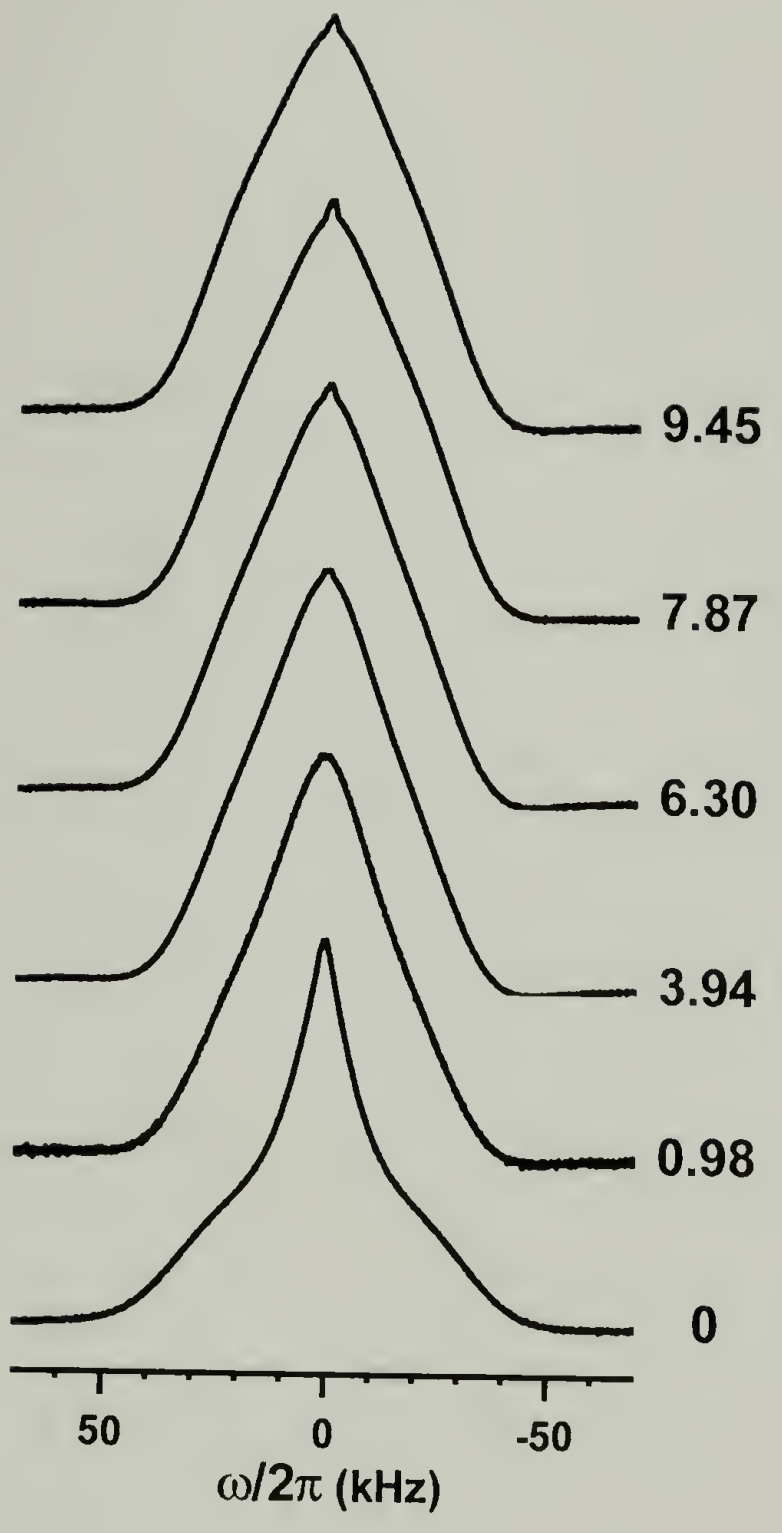

Figure 5.1: ^{1}H wideline spectra of the HDPE at different drawing strains, as indicated. The very small, narrow peak in the cold-drawn sample spectra has been identified by Hu and Schmidt-Rohr[16] with a highly mobile, second amorphous phase.

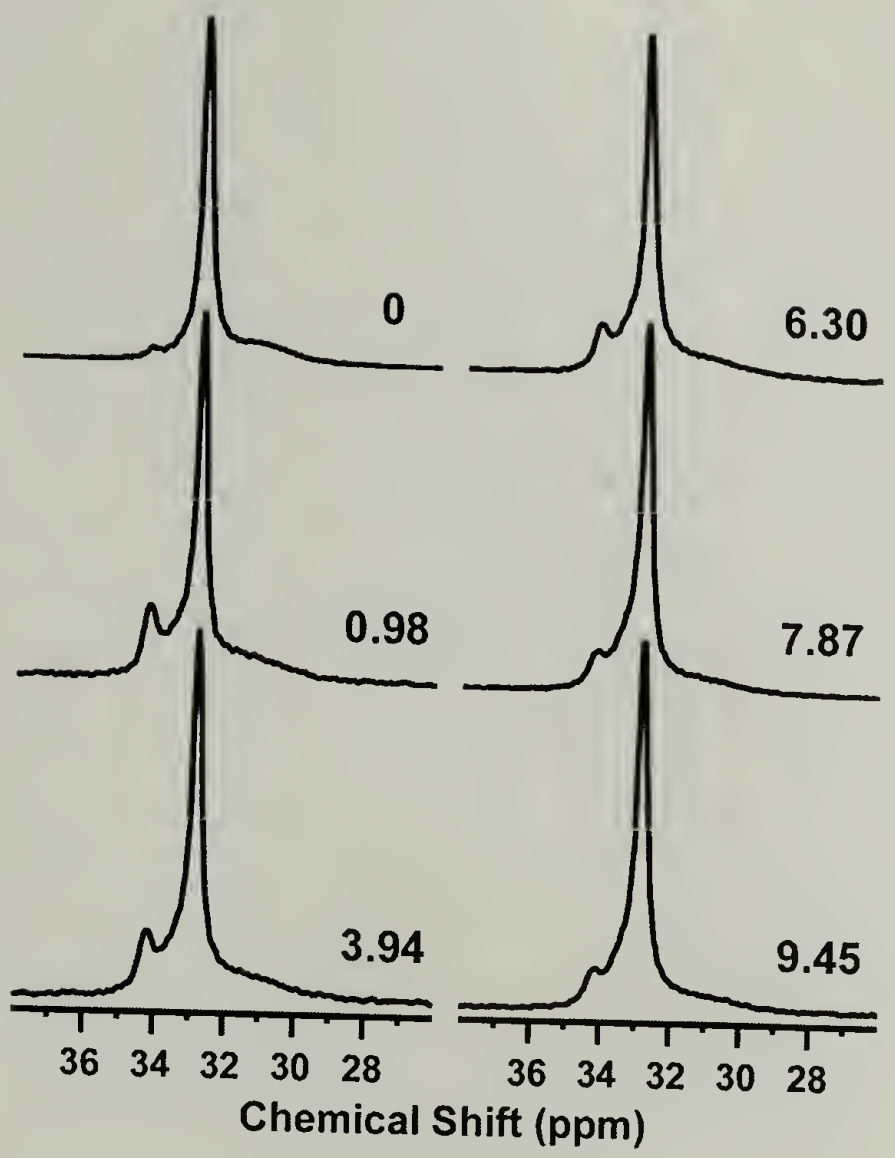

Figure 5.2: ^{13}C CP/MAS spectra of the HDPE at different drawing strains, as indicated. Note the increase in line width of the orthorhombic crystal resonance (32.8 ppm) upon necking and subsequent deformation.

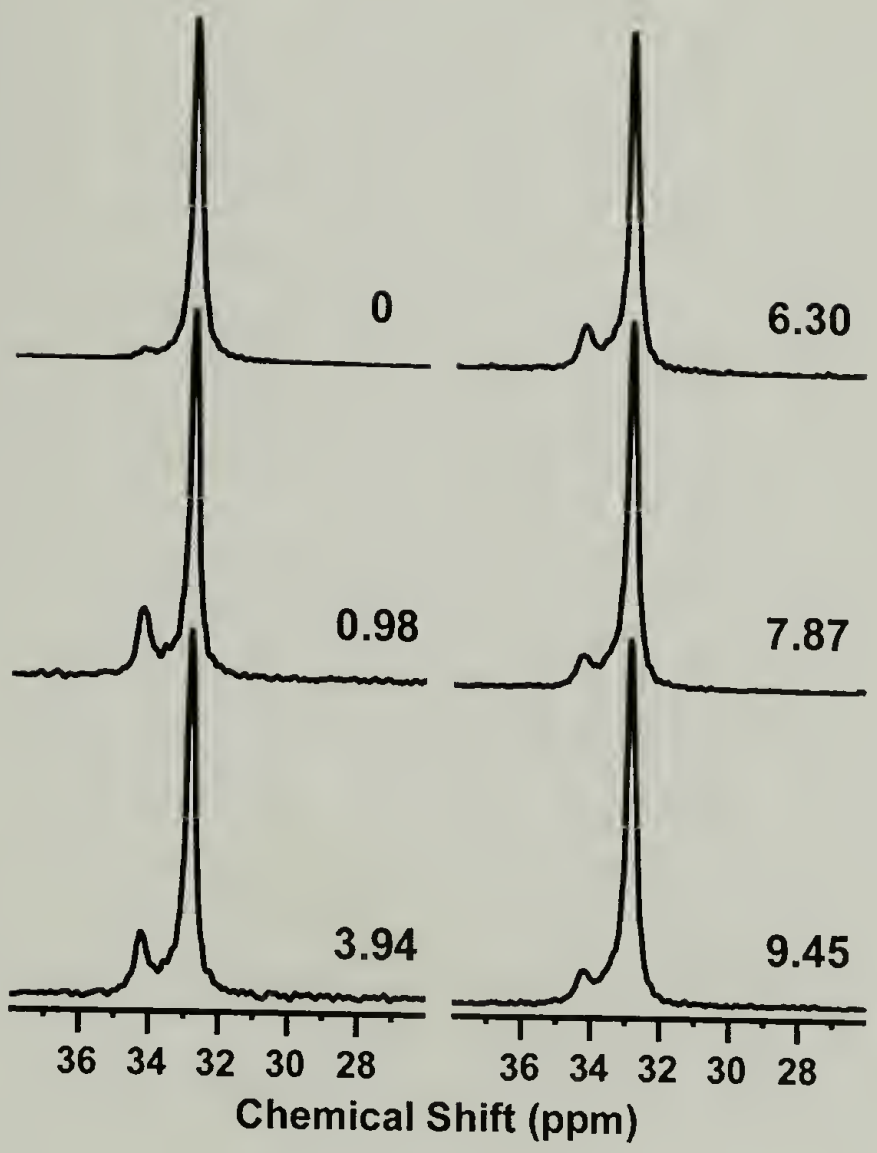

Figure 5.3: ^{13}C CP/MAS 10-s $T_{1,C}$ filtered spectra (rigid components) of the HDPE at different drawing strains, as indicated. Again, note the increased line width of the orthorhombic crystal resonance with necking and drawing.

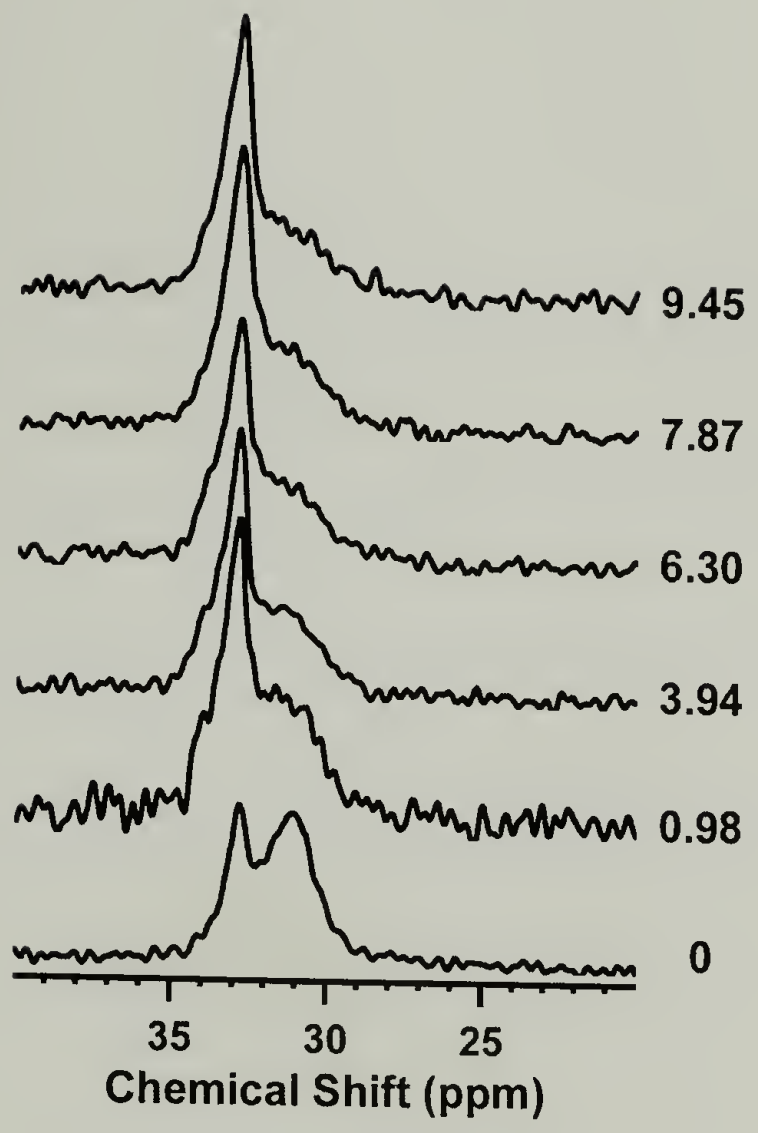

Figure 5.4: ^{13}C DP/MAS spectra with 10-s recycle delay (mobile components) of the HDPE at different drawing strains, as indicated. The spectra have been presented so that their integrated intensities (spectral areas) reflect the relative amounts of mobile components in the material bulk that have $T_{1,C}$ relaxed by 10 s, as determined in Section 5.3.2.

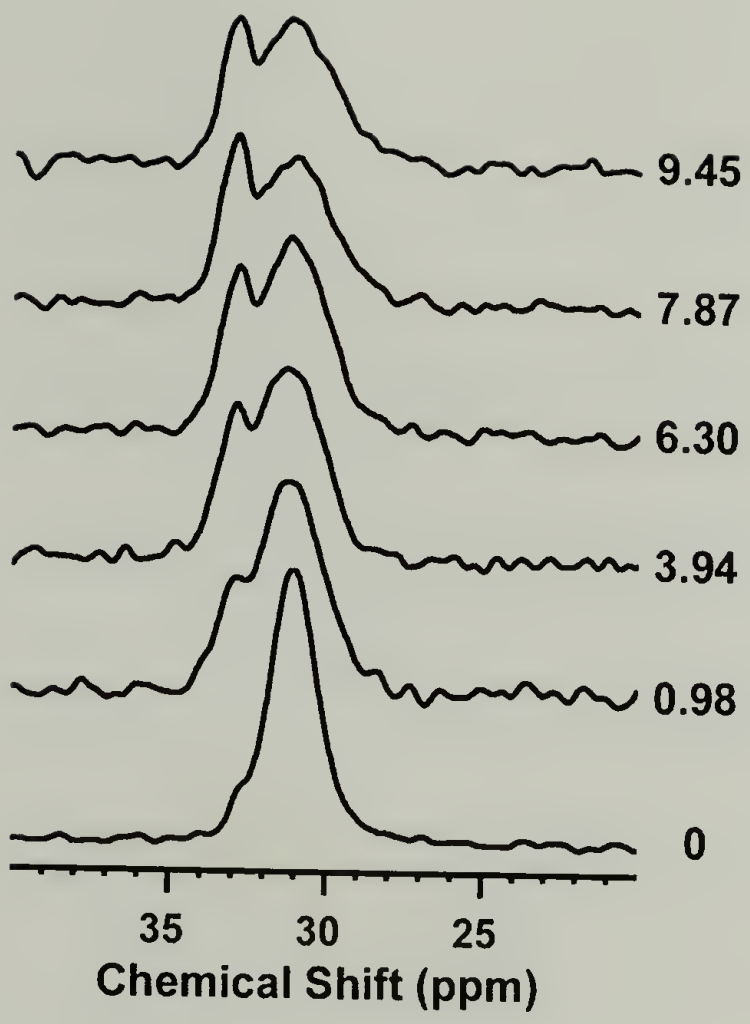

Figure 5.5: ^{13}C CP/MAS spectra with a dipolar filter before CP (very mobile components) of the HDPE at different drawing strains, as indicated. The spectra have been presented so that their integrated intensities (spectral areas) reflect the relative amounts of very mobile components in the material bulk, as determined in Section 5.3.2.

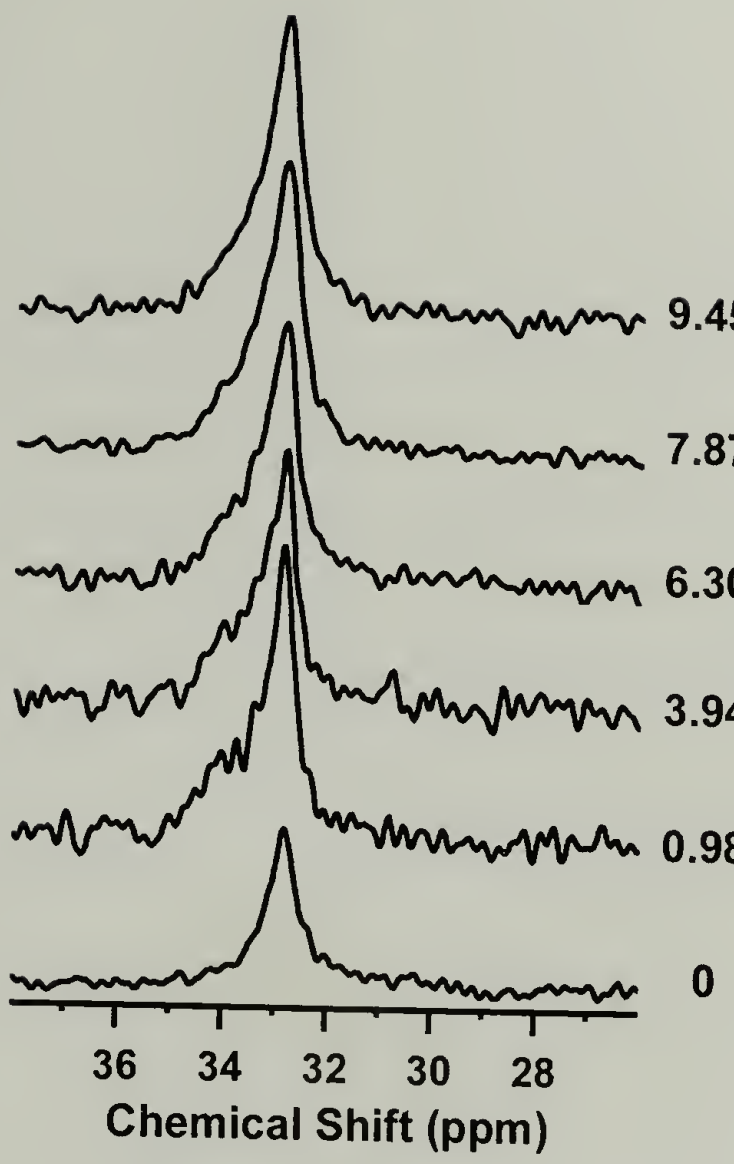

Figure 5.6: Difference spectra between ^{13}C CP/MAS 1-s and 10-s $T_{1,C}$ filtered spectra (intermediate component) of the HDPE at different drawing strains, as indicated. The spectra have been presented so that their integrated intensities (spectral areas) reflect the relative amounts of the 'mid-range $T_{1,C}$' intermediate component in the material bulk, as determined in Section 5.3.2.

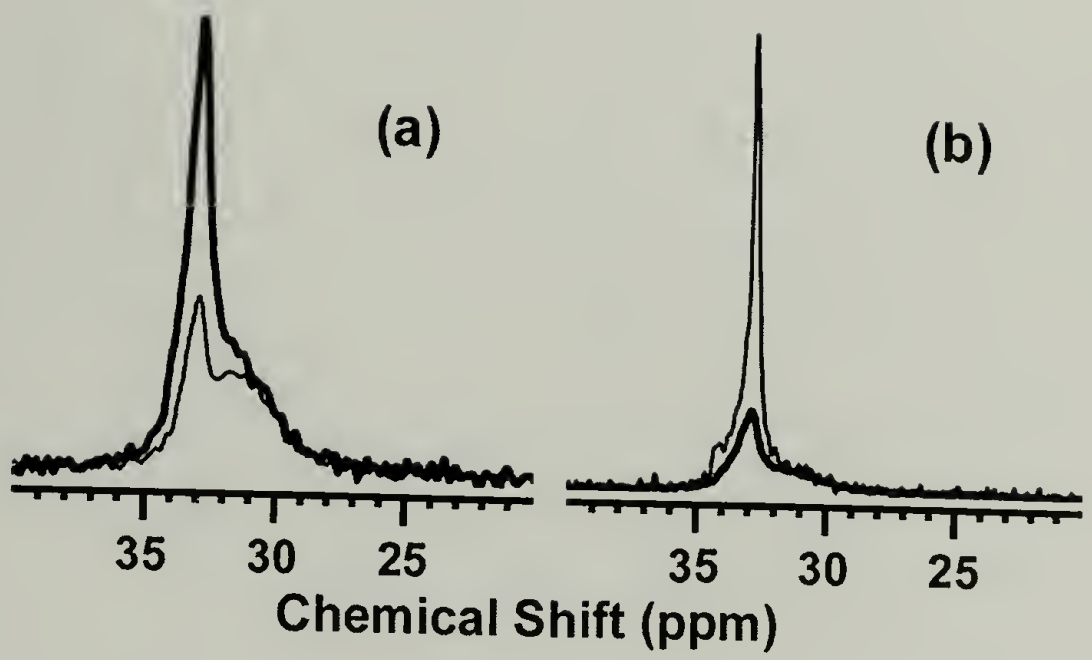

Figure 5.7: Demonstration of the quantitative ^{13}C DP/MAS procedure introduced by Hu and Schmidt-Rohr[16] to measure component composition in polyethylene. Spectra are of the HDPE sample cold drawn to 945% strain. Three DP spectra acquired with different recycle delays and numbers of scans are shown in two sets: (a) 1 s (1024 scans) and 10 s (512 scans); (b) 10 s (512 scans) and 2000 s (32 scans). For direct comparison, spectra are scaled to compensate for the different number of scans. The 10-s spectrum is indicated by a thick line in both sets. The transient heteronuclear NOE is suppressed in all DP experiments used in the quantitative procedure.

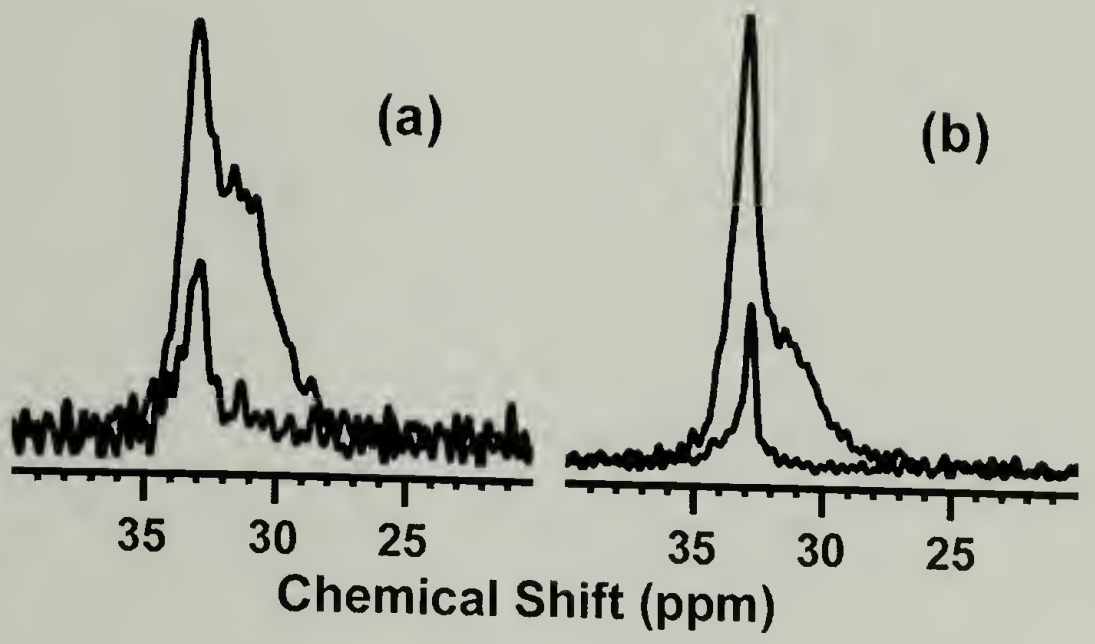

Figure 5.8: MAS spectra of the sample drawn to 945% strain acquired with ^{13}C direct polarization (DP) followed by a $T_{1,C}$ filter. The spectra of each pair presented were measured with the same number of scans and the same recycle delay. Recycle delays employed for the spectral pairs shown were (a) 1 s and (b) 10 s. The spectrum with the largest intensity in each pair was obtained with a very short $T_{1,C}$ filter time (1 ms), while the spectrum of smaller area was acquired with a $T_{1,C}$ filter equal to the recycle delay. These pairs of spectra are used to correct for partially relaxed ^{13}C signals in DP experiments, as described in the text.

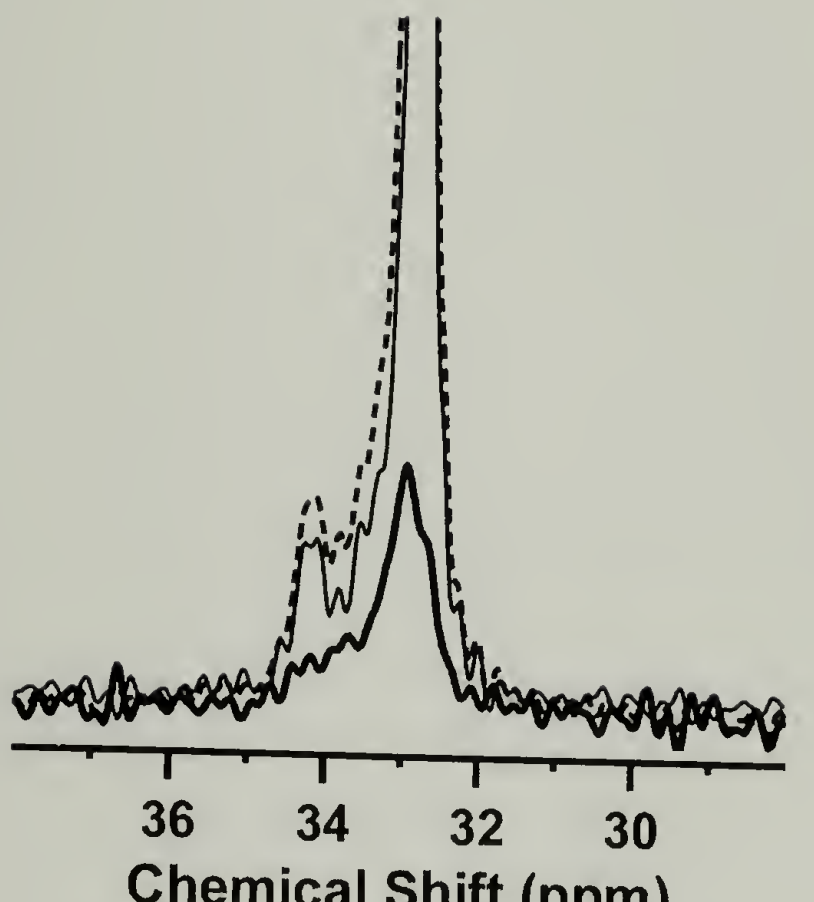

Figure 5.9: Derivation of pure non-crystalline ^{13}C signals that relax after a specific time t_z using a scaling method. Spectra shown are of the HDPE sample cold drawn to 945% strain. A pair of ^{13}C CP/MAS $T_{1,C}$ filtered spectra were acquired with the same number of scans, one with a filter delay t_z (dashed spectrum, t_z = 10 s in this case) and the other representing the true crystalline line shape (thin solid spectrum, 60-s $T_{1,C}$ filter, shown scaled in the figure). The crystal spectrum was then scaled manually to the intensity given in the figure to yield a residual (thick solid spectrum) of reasonable line shape where no apparent traces of underestimation or overestimation of the scaling factor are seen. The area ratio of the residual and the 10-s $T_{1,C}$ filtered spectrum is used to determine the long-$T_{1,C}$ intermediate contribution. Uncertainties in the area of the residual due to the scaling method are indicated in Figure 5.10 and Figure 5.11.

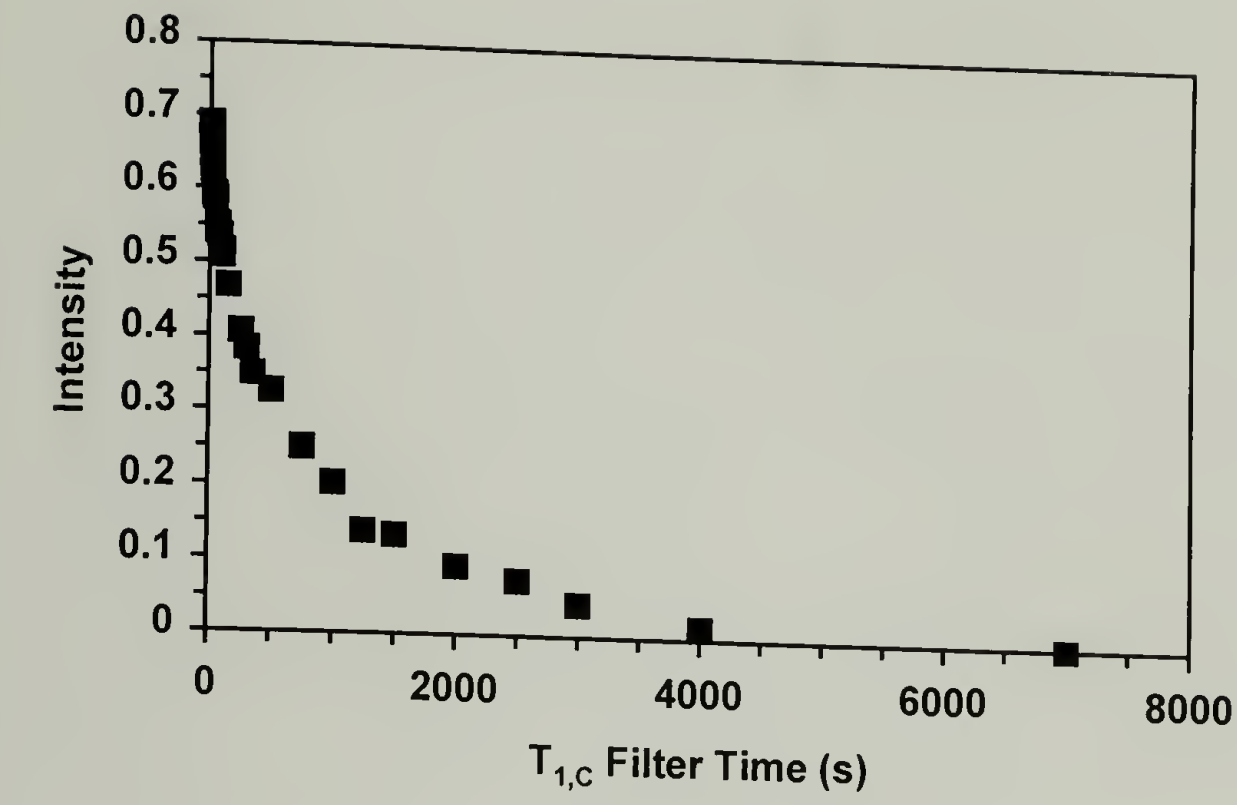

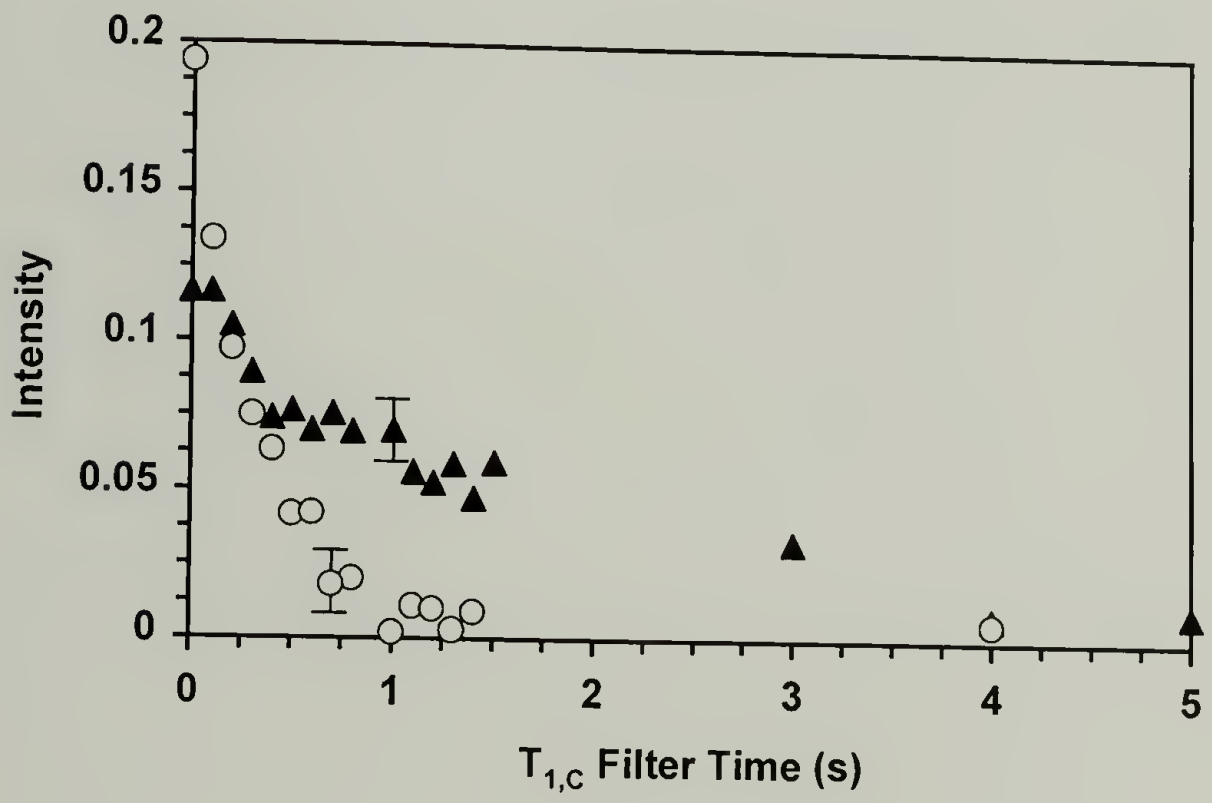

Figure 5.10: ^{13}C T_1 relaxation curves (or 'Torchia' curves) of the morphological components in the undrawn HDPE. Crystalline (■); intermediate (▲); amorphous (○). Intensities are spectral areas relative to the original 1-ms CP/$T_{1,C}$ filtered spectrum of all components. The amorphous fraction is underrepresented to its true amount due to differences in CP efficiencies. Error bars indicate uncertainties introduced by the scaling method of Figure 5.9 and are applicable to all data points before a filter time of 6 s.

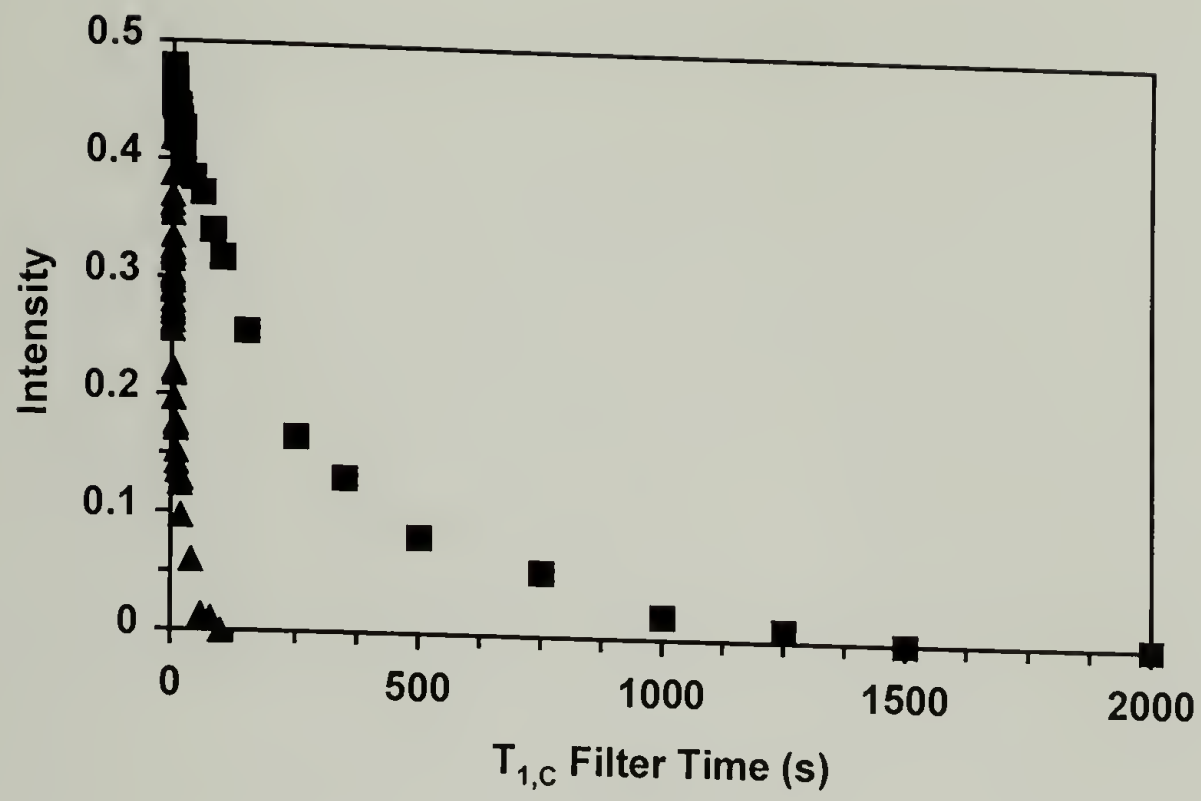

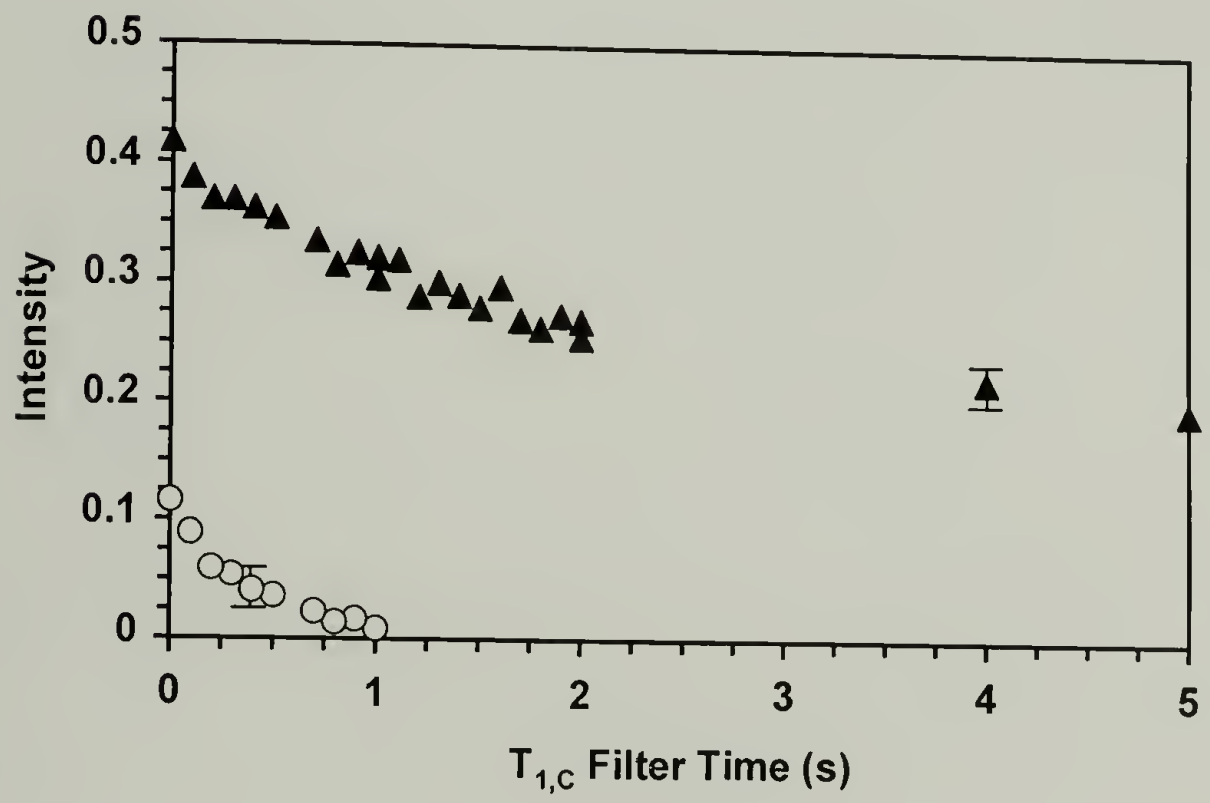

Figure 5.11: ^{13}C T_1 relaxation curves (or 'Torchia' curves) of the morphological components in the HDPE sample cold drawn to 945% strain. Crystalline (■); intermediate (▲); amorphous (○). Intensities are spectral areas relative to the original 1-ms CP/$T_{1,C}$ filtered spectrum of all components. The amorphous fraction is underrepresented to its true amount due to differences in CP efficiencies. Error bars indicate uncertainties introduced by the scaling method of Figure 5.9 and are applicable to all data points before a filter time of 100 s.

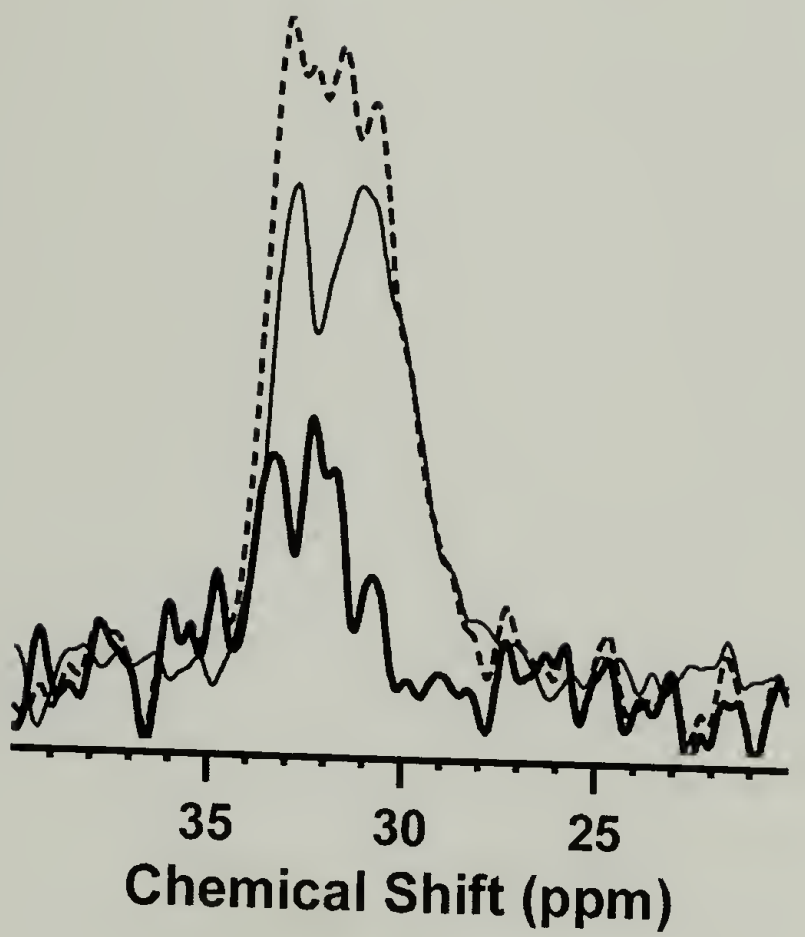

Figure 5.12: Manual selection of the short-$T_{1,C}$ intermediate signals from the 1-s DP spectrum. Spectra shown are of the HDPE sample drawn to 945% strain. The 'corrected' 1-s DP spectrum (dashed line) only contains signals sufficiently relaxed by 1 s; it is obtained as the unscaled difference of the spectra in Figure 5.8(a). The dipolar filtered CP/MAS spectrum is indicated by the thin solid line. The dipolar-filtered spectrum was scaled so that the residual (thick solid spectrum) showed a reasonable line shape. The area of this residual relative to the corrected 1-s DP spectrum gives the fraction of the intermediate component $T_{1,C}$ relaxed by 1 s, i.e. the short-$T_{1,C}$ portion.

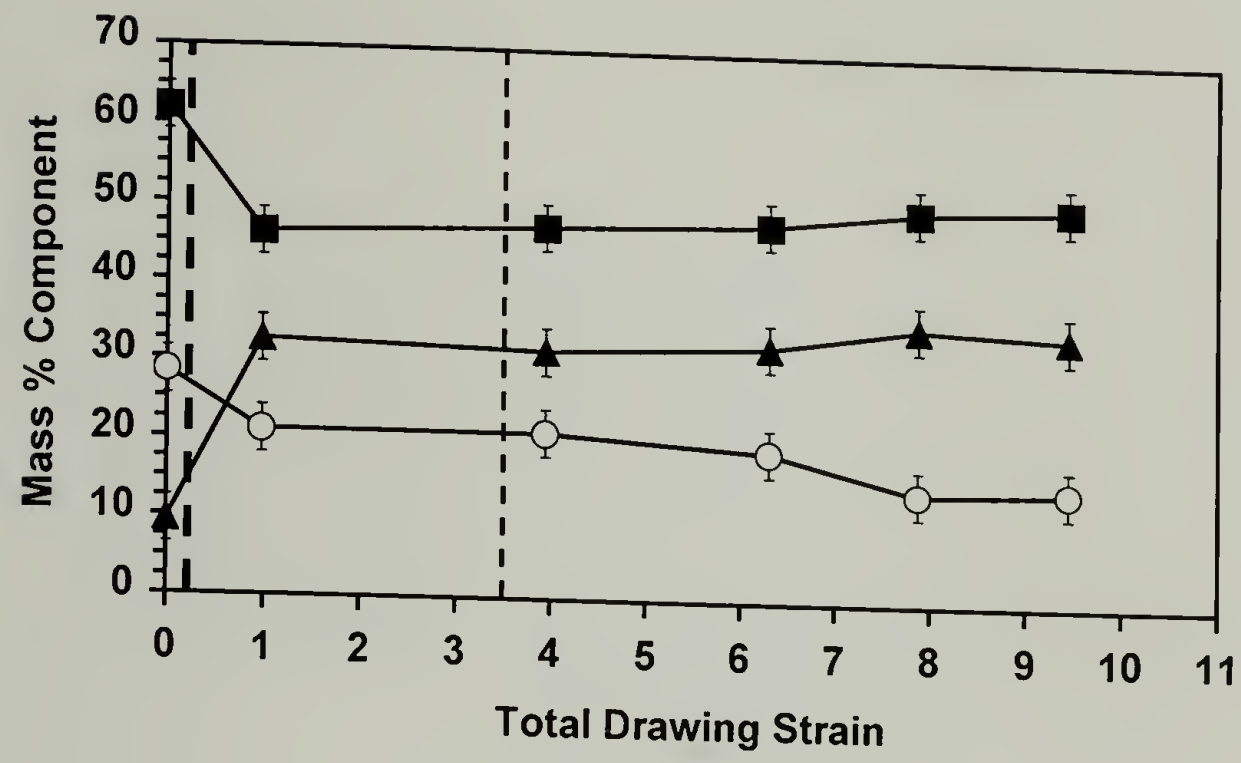

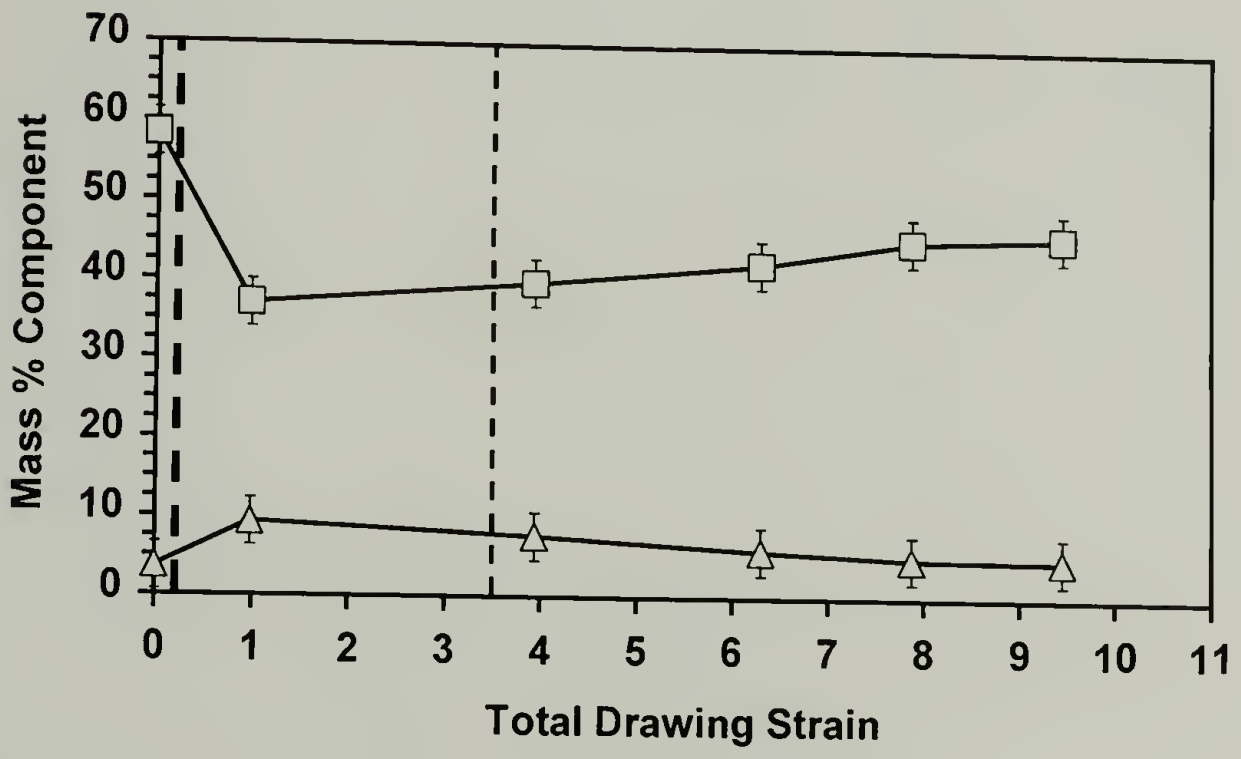

Figure 5.13: Changes in the morphological component composition of the HDPE (DOW HD-12450N) subjected to uniaxial cold drawing (ambient conditions; 0.0013 s^{-1} strain rate). The macroscopic cold-drawing response of the HDPE was described in Chapter 3. Mass-percentages of the total material bulk are shown for the total crystalline (■); total intermediate (▲); amorphous (○); orthorhombic crystalline (□); and monoclinic crystalline (Δ) components. The thick vertical dashed line indicates the total drawing strain at which the neck forms; the thin vertical dashed line marks the end of neck propagation (stage 4) and the onset of strain hardening (stage 5).

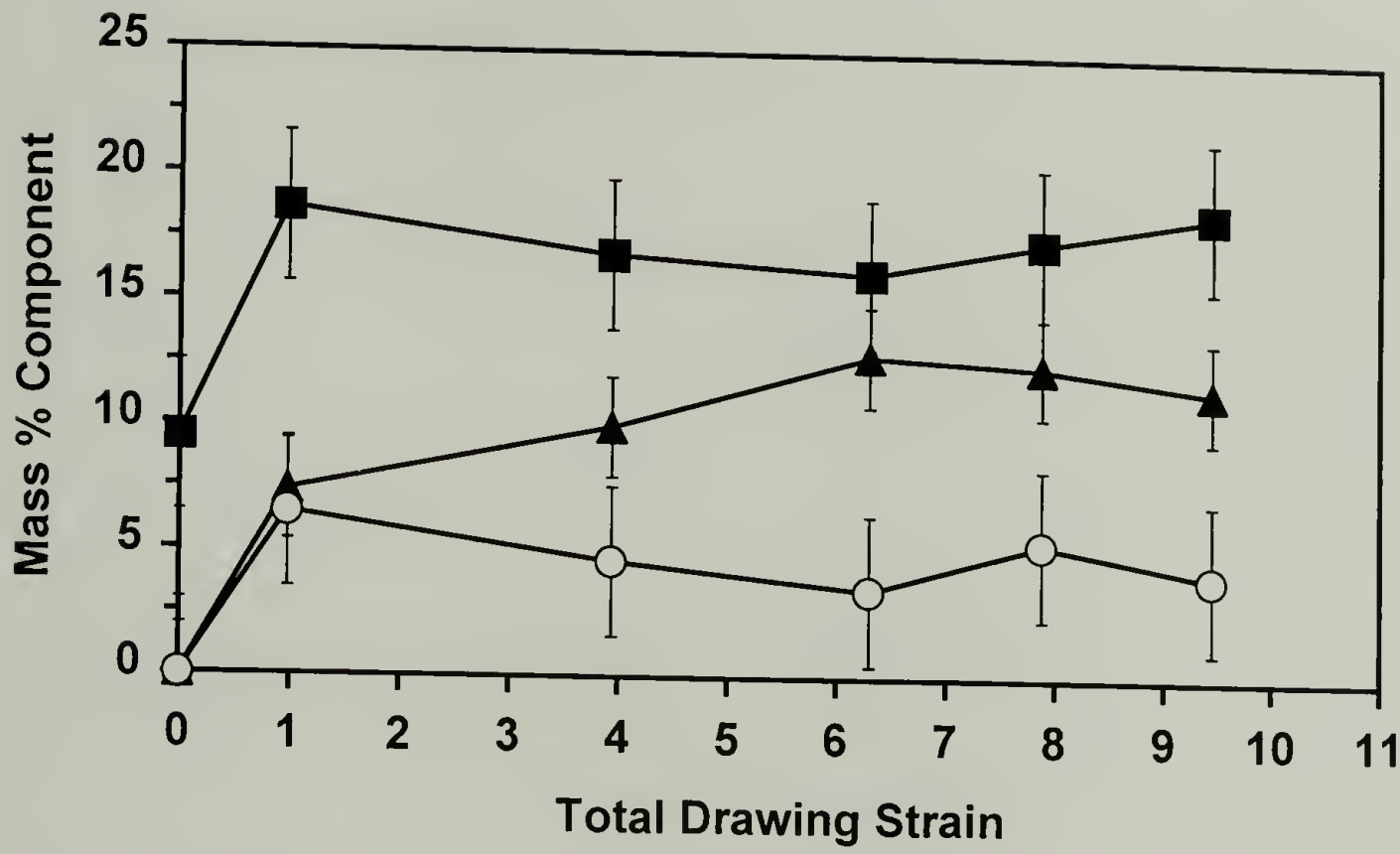

Figure 5.14: Changes with drawing strain in the bulk fractions of the intermediate component constituents, as defined in the text. 'Mid-range $T_{1,C}$' intermediate (■); 'long-$T_{1,C}$' intermediate (▲); 'short-$T_{1,C}$' intermediate (○).

5.6 References

1. Mandelkern, L.; Peacock, A.J. *Studies in Physical and Theoretical Chemistry*, 1988. **54**: p. 201-227.

2. Popli, R.; Mandelkern, L. *Journal of Polymer Science: Part B: Polymer Physics*, 1987. **25**: p. 441-483.

3. Alamo, R.G.; Mandelkern, L. *Macromolecules*, 1989. **22**(3): p. 1273-1277.

4. Mandelkern, L. *Polymer Journal*, 1985. **17**(1): p. 337-350.

5. Lagaron, J.M.; Dixon, N.M.; Reed, W.; Pastor, J.M.; Kip, B.J. *Polymer*, 1999. **40**: p. 2569-2586.

6. Saraf, A.W.; Desai, P.; Abhiraman, A.S. *Journal of Applied Polymer Science: Applied Polymer Symposium*, 1991. **47**: p. 67-86.

7. Eckman, R.R.; Henrichs, P.M.; Peacock, A.J. *Macromolecules*, 1997. **30**(8): p. 2474-2481.

8. Kitamaru, R.; Horii, F. *Advances in Polymer Science*, 1978. **26**: p. 138-178.

9. Smith, J.B.; Manuel, A.J.; Ward, I.M. *Polymer*, 1975. **16**: p. 57-65.

10. Axelson, D.E.; Mandelkern, L.; Popli, R.; Mathieu, P. *Journal of Polymer Science: Polymer Physics Edition*, 1983. **21**: p. 2319-2335.

11. Schmidt-Rohr, K.; Spiess, H.W. *Macromolecules*, 1991. **24**(19): p. 5288-5293.

12. VanderHart, D.L.; Khoury, F. *Polymer*, 1984. **25**: p. 1589-1599.

13. Cheng, J.; Fone, M.; Reddy, V.N.; Schwartz, K.B.; Fisher, H.B.; Wunderlich, B. *Journal of Polymer Science: Part B: Polymer Physics*, 1994. **32**(2683-2693).

14. Kitamaru, R.; Horii, F.; Murayama, K. *Macromolecules*, 1986. **19**(3): p. 636-643.

15. Kuwabara, K.; Kaji, H.; Horii, F.; Bassett, D.C.; Olley, R.H. *Macromolecules*, 1997. **30**(24): p. 7516-7521.

16. Hu, W.-G.; Schmidt-Rohr, K. *Polymer*, 2000. **41**: p. 2979-2987.

17. Wunderlich, B. *Macromolecular Physics*. Vol. 1. 1973, New York: Academic Press.

18. Strobl, G.R.; Hagedorn, W. *Journal of Polymer Science: Polymer Physics Edition*, 1978. **16**: p. 1181-1193.

19. Rull, F.; Prieto, A.C.; Casado, J.M.; Sobron, F.; Edwards, H.G.M. *Journal of Raman Spectroscopy*, 1993. **24**: p. 545-550.

20. Steidl, J.; Pelzbauer, Z. *Journal of Polymer Science: Part C*, 1972. **38**: p. 345-356.

21. Zhurkov, S.N.; Kuksenko, V.S. *International Journal of Fracture*, 1975. **11**(4): p. 629-639.

22. Egger, N.; Schmidt-Rohr, K.; Blümich, B.; Domke, W.-D.; Stapp, B. *Journal of Applied Polymer Science*, 1992. **44**: p. 289-295.

23. Axelson, D.E. *Carbon-13 Solid-State NMR of Semicrystalline Polymers*, in *High Resolution NMR Spectroscopy of Synthetic Polymers in Bulk*, Komoroski, R.A., Editor. 1986, VCH Publishers, Inc.: Deerfield Beach, Florida, USA. p. 157-226.

24. Torchia, D.A. *Journal of Magnetic Resonance*, 1978. **30**: p. 613-616.

25. Kaji, A.; Yamanaka, A.; Murano, M. *Polymer Journal*, 1990. **22**(10): p. 893-900.

26. Kaji, A.; Ohta, Y.; Yasuda, H.; Murano, M. *Polymer Journal*, 1990. **22**(6): p. 455-462.

27. Earl, W.L.; VanderHart, D.L. *Macromolecules*, 1979. **12**(4): p. 762-767.

28. Hiss, R.; Hobeika, S.; Lynn, C.; Strobl, G. *Macromolecules*, 1999. **32**(13): p. 4390-4403.

29. Hughes, D.J.; Mahendrasingam, A.; Oatway, W.B.; Heeley, E.L.; Martin, C.; Fuller, W. *Polymer*, 1997. **38**(26): p. 6427-6430.

30. Brooks, N.W.J.; Unwin, A.P.; Duckett, R.A.; Ward, I.M. *Journal of Macromolecular Science -- Physics*, 1995. **B34**(1&2): p. 29-54.

31. Butler, M.F.; Donald, A.M.; Bras, W.; Mant, G.R.; Derbyshire, G.E.; Ryan, A.J. *Macromolecules*, 1995. **28**(19): p. 6383-6393.

32. Vickers, M.E.; Fischer, H. *Polymer*, 1995. **36**(13): p. 2667-2670.

33. Seto, T.; Hara, T.; Tanaka, K. *Japanese Journal of Applied Physics*, 1968. **7**(1): p. 31-42.

34. Rodríguez-Cabello, J.C.; Martín-Monge, J.; Lagarón, J.M.; Pastor, J.M. *Macromolecular Chemistry and Physics*, 1998. **199**(12): p. 2767-2776.

35. Lagarón, J.M.; López-Quintana, S.; Rodriguez-Cabello, J.C.; Merino, J.C.; Pastor, J.M. *Polymer*, 2000. **41**: p. 2999-3010.

36. Peterlin, A. *Journal of Materials Science*, 1971. **6**: p. 490-508.

37. Peterlin, A. *Colloid & Polymer Science*, 1987. **265**(5): p. 357-382.

38. Peterlin, A. *Colloid and Polymer Science*, 1975. **253**(10): p. 809-823.

CHAPTER 6

MODELING THE MICROSTRUCTURE OF COLD-DRAWN HDPE WITH SOLID-STATE NMR

6.1 Introduction

In previous chapters, major morphological components in the microstructure of cold-drawn high-density polyethylene (HDPE) have been identified and distinguished. Their roles during the cold-drawing process have been investigated. An intermediate component of considerable bulk (up to 35 mass-% in the necked material) has been detected, and its importance discussed. However, the microstructural form (e.g. interfacial matter, tie molecules) of this intermediate component has not been addressed. Understanding its nature and its proximity to other microstructural units is of great interest in building an accurate and more comprehensive picture of the morphology of cold-drawn HDPE.

Peterlin[1-3] has developed the most commonly accepted morphological model for drawn semi-crystalline polymers such as HDPE. In his model, the necked material is characterized by a fibrillar texture in which the macroscopic fibrils comprising the neck are themselves composed of bundles of microfibrils. Within the microfibrils are small 'mosaic-block' crystallites that are joined by 'tie' molecules to give the highly oriented neck its structural integrity under the applied tensile strain. These tie molecules are either interfibrillar or intrafibrillar in nature.

In this chapter, the morphology of the cold-drawn and necked HDPE is explored using solid-state NMR. The determination of the size, proximity, and form of the intermediate component in relation to the other domains is of greatest interest in the

experimental data and analyses presented. Several of the NMR experiments conducted employed the 'inverse ^{13}C T_1 filter' described in Chapter 4. ^1H longitudinal relaxation times in the rotating frame ($T_{1\rho,H}$) were measured for each of the morphological components. $T_{1\rho,H}$ relaxation times are influenced by molecular mobility and domain size, as in the crystallites of the PE microstructure.[4-6] ^1H spin diffusion experiments with ^{13}C detection were performed to measure domain sizes and detect proximities in all directions.[7,8] ^{13}C CP/MAS experiments with $T_{1,C}$ filtering[9] were carried out in the determination of ^{13}C T_1 relaxation times, which are also indicative of molecular mobility[7], crystallite thickness[10], and crystalline chain diffusion rates[11]. 2D ^{13}C exchange spectra following the work of Schmidt-Rohr and Spiess[11] were acquired to measure component proximities along the chain direction. From the results of these experiments, a model of cold-drawn and necked HDPE is offered.

6.2 Experimental

6.2.1 Sample Preparation

Samples of DOW HD-12450N were prepared in the same fashion used in Chapters 4 and 5. Details of these preparation and testing procedures were given in Chapter 3. Samples designated as 'undrawn' or 'undeformed' in this chapter were extracted directly from melt-crystallized, compression-molded test sheets. As in Chapter 4, they were used as reference specimens to show the effects of cold drawing on the HDPE microstructure. Standard dumbbell-shaped test specimens punched from the molded sheets were drawn at 2 mm/min (0.0013 s^{-1} drawing strain rate) to various extensional changes ΔL. The cold-drawing procedure was detailed in Chapter 3.

Extensional changes ΔL of 30 mm (118% nominal drawing strain) and 240 mm (945% drawing strain) were analyzed. The cold-drawn sample strained to 118% was not discussed in Chapter 3, but is very similar in deformation history to the sample of 98% strain. Samples were cut from the necked regions for characterization.

For NMR experiments, samples of the HDPE were wrapped in Teflon tape for better packing and alignment during ^{13}C magic-angle spinning (MAS) NMR measurements. The draw directions of pieces from the necked samples were aligned parallel to the long axis of the sample rotor and, hence, the sample coil.

6.2.2 Solid-State NMR Experiments

6.2.2.1 ^{1}H Spin Diffusion

Proton spin diffusion data were acquired using a Bruker DSX 400 spectrometer (B_o = 9.4 T) at a ^{13}C resonance frequency of 100 MHz. Experiments were performed with magic-angle spinning (MAS) at ambient temperature. 4-mm diameter zirconia rotors with Kel-F caps were used to hold the sample; a 4-kHz spinning speed was chosen. A ^{1}H 90° pulse length of 3.9 μs and a cross-polarization (CP) contact time of 50 μs were employed. The short CP time was used to suppress ^{1}H spin diffusion during spin lock. High-power proton decoupling with two-pulse phase modulation (TPPM)[12] at $\gamma B_1/2\pi$ = 64 kHz was utilized during signal detection.

6.2.2.2 Other NMR Experiments

All other solid-state NMR experiments were conducted using a Bruker DSX 300 spectrometer (B_o = 7 T) at a ^{13}C resonance frequency of 75.5 MHz. Measurements were

made under MAS conditions. 4-mm diameter zirconia rotors with Kel-F caps were used to hold the samples; a 5-kHz spinning speed and decoupling with two-pulse phase modulation (TPPM)[12] at $\gamma B_1/2\pi$ = 62.5 kHz were utilized.

For standard CP measurements, a ^1H 90° pulse length of 4 μs and a contact time of 0.5 ms were used. For $T_{1\rho,H}$ experiments, magic-angle spin lock[13] (MASL) was applied during the $T_{1\rho,H}$ filter locking pulse and the CP contact pulse. MASL is used to suppress ^1H spin diffusion and was briefly described in Chapter 4. A ^1H 90° pulse length of 4 μs was also employed in $T_{1\rho,H}$ measurements, producing a locking field $\gamma B_1/2\pi$ = 62.5 kHz. However, a short CP contact time (0.2 ms) was used to further inhibit spin diffusion. Most experiments were performed at ambient temperature. However, ^{13}C exchange experiments were done at variable temperature. The uncertainty of recorded temperatures was ± 3°C.

6.3 Results and Discussion

6.3.1 ^1H $T_{1\rho}$ Measurements

In conjunction with the selective ^{13}C T_1 filtering methods described in Chapter 4, the $T_{1\rho,H}$ relaxation times of the morphological components in undrawn and drawn samples of the HDPE were measured (Table 6.1). By applying the $T_{1\rho}$ filter locking pulse on ^1H before CP and detecting on ^{13}C after CP with selective filtering, $T_{1\rho,H}$ values for each of the components can be readily determined. Such experiments are yet another example of the great advantage of the inverse $T_{1,C}$ filter that was detailed in Chapter 4. $T_{1\rho,H}$ times for the crystalline forms were obtained using a 10-s $T_{1,C}$ filter after CP. Corresponding values for the amorphous and intermediate components were measured

from inverse $T_{1,C}$ filtered spectra that were derived from pairs of $T_{1,C}$ filtered experiments with the same locking pulse length. Amorphous signals were selected using a 1-s inverse $T_{1,C}$ filter; intermediate component signals were acquired from the difference of 1-s and 10-s $T_{1,C}$ filtered spectra. For each component, a series of experiments were run in which the $T_{1\rho}$ locking pulse length was varied. The intensities of the spectra decayed with increasing locking pulse length. $T_{1\rho,H}$ times were determined by fitting the decay in intensities with an exponential function. However, locking pulse lengths only up to 20 ms were employed, as higher times would have risked damaging the spectrometer hardware. Hence, the relaxation behavior for the component magnetization had to be estimated from the initial portion of the decay curve.

In Table 6.1 significant differences in the $T_{1\rho,H}$ relaxation times of the morphological components are observed in both the undrawn and drawn samples. In the undeformed, melt-crystallized material, $T_{1\rho,H}$ values for the crystalline components are much greater than for the intermediate and amorphous domains. $T_{1\rho,H}$ is influenced by molecular mobility, and the larger times of the crystalline phase indicate lower mobility relative to the non-crystalline domains. Gelfer and co-workers[5,6] have calibrated the $T_{1\rho,H}$ times of PE orthorhombic crystals with the thickness of the crystals along the chain direction. Qualitatively, the magnitude of $T_{1\rho,H}$ increases with the crystal thickness. Using the calibration curve derived by Gelfer et al.[5] and the value for the orthorhombic crystalline $T_{1\rho,H}$ displayed in Table 6.1, the average lamellar thickness in the undrawn HDPE precursor is estimated at about 23 nm.

True to its 'name', the intermediate component in the undrawn sample shows a $T_{1\rho,H}$ relaxation time between the crystalline and amorphous times (Table 6.1) as a result

of intermediate molecular mobility. The shorter $T_{1\rho,H}$ time of the amorphous component indicates fast molecular mobility. The relaxation behavior of the amorphous magnetization is best fit with a stretched exponential function, as indicated in Table 6.1. Relaxation characterized by a stretched exponential function denotes a superposition of monoexponential functions with different relaxation times, i.e. a distribution of $T_{1\rho,H}$ times. Also note that for both HDPE samples, the $T_{1\rho,H}$ relaxation in the monoclinic crystals is faster compared to the orthorhombic crystals (Table 6.1). Hu et al.[4] have determined a direct dependence between the correlation time of the 180° flip motion of chains in PE crystallites and the crystalline $T_{1\rho,H}$ time. The smaller $T_{1\rho,H}$ times of the monoclinic crystals thus indicate larger chain flip rates.

Considerable changes in the $T_{1\rho,H}$ times of the various components occur upon cold drawing. As seen from the data in Table 6.1, the drawn sample (945% strain) shows much lower $T_{1\rho,H}$ values for the crystalline and intermediate components compared to the undrawn precursor. The reduction in crystalline $T_{1\rho,H}$ times reflects a decrease in crystallite thickness and an increase in the chain flip rate as a result of drawing deformation. From the calibration study of Gelfer et al.[5], the average crystallite thickness in the cold-drawn sample is estimated at approximately 13 nm along the chain direction, indicating a decrease in the crystal thickness of over 40% during the cold-drawing process.

Overall, the distribution of $T_{1\rho,H}$ values between the various morphological components diminishes greatly due to cold drawing (Table 6.1). This shows a significant rise in the bulk chain mobility induced by the drawing strain. No doubt, the increased chain mobility is essential in the dramatic restructuring and deformation that takes place

during necking. The reduction in the range of $T_{1\rho,H}$ times also indicates a more intimate proximity of the various components, particularly the intermediate and amorphous material. Note also in Table 6.1 that both the intermediate and amorphous $T_{1\rho,H}$ decay curves of the drawn sample are best fit with a stretched exponential using $\beta \sim 0.8$, as used for the amorphous component in the undrawn sample. This also reflects a closer proximity of the intermediate and amorphous domains.

6.3.2 ^{1}H Spin Diffusion

Proton spin diffusion with detection on ^{13}C provides a powerful means of analyzing the size, proximity, and distribution of microstructural domains that are distinguishable by NMR.[7,8] When utilized in conjunction with the inverse ^{13}C T_1 filter, the distinction between components is even more pronounced, and the non-crystalline domains are better analyzed. ^{1}H spin diffusion experiments conducted in this study were based on the classic method of Goldman and Shen[14]. A freshly necked HDPE cold drawn to 118% strain was characterized. The magnetization of the mobile domains in the sample was selected using the 'dipolar filter'[15] described in Section 5.3.1. The dipolar filter pulse sequence with twenty-four pulses separated by 11-μs windows was applied to ensure exclusive excitation of the ^{1}H magnetization in mobile domains.

The signals of the crystalline material reappearing after spin diffusion were analyzed using a 5-s $T_{1,C}$ filter after the CP pulse. A 5-s filter delay was used rather than a 10-s delay so that the increased scans per unit time would yield spectra with better signal-to-noise in a reasonable experiment time. Intermediate and amorphous signals were measured via 5-s inverse $T_{1,C}$ filtered spectra. Amorphous signals were determined

from the gauche-containing resonances at shifts less than 32 ppm. Intermediate component signals were measured from the intensity of the mobile all-trans peak at ~33 ppm after subtraction of the zero mixing time ($t_m = 0$) spectrum, scaled to match the gauche-containing resonances.

Results of the ^1H spin diffusion experiments are shown in Figure 6.1 and Figure 6.2. Note that the data points shown in all the plots of both figures are the same. Only the simulated fits to the data points differ for each plot. In simulating the ^1H spin diffusion for the cold-drawn HDPE sample, a two-dimensional lattice calculation corresponding to classic Fickian diffusion theory was applied. The input parameters were the domain sizes and the ^1H spin diffusion coefficients for each component. Because the sample was drawn to 118% strain, its deformation history is very similar to samples drawn to 98%, which have been well characterized throughout the previous chapters of the dissertation. Estimation of the component composition was made from the findings of Chapter 5 (Figure 5.13) and by taking into account the 5-s $T_{1,C}$ filter delay employed in the spin diffusion experiments. A component composition of 45% crystalline (including some contribution from the long-$T_{1,C}$ intermediate component), 31% amorphous, and 25% intermediate was therefore used in simulations. Diffusion coefficients for the three microstructural domains were estimated based on molecular mobility and previous experiments conducted on polyethylene materials. Values of 1 nm^2/ms, 0.9 nm^2/ms, and 0.3 nm^2/ms were used for the diffusion coefficients of the crystalline, intermediate, and amorphous domains, respectively.

Two general pictures of the component microstructure in cold-drawn HDPE were considered. In one view, the intermediate component was regarded as an interfacial layer

between the crystallites and the amorphous regions (Figure 6.1). Data simulations that included an interfacial component were performed using three models, each model taking into account varying spatial dimensionalities of the crystallites (Figure 6.1). Since the amorphous magnetization is preferentially selected in the experiments, ^{1}H spin diffusion to the rigid crystalline domains would have to pass through the interfacial layers. This would lead to delayed diffusion of polarized magnetization into the crystallites. However, no time delay in the growth of the crystalline signal intensity is evident from the recorded data points (Figure 6.1), which indicates direct contact of the amorphous and crystalline domains. A thinner interfacial layer, which would reduce the delay, is excluded based on the large intermediate component fraction coupled with fast diffusion into the crystallites and the relatively slow diffusion into the intermediate component. As a result, simulations using interfacial models gave poor fits to the data, particularly at short mixing times (Figure 6.1).

The other microstructural view of cold-drawn HDPE considered in this study invoked the 'tie-molecule' structures proposed by Peterlin[1-3,16] (Figure 6.2). In this model, the intermediate component is identified with the tie molecules linking the crystallites. However, tie molecules are arranged in bundles, not as individual chains finely dispersed in an amorphous medium. The results of Chapter 4 gave convincing evidence that the intermediate component is a morphological domain distinct from the crystalline and amorphous phases. In Chapter 5, the $T_{1,C}$ relaxation behavior of the various components was found to clearly change with component type. Although the $T_{1\rho,H}$ relaxation times of the intermediate and amorphous components in the drawn

sample are close in value (Table 6.1), they are still different, which is a further indication of distinct domains.

A representation of this 'tie-molecule bundle' model is depicted in Figure 6.2. The model is two-dimensional with regards to the directions of spin diffusion considered in the simulation process. Simulated fits to the spin diffusion data were excellent, especially at short mixing times (Figure 6.2), thus supporting the tie-molecule bundle model. Estimated length scales from a two-dimensional perspective are indicated in the model schematic shown in Figure 6.2. If the model was extended to three dimensions, and the crystallites were represented as cubic blocks, their average dimension is estimated at 10–15 nm, which agrees well with the value determined from $T_{1\rho,H}$ experiments (13 nm). Also, the average diameter and longitudinal length of the cylindrical tie-molecule bundles are calculated to be about 2.5 nm and 3 nm, respectively. Hence, the ratio of the tie-molecule bundle diameter to the crystallite diameter would be about 25%.

The spin diffusion results also reveal the three major morphological components to be in direct contact with each other, which agrees with the reduced range of $T_{1\rho,H}$ relaxation times observed due to drawing (Table 6.1). Simulations employing the tie-molecule bundle model estimate the fractions of the crystallite surface areas in contact with the amorphous and intermediate domains to be equivalent. It is apparent from these studies that in the necked morphology, the domains are small in size and intimately mixed, due to the major microstructural disordering incurred during the necking process.

The ^{1}H spin diffusion study presented here gives considerable evidence to the existence of tie-molecule bundles with a morphological character intermediate to the

crystalline and amorphous phases. The study further provides details regarding the proximity and size of these microstructural units. However, several more questions are posed by the results. First, do chains in the tie-molecule bundles pass parallel or perpendicular to the bundle long axis, or both? The results of the static ^{13}C NMR experiments performed in Chapter 4 clearly showed the chains in the crystalline and intermediate components to be generally aligned with the draw direction and, hence, with each other. As depicted in the model presented in Figure 6.2, the tie-molecule bundles can link crystals that are arranged parallel or transverse to the draw direction. Hence, the chains comprising an individual tie-molecule bundle could pass through the bundle at different directions with respect to the bundle's long axis. Of course, an intuitive view of the tie-molecule bundles would immediately suggest the chains to be parallel with the long axis, as this provides for better structural integrity.

Another important question considers the distribution and location of contact surfaces between the amorphous and intermediate components and the oriented crystallites. Is there an even distribution? Or does one of the components dominate the crystal basal plane (transverse to the chain axis) while the other covers mostly the crystal side surfaces? These questions will be addressed in the next section.

6.3.3 ^{13}C T_1 Relaxation and 2D ^{13}C Exchange

Schmidt-Rohr and Spiess[11] proved the solid-state diffusion of chains between the amorphous and crystalline domains of linear polyethylene at ambient to near melting temperatures. This chain diffusion in the crystalline material, which is directly linked to the α_c-relaxation[17-19], explained the nonexponential ^{13}C T_1 relaxation behavior observed

in the crystals of PE[10,20] and the dependence of $T_{1,C}$ relaxation times on the crystal thickness[10]. Therefore, crystalline chain diffusion was shown to be the predominant mechanism of ^{13}C T_1 relaxation in PE lamellar crystals. The magnetization of the fast-relaxing amorphous domains is transported into the crystals by the diffusion of chains.

The crystalline chain diffusion was detected by means of one- and two-dimensional ^{13}C exchange experiments under MAS. For the 1D case, a series of ^{13}C direct-polarization (DP) experiments were conducted with variable recycle delays. The intensity of the crystalline signals grew with time until a sufficient equilibrium was reached, due to ^{13}C T_1 relaxation. When the crystalline intensity was plotted versus square-root recycle delay, which acts as a mixing time for ^{13}C magnetization exchange, a curve characteristic of Fickian-type diffusion was obtained.

A brief introduction to 2D ^{13}C exchange experiments has been given in Chapter 2. The exchange of a ^{13}C spin between two different sites results in a shift in its NMR frequency. This shift appears as off-diagonal intensities in the 2D spectrum. In their study, Schmidt-Rohr and Spiess[11] observed significant off-diagonal intensities at the intersection of the crystalline isotropic chemical shift on one frequency axis and the amorphous isotropic chemical shift on the other axis in the 2D ^{13}C exchange spectra of linear polyethylenes. These off-diagonal intensities were more pronounced as the linear PE samples were heated to relatively high temperatures below melting. The off-diagonal 'cross peaks' were direct evidence of the transport of ^{13}C magnetization by chain diffusion between the amorphous and crystalline domains. Hence, these various 1D and 2D ^{13}C exchange experiments showed a 'connectivity' between the amorphous and crystalline domains along the chain direction by the chain diffusion process.

One-dimensional ^{13}C CP/MAS $T_{1,C}$ filtered experiments were used in Chapters 4 and 5 to determine times when ^{13}C magnetization was sufficiently relaxed in the separate components. ^{13}C T_1 relaxation curves, or 'Torchia' curves[9], of the various morphological components in undrawn and drawn samples of the HDPE were derived in Chapter 5. As mentioned in Chapter 5, the decay constant of ^{13}C magnetization during the $T_{1,C}$ filter delay following CP equals the time constant for equilibrium in the recycle delay of a ^{13}C DP experiment. If the intensities of the crystalline signals in the Torchia curves (Figure 5.10 and Figure 5.11) are normalized by the crystalline intensity near zero filter delay time (1 ms) for each curve, the resulting plots will show the decay of the crystalline signals from unity to zero. Plotting the differences between these normalized intensities and unity versus square-root filter delay time will produce 'chain diffusion' curves like those derived by Schmidt-Rohr and Spiess[11] from ^{13}C DP experiments. The $T_{1,C}$ filter acts as a mixing time t_m for ^{13}C exchange, just as the recycle delay in DP experiments.

Chain diffusion curves for the crystalline material in samples of the undrawn and cold-drawn HDPE are presented in Figure 6.3. At short mixing times, the initial slope is fairly linear for both samples, particularly in the diffusion curve of the undrawn sample. The presence of this initial linear slope is characteristic of Fickian-type diffusion. The slope of the linear regime is related to the rate of chain diffusivity[11]; the larger the slope, the faster the rate of chain diffusion in the crystallites. The drawn sample shows a steeper initial slope and shorter time for equilibrium of the ^{13}C magnetization. Hence, crystalline chains in the cold-drawn material demonstrate faster chain mobility and, consequently, faster $T_{1,C}$ relaxation relative to the undrawn material. This agrees with

findings from the Torchia curves of Chapter 5 (Figure 5.10 and Figure 5.11) and the $T_{1\rho,H}$ results discussed above.

If 2D ^{13}C exchange experiments like those performed by Schmidt-Rohr and Spiess[11] are to be used in comparing the microstructures of the undeformed and cold-drawn HDPE samples, the crystalline chain diffusion rate in a sample of the undeformed, melt-crystallized material must be increased to match the chain diffusion rate in a sample of the necked material. Since the chain diffusivity is a thermally-activated process[11], the temperature of the undrawn sample can be raised until the initial linear slope of the crystalline chain diffusion curve is equivalent to the corresponding slope in the drawn sample curve. This in effect equalizes the chain diffusion rates in the two samples for proper comparison by 2D exchange NMR.

Using this method, the crystal chain diffusion rates in the two samples initially characterized in Figure 6.3 were made roughly equal. It was found that at a temperature of 342 K (69°C), the chain diffusion rate in the undrawn sample was approximately equivalent to the rate in the drawn sample (Figure 6.4). In essence, this time-temperature superposition reveals the necking process to induce an increase in the crystal chain diffusion rate that is equivalent to heating the undrawn material by about 50 K. This rise in chain diffusion mobility is prompted by a decrease in crystallite thickness during necking. Another interesting feature in the chain diffusion curves of Figure 6.4 is the short mixing time behavior of the crystalline signals in the cold-drawn sample. A time delay in the rise of the crystalline ^{13}C magnetization is observed, which could indicate the effect of the intermediate component initially 'blocking' part of the crystal basal plane, but later contributing to T_1 relaxation relayed by chain diffusion. Alternatively, it might

denote a more exponential ^{13}C T_1 relaxation behavior. Such behavior could result from localized chain mobility acting as the dominant source of ^{13}C T_1 relaxation in the crystallites.

Based on the results of the chain diffusivity study, 2D ^{13}C exchange experiments using direct excitation of ^{13}C and MAS were performed on the undrawn and drawn HDPE samples. An initial recycle delay of 0.5 s was employed in the analysis of both samples to select primarily mobile components, i.e. mobile, all-trans intermediate and amorphous material. A mixing time t_m = 0.5 s was used for both samples to prohibit significant ^{13}C T_1 relaxation during the mixing time delay. The drawn sample was tested at ambient temperature (292 K), while the undrawn sample was heated to 342 K (69°C).

The resulting 2D ^{13}C exchange spectra are displayed in Figure 6.5. Cross-peaks caused by ^{13}C exchange via chain diffusion are visible in the undrawn sample spectrum (Figure 6.5, a). Only traces of exchange are detectable in the drawn sample (Figure 6.5, b). Because of the short recycle delay, any detectable exchange occurs primarily between the mobile, all-trans intermediate component and the amorphous domains. Exchange between these components in the undrawn sample takes place because the intermediate component is interfacial in nature. In this scenario, the chains diffuse from the amorphous regions to the crystallites through the interfacial material comprising the intermediate component.

The lack of significant exchange in the cold-drawn sample (Figure 6.5, b) shows that chains in the tie-molecule bundles comprising the intermediate component mostly do not pass immediately into amorphous regions. Therefore, chains in the tie-molecule bundles must be arranged in parallel with amorphous domains. From the ^{13}C static

experiments in Chapter 4, it can then be concluded that the long axis of each tie-molecule bundle must be generally aligned with the draw direction and the chain direction in the crystallites. The tie-molecule bundles cannot exist predominantly on the crystallite side surfaces, as the chains would then pass into the amorphous domains at the ends of the bundles. Therefore, the tie-molecule bundles are joined to crystallites at both ends, which agrees with the model of Peterlin[1-3].

Based on the method developed by Torchia[9], the ^{13}C T_1 relaxation times of the various morphological components in undrawn and cold-drawn HDPE samples were measured (Table 6.2). The Torchia curves of Figure 5.10 and Figure 5.11 were used in these analyses. A log–linear plot of intensity versus $T_{1,C}$ filter delay time is utilized in the determination of apparent $T_{1,C}$ relaxation times in the long-time limit (i.e. 'long-time' $T_{1,C}$ relaxation times), as shown for the crystalline and intermediate components in Figure 6.6 and Figure 6.7, respectively. Deviation of a log-linear plot from a linear slope at short filter delay times is caused by nonexponentiality in the linear-linear relaxation curve. The nonexponentiality in the $T_{1,C}$ decay of crystalline signals is produced by the influence of chain diffusion in the crystallites[11]. Such deviations from the monoexponential ^{13}C T_1 relaxation behavior in polyethylenes have been observed by Axelson et al.[10] and many others[20-23]. In such cases, the 'long-time' $T_{1,C}$ relaxation time can be computed, based on the linear portion of the log-linear plot at longer $T_{1,C}$ filter delay times.

The crystalline $T_{1,C}$ relaxation curves for both samples are presented in Figure 6.6. The ^{13}C magnetization in the drawn sample clearly relaxes faster. This indicates a smaller average crystallite thickness[10]. A comparison of the $T_{1,C}$ relaxation times

computed for the crystalline components in both samples (Table 6.2) shows an order of magnitude decrease in the $T_{1,C}$ relaxation time due to cold drawing. Axelson et al.[10] derived a quantitative correlation between $T_{1,C}$ time and crystal thickness. From the values listed in Table 6.2, the crystal thicknesses for the undrawn and drawn HDPE samples were estimated at about 28 nm and 14 nm, respectively, which agree fairly well with dimensions obtained by $T_{1\rho,H}$ and ^1H spin diffusion measurements discussed above. Independent small-angle X-ray scattering (SAXS) studies of the undrawn HDPE sample yielded a value of 21 nm for the crystal thickness.[24]

In both samples, the $T_{1,C}$ values were computed for the long-time relaxation regime due to short-time deviations from monoexponential relaxation behavior. However, the deviation is considerably more pronounced in the undrawn sample relative to the drawn sample (Figure 6.6), which agrees with observations made from Figure 6.4. This suggests that in the crystallites of the cold-drawn HDPE, ^{13}C T_1 relaxation is more 'normal', being driven by local high frequency, small-amplitude chain mobility rather than just chain diffusion. This relaxation behavior could result from a reduction of chain diffusion from amorphous regions into the crystallites that could be explained by the regions on the crystallite surfaces contacted by the intermediate component rather than the amorphous material.

The 2D exchange experiments indicate that the tie-molecule bundles comprising the intermediate component join crystals along the chain axis. As a result, the suppression in chain diffusion from the amorphous domains could be explained by a tie-molecule bundle model where the basal planes (transverse to the chain direction) of the crystallites are in contact more with tie-molecule bundles than with amorphous material.

The side surfaces of the crystallites would be in contact more with the amorphous regions, which would require that the tie-molecule bundles joining the crystallites be arranged close together with only small amorphous regions between them.

^{13}C T_1 relaxation curves for the intermediate component in both the undrawn and drawn HDPE samples are displayed in Figure 6.7. Corresponding $T_{1,C}$ relaxation times are presented in Table 6.2. The intermediate component in the undrawn sample shows reasonably monoexponential relaxation behavior (Figure 6.7). However, the intermediate component of the drawn sample demonstrates some deviation from monoexponentiality at short times, which could result from a distribution of $T_{1,C}$ relaxation times in the very mobile (short $T_{1,C}$) portions. Cold drawing causes an order of magnitude increase in the intermediate component $T_{1,C}$ relaxation time (Table 6.2). The amorphous relaxation behavior is described well by a monoexponential function in both samples and changes little in the cold-drawing process (Table 6.2).

Finally, the Torchia method was applied to the undeformed and cold-drawn HDPE samples used in the 2D ^{13}C exchange experiments (Figure 6.5). From the crystalline chain diffusion data of Figure 6.4, it was found that to equalize crystalline chain diffusion rates in the undrawn and cold-drawn material, the sample of undrawn HDPE would need to be heated to about 342 K. ^{13}C T_1 relaxation plots of the undrawn sample at 342 K and the drawn sample at ambient temperature (292 K) are presented in Figure 6.8. Compared to Figure 6.6, where both samples were characterized at ambient temperature, the undrawn sample shows a much faster $T_{1,C}$ relaxation rate that is similar to the drawn sample (Figure 6.8) This agrees with the roughly equivalent crystalline chain diffusion rates (Figure 6.4). Even at the higher temperature, the crystalline

component in the undrawn HDPE exhibits a larger deviation from monoexponential relaxation at short times relative to the cold-drawn material (Figure 6.8).

6.4 A Model of the Cold-Drawn HDPE Microstructure

From the experiments of this chapter and previous chapters, a microstructural model of cold-drawn and necked high-density polyethylene is offered. The model follows many of the basic characteristics of Peterlin's classic depiction[1-3] of the morphology in drawn semi-crystalline polymers but differs in some important aspects, such as the bundling of tie molecules. Small 'mosaic block' crystallites, about 10–15 nm in diameter and thickness, are dispersed throughout the bulk of the necked material. Their chain axes are aligned with the draw direction. The crystallites are connected along the draw direction by bundles of tie molecules with diameters about one-fourth the crystalline dimension (2.5 nm) and about 3 nm in length. They comprise much of the material between the crystallites along the draw direction. The series of crystals and interconnecting tie-molecule bundles form nanofibrils that are interspersed by amorphous material, forming a dense network of nanofibrils, microfibrils, and macrofibrils.

Based on the 2.5-nm diameter, a tie-molecule bundle consists of about 30 chains. The chains show properties intermediate to the crystalline and amorphous domains. They are generally aligned with the draw direction, but at a greater distribution of angles relative to the crystalline chains. The tie molecules are poorly packed, which allows them to undergo fast, intermediate-amplitude chain motions about their axes. The tie-molecule bundles form during necking as a result of large strain-induced mobilization and disordering of the rigid crystalline structure. Their presence is detected throughout

the cold-drawing process after necking, indicating their importance in maintaining the structural integrity of the fibrillar system.

6.5 Tables and Figures

Table 6.1: ^{1}H $T_{1\rho}$ relaxation times for the various morphological components in samples of the HDPE. A stretched exponential $\exp(-(t/T_{1\rho,H})^{\beta})$ was employed in fitting the $T_{1\rho}$ decay curve of a specific component if the β factor is presented in the table. Displayed uncertainties are derived from the standard errors of fitting the $T_{1\rho}$ decay curve by a regression analysis.

Morphological Component	**Undrawn Sample**	**Drawn Sample 945% strain**
Orthorhombic crystalline	149 ms ± 9 ms	35 ms ± 1 ms
Monoclinic crystalline	115 ms ± 10 ms	22 ms ± 1 ms
Intermediate	38 ms ± 2 ms	19 ms ± 4 ms $\beta = 0.78 \pm 0.05$
Amorphous	12 ms ± 1 ms $\beta = 0.84 \pm 0.02$	16 ms ± 2 ms $\beta = 0.79 \pm 0.03$

Table 6.2: ^{13}C T_1 relaxation times for the various morphological components in samples of the HDPE. An asterick (*) indicates a 'long-time' relaxation time, as described in the text. Displayed uncertainties are derived from the standard errors of fitting the $T_{1,C}$ decay curve by a regression analysis.

Morphological Component	**Undrawn Sample**	**Drawn Sample 945% strain**
Crystalline	1245 s ± 52 s*	336 s ± 10 s*
Intermediate	2.2 s ± 0.1 s	24 s ± 1 s*
Amorphous	0.35 s ± 0.02 s	0.43 s ± 0.02 s

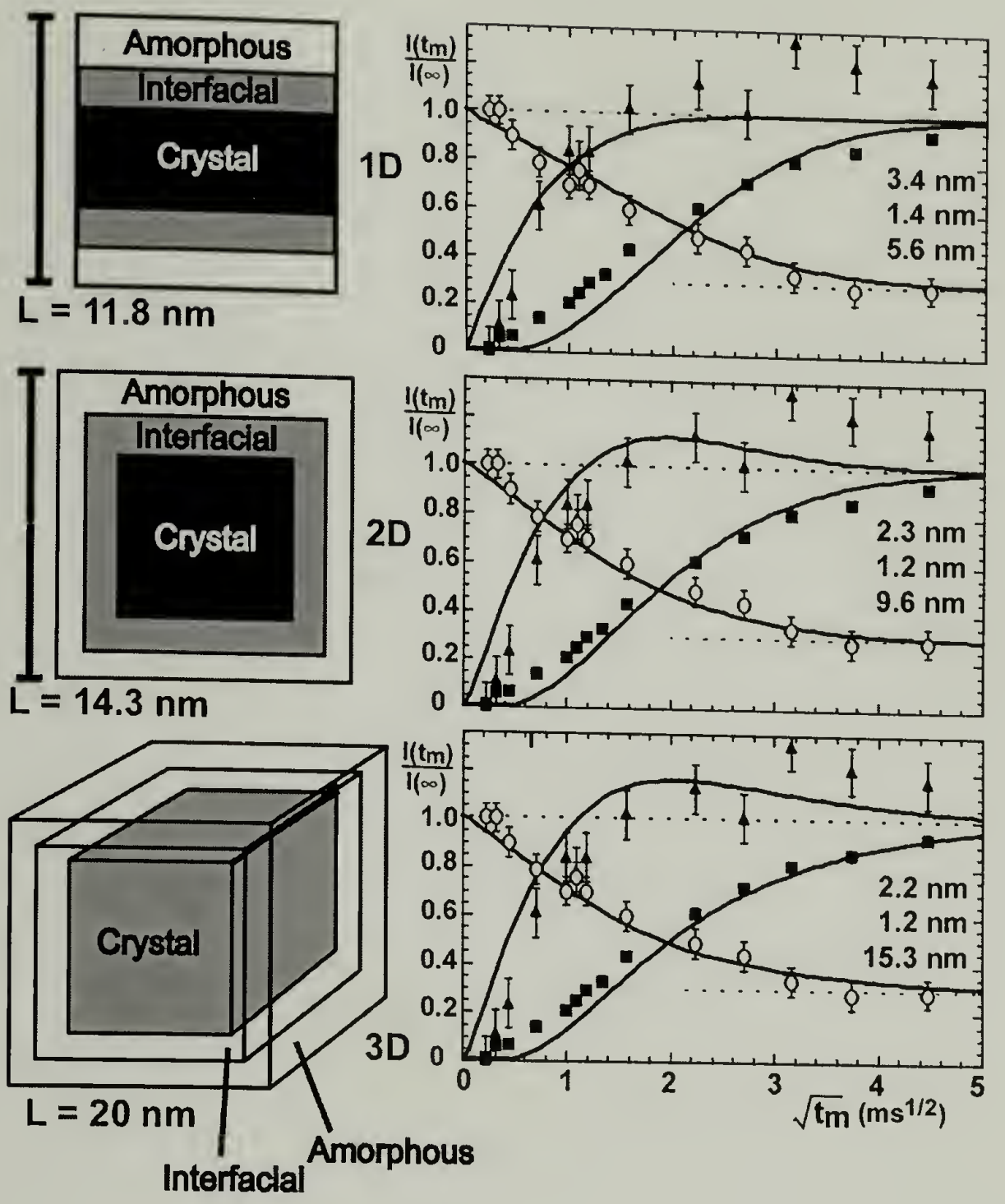

Figure 6.1: Simulations of ^{1}H spin diffusion data of an HDPE sample cold drawn to 118% strain. Actual data from the spin diffusion experiments are shown in the plots. Crystalline (■); intermediate (▲); amorphous (○). The simulations are based on models where the intermediate component is regarded as interfacial material between the crystallites and amorphous regions. The various models considered were based on the number of spatial dimensions and are displayed on the left. Corresponding fits to the data resulting from the simulations are shown to the right of each model. Estimated values of the average thickness of the amorphous, intermediate, and crystalline domains are listed from top to bottom, respectively, in each plot of fitted data. Parameters for the simulation process are given in the text. The mixing time for spin diffusion is identified by t_m in the plots.

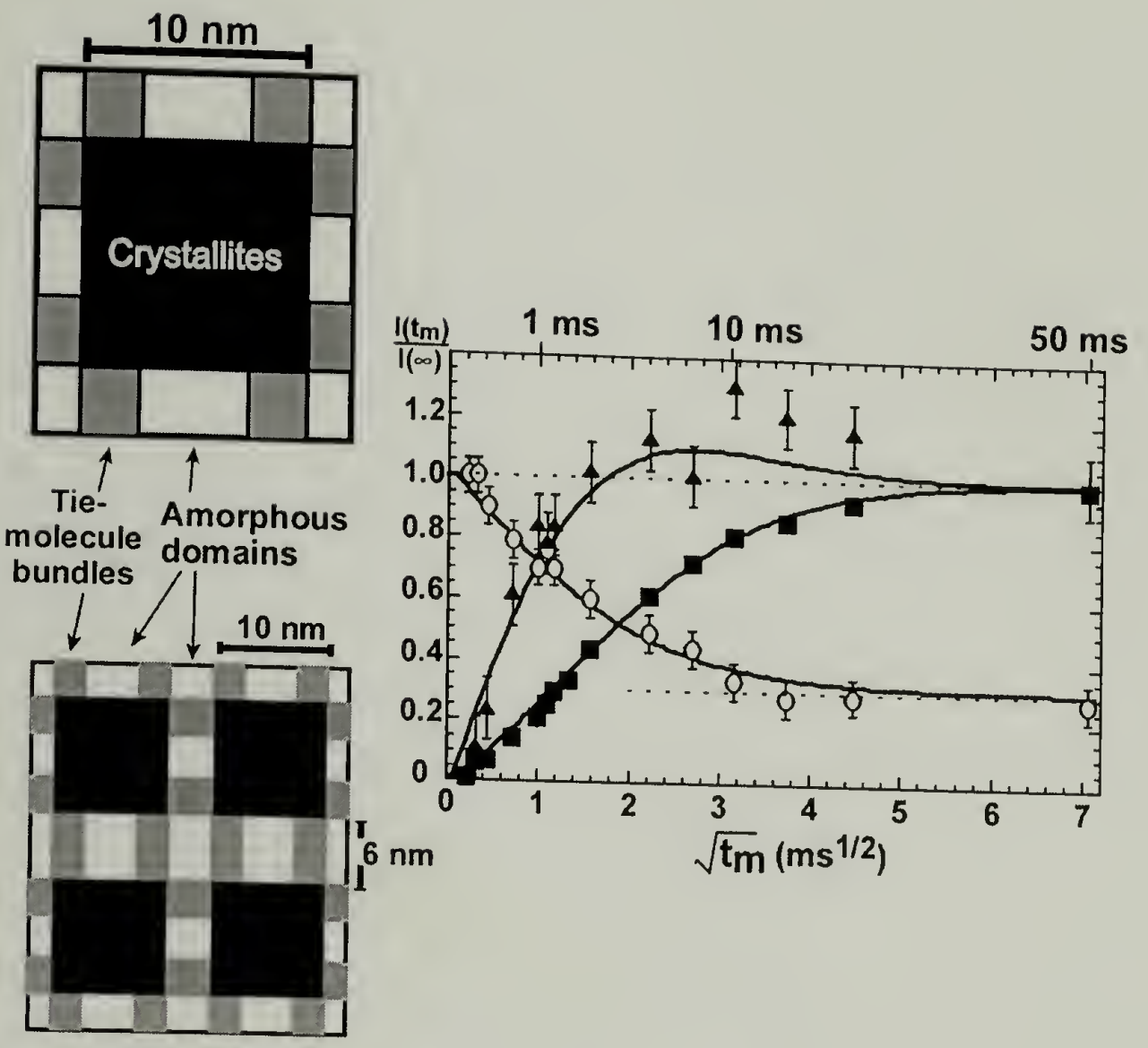

Figure 6.2: Simulation of ^1H spin diffusion data of an HDPE sample cold drawn to 118% strain. Actual data from the spin diffusion experiments are shown in the plot. Crystalline (■); intermediate (▲); amorphous (○). The simulation is based on a model where the intermediate component is regarded as bundles of tie molecules connecting the crystallites and dispersed in the amorphous regions. A representation of the model is displayed on the left. Fits to the data resulting from the simulation are presented in the right-hand side of the figure. Estimated values of the domains are shown in the model schematic. Parameters for the simulation process are given in the text. The mixing time for spin diffusion is identified by t_m in the plot.

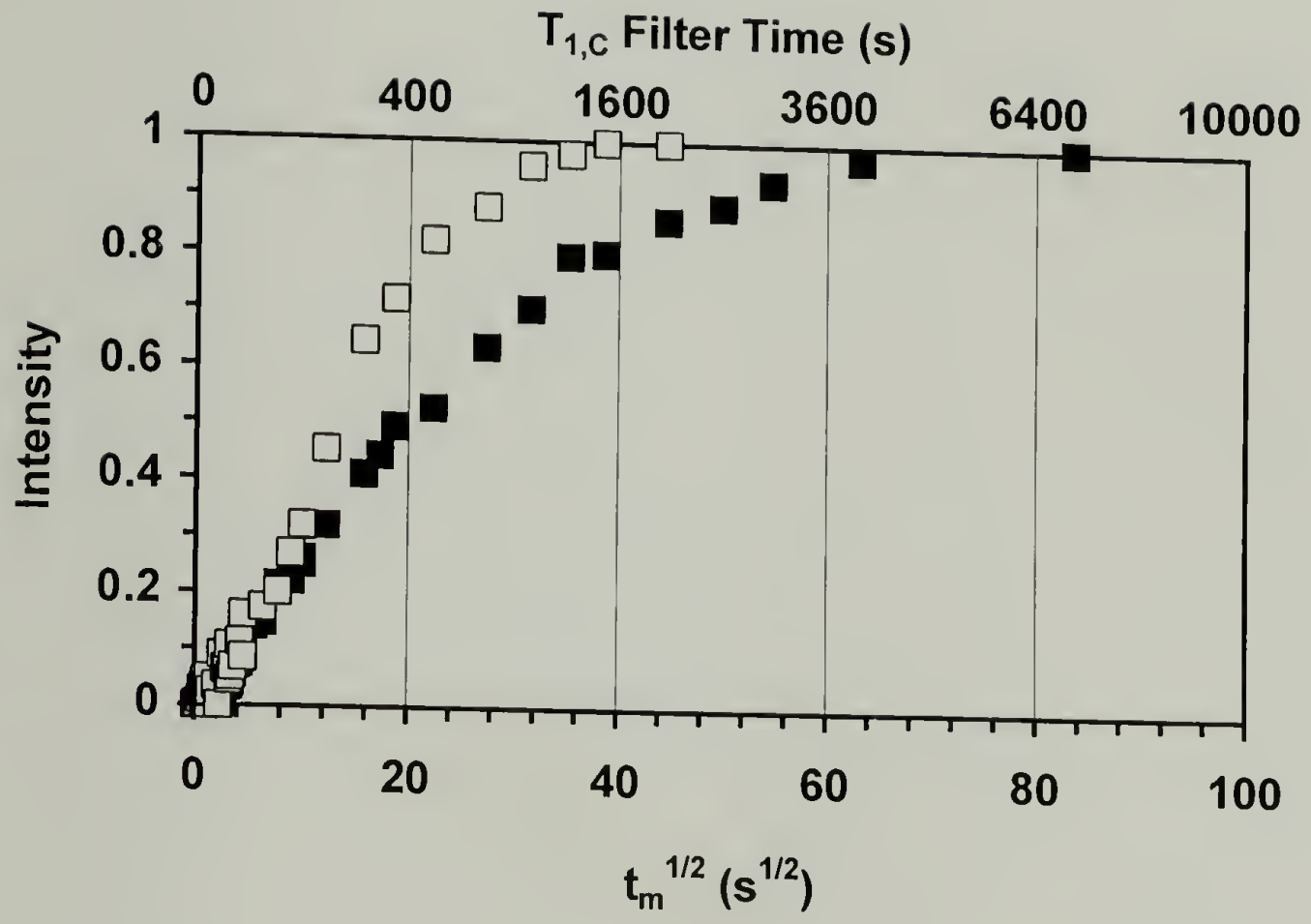

Figure 6.3: Crystalline chain diffusion curves for samples of the undrawn (■) and drawn (□) HDPE at ambient temperature (292 K). The drawn sample was strained to 945%. The intensities are derived from the Torchia curves in Chapter 5. The $T_{1,C}$ filter delay time acts as a mixing time t_m in these experiments.

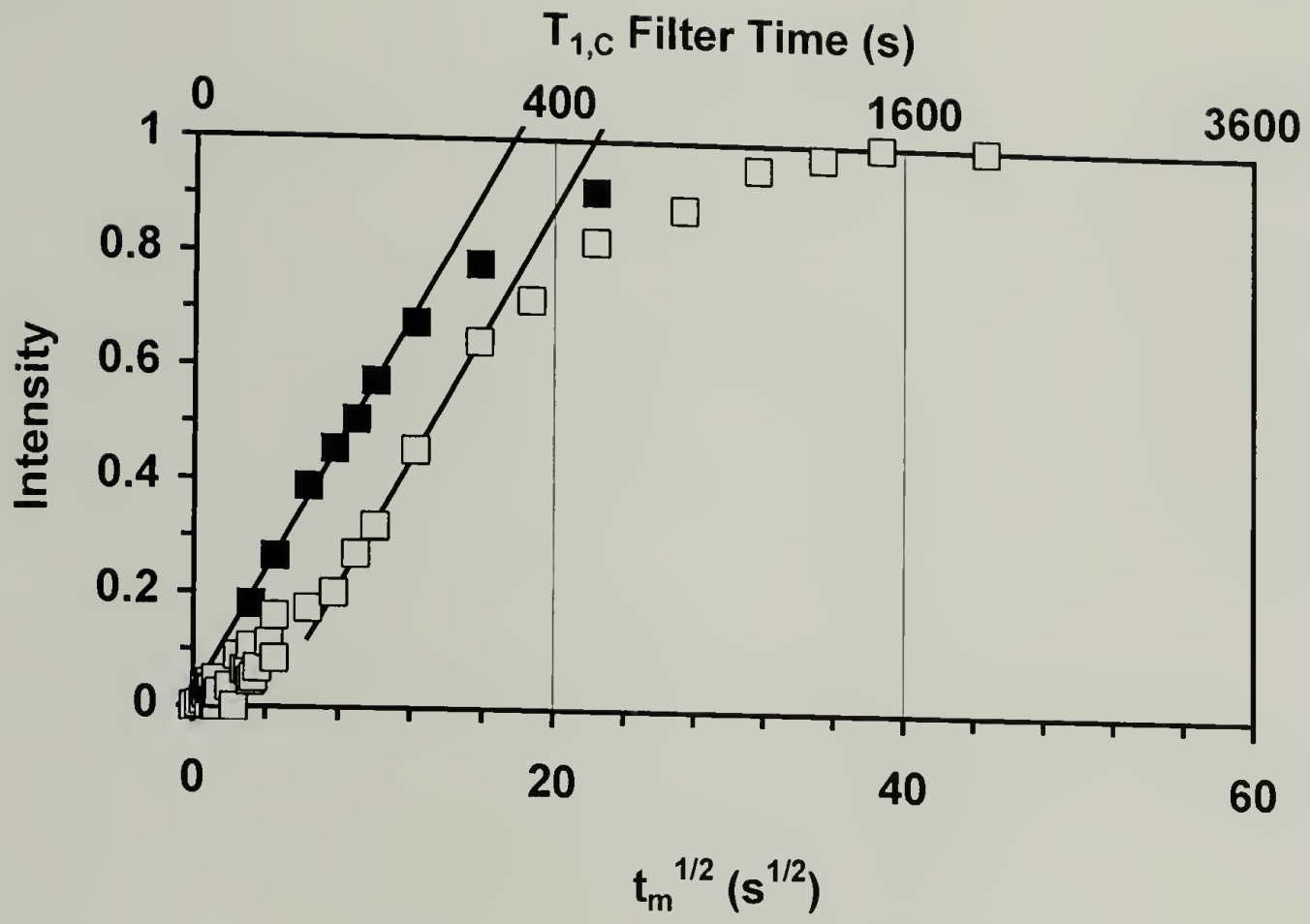

Figure 6.4: Crystalline chain diffusion curves for the same undrawn and drawn HDPE samples characterized in Figure 6.3. Data points for the drawn sample (□) were acquired at ambient temperature (292 K). Data points for the undrawn sample (■) were obtained after the sample had been heated to 342 K to equalize the crystalline chain diffusion rates in the two samples. The lines indicate the initial linear slopes of the curves for each sample. The slopes of these lines are proportional to the chain diffusion rates[11]. Note the slight delay in the drawn sample curve at the smallest mixing times t_m due to some exponential character in the $T_{1,C}$ relaxation behavior of the crystallites.

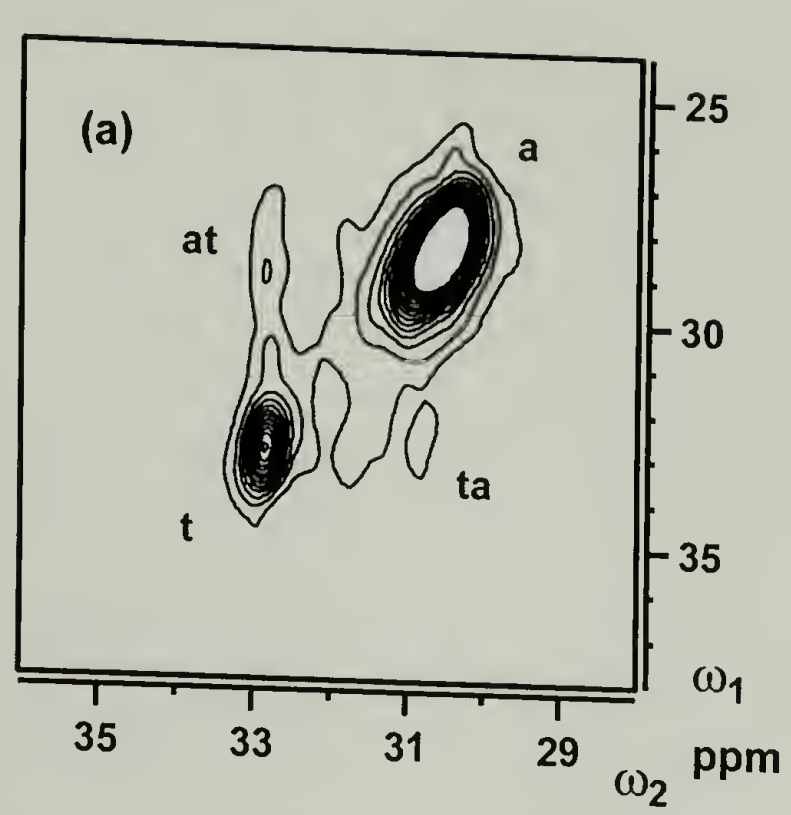

Figure 6.5: MAS 2D ^{13}C exchange spectra of the HDPE with a recycle delay of 0.5 s and a mixing time t_m of 0.5 s. (a) undrawn sample analyzed at a temperature of 342 K (69°C); (b) cold-drawn sample (945% drawing strain) analyzed at ambient temperature (292 K). Chain diffusion rates in the crystals are roughly equivalent for both samples (Figure 6.4). Off-diagonal cross peaks 'ta' and 'at' indicate exchange between the amorphous (a) and all-trans (t) domains. Contour lines are evenly spaced at 1/15 of half the maximum intensity in each spectrum.

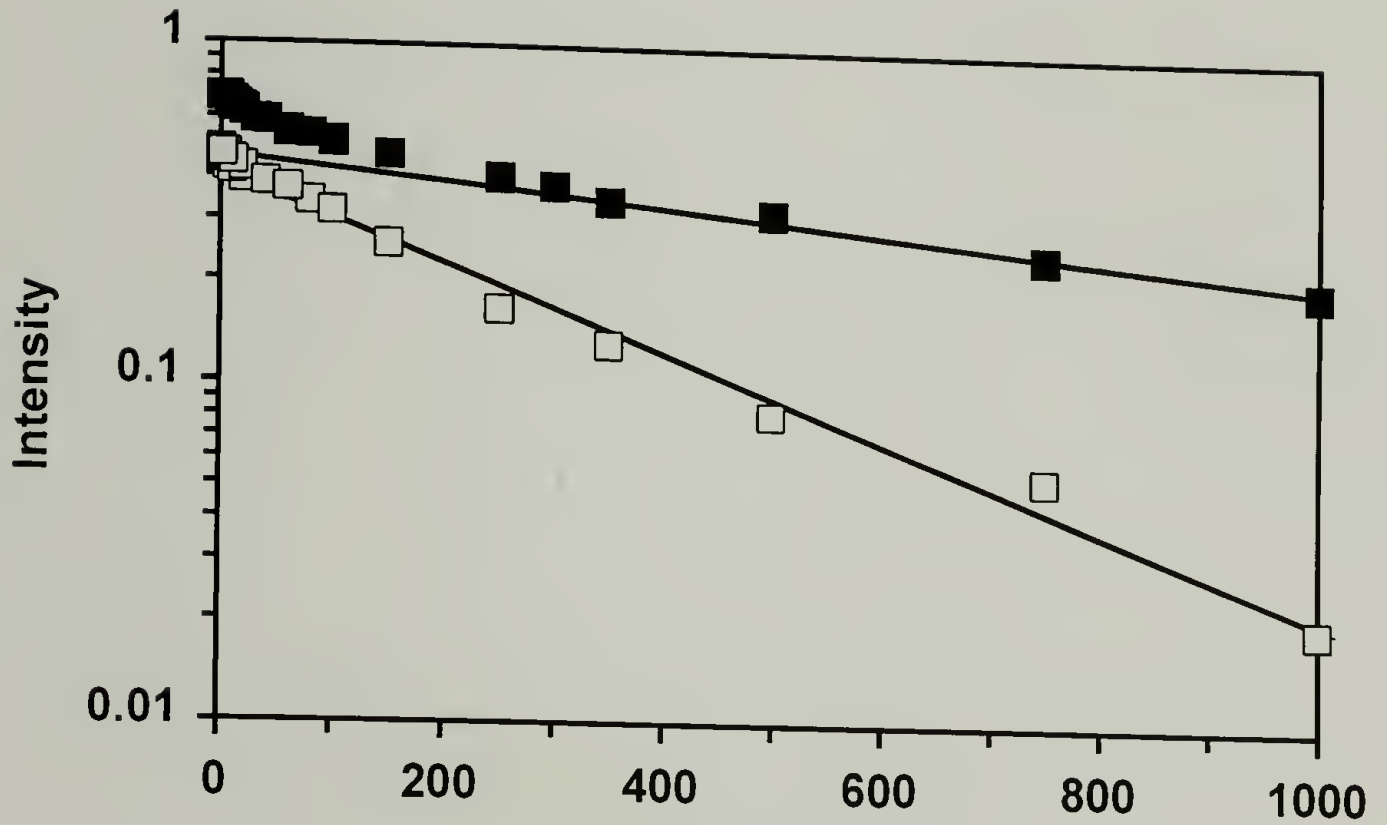

Figure 6.6: ^{13}C T_1 relaxation plots for the crystalline component in samples of the undrawn (■) and drawn (□) HDPE. The drawn sample was strained to 945%. Lines indicate best-fits to the data at long $T_{1,C}$ filter delay times using a monoexponential function. Intensities are relative to the original 1-ms $T_{1,C}$ filtered ^{13}C CP/MAS spectrum for each sample.

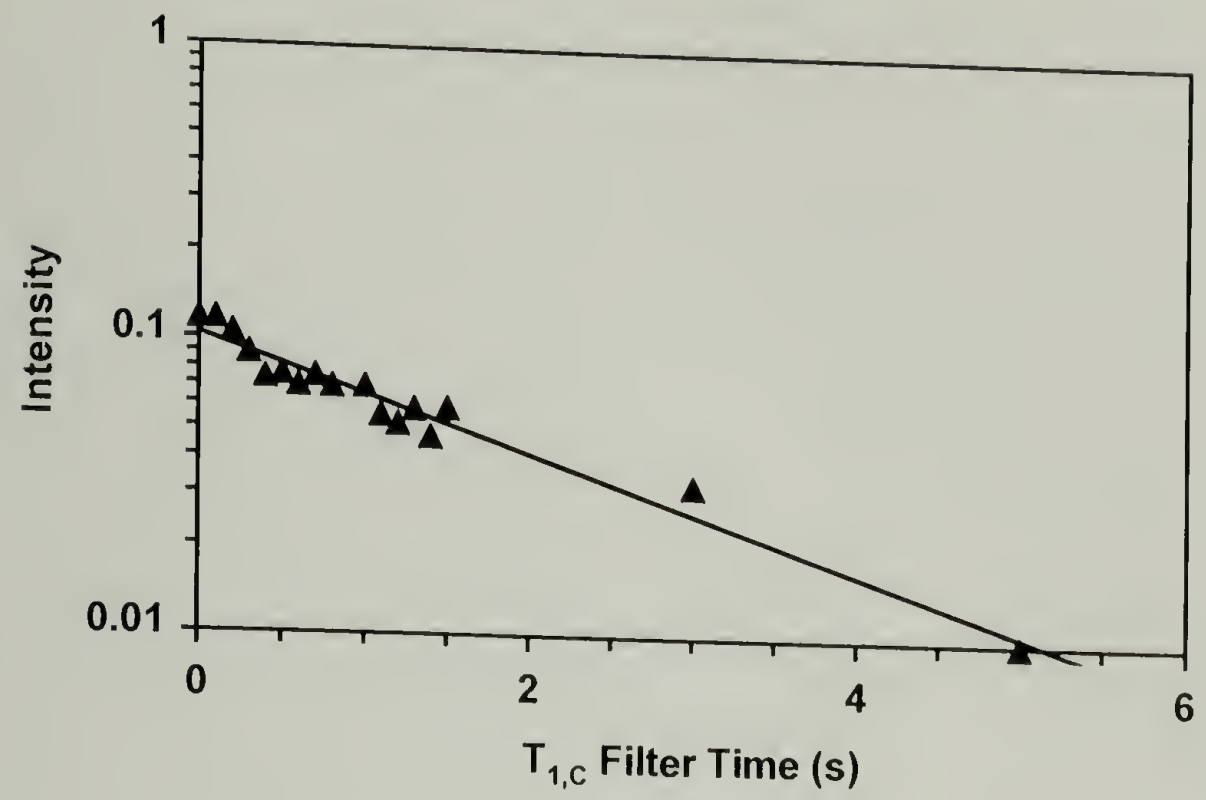

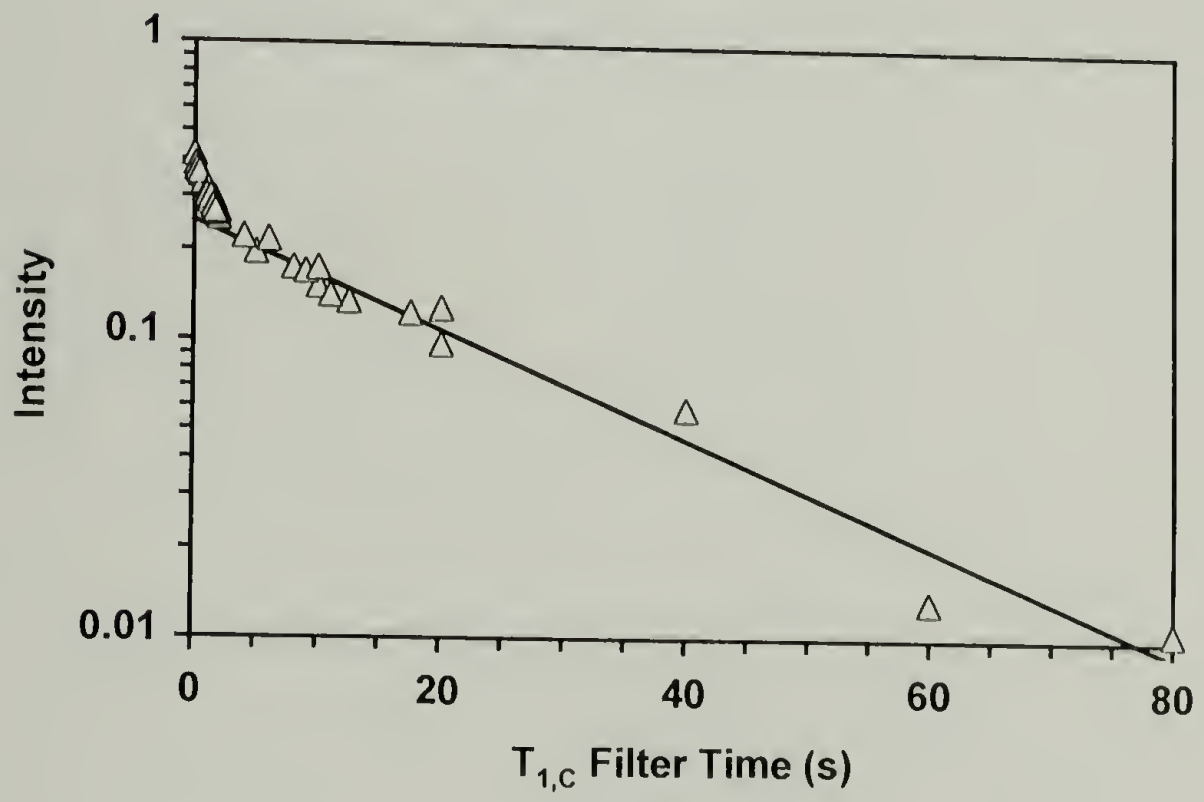

Figure 6.7: ^{13}C T_1 relaxation plots for the intermediate component in samples of the undrawn (▲) and drawn (Δ) HDPE. The drawn sample was strained to 945%. Lines indicate best-fits to the data using a monoexponential function; in the drawn sample, only the long-time relaxation data points were fit. Intensities are relative to the original 1-ms $T_{1,C}$ filtered ^{13}C CP/MAS spectrum for each sample.

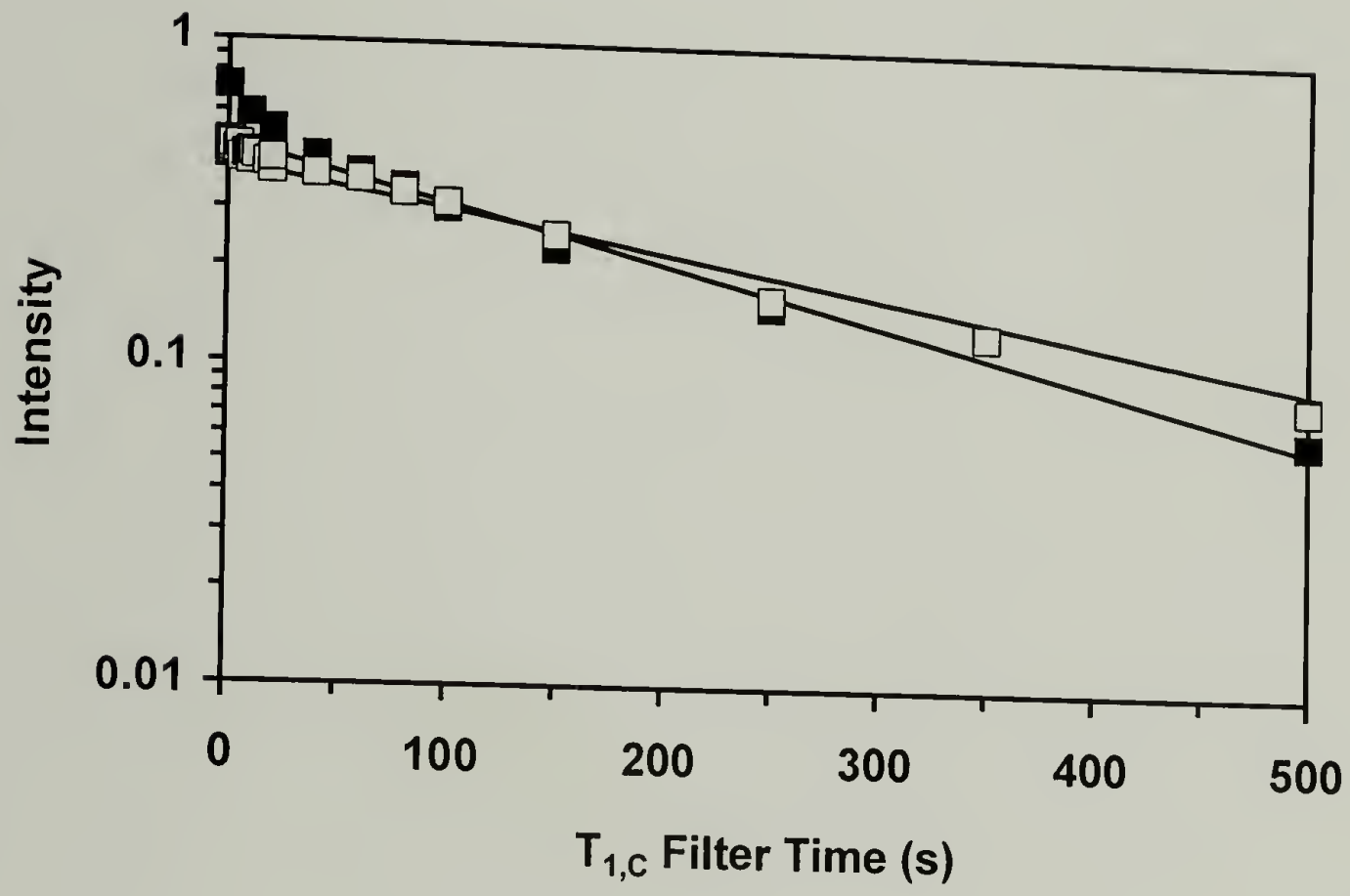

Figure 6.8: ^{13}C T_1 relaxation plots for the crystalline component in samples of the undrawn (■) and drawn (□) HDPE, corresponding to the chain diffusion curves in Figure 6.4. Data points for the drawn sample were acquired at ambient temperature (292 K). Data points for the undrawn sample were obtained after the sample had been heated to 342 K. As a result, the chain diffusion rates were roughly equivalent in the two samples. Lines indicate best-fits to the data at long $T_{1,C}$ filter delay times using a monoexponential function. Intensities are relative to the original 1-ms $T_{1,C}$ filtered ^{13}C CP/MAS spectrum for each sample.

6.6 References

1. Peterlin, A. *Colloid & Polymer Science*, 1987. **265**(5): p. 357-382.

2. Peterlin, A. *Colloid and Polymer Science*, 1975. **253**(10): p. 809-823.

3. Peterlin, A. *Journal of Materials Science*, 1971. **6**: p. 490-508.

4. Hu, W.-G.; Boeffel, C.; Schmidt-Rohr, K. *Macromolecules*, 1999. **32**(5): p. 1611-1619.

5. Gelfer, M.; Beyer, F.; Gido, S.P.; Alamo, R.; Schmidt-Rohr, K. *Macromolecules*, submitted.

6. Gelfer, M.Y.; Schmidt-Rohr, K. *Polymeric Materials: Science and Engineering*, 1999. **80**: p. 380-381.

7. Schmidt-Rohr, K.; Spiess, H.W. *Multidimensional Solid-State NMR and Polymers*. 1994, San Diego: Academic Press, Inc.

8. Clauss, J.; Schmidt-Rohr, K.; Spiess, H.W. *Acta Polymerica*, 1993. **44**: p. 1-17.

9. Torchia, D.A. *Journal of Magnetic Resonance*, 1978. **30**: p. 613-616.

10. Axelson, D.E.; Mandelkern, L.; Popli, R.; Mathieu, P. *Journal of Polymer Science: Polymer Physics Edition*, 1983. **21**: p. 2319-2335.

11. Schmidt-Rohr, K.; Spiess, H.W. *Macromolecules*, 1991. **24**(19): p. 5288-5293.

12. Bennett, A.E.; Rienstra, C.M.; Auger, M.; Lakshmi, K.V.; Griffin, R.G. *Journal of Chemical Physics*, 1995. **103**(16): p. 6951-6958.

13. Lee, M.; Goldburg, W.I. *Physical Review*, 1965. **140**(4A): p. A1261-A1271.

14. Goldman, M.; Shen, L. *Physical Review*, 1966. **144**(1): p. 321-331.

15. Egger, N.; Schmidt-Rohr, K.; Blümich, B.; Domke, W.-D.; Stapp, B. *Journal of Applied Polymer Science*, 1992. **44**: p. 289-295.

16. Peterlin, A. *Journal of Polymer Science: Part A-2*, 1969. **7**: p. 1151-1163.

17. Boyd, R.H. *Polymer*, 1985. **26**(8): p. 1123-1133.

18. Boyd, R.H. *Polymer*, 1985. **26**(3): p. 323-347.

19. McCrum, N.G.; Read, B.E.; Williams, G. *Anelastic and Dielectric Effects in Polymeric Solids*. 1967, New York: Dover Publications, Inc.

20. Kitamaru, R.; Horii, F.; Murayama, K. *Macromolecules*, 1986. **19**(3): p. 636-643.

21. Kuwabara, K.; Kaji, H.; Horii, F.; Bassett, D.C.; Olley, R.H. *Macromolecules*, 1997. **30**(24): p. 7516-7521.

22. Kaji, A.; Yamanaka, A.; Murano, M. *Polymer Journal*, 1990. **22**(10): p. 893-900.

23. Kaji, A.; Ohta, Y.; Yasuda, H.; Murano, M. *Polymer Journal*, 1990. **22**(6): p. 455-462.

24. Kent, M.S.; Rieker, T. private communication, 2000.

BIBLIOGRAPHY

Designer plastics, in *The Economist Technology Quarterly*. Dec 8, 2001. p. 26-28.

Abragam, A. *The Principles of Nuclear Magnetism*. The International Series of Monographs on Physics. 1961, New York: Oxford University Press Inc.

Alamo, R.G.; Mandelkern, L. *Thermodynamic and Structural Properties of Ethylene Copolymers*. Macromolecules, 1989. **22**(3): p. 1273-1277.

Aoki, A.; Asakura, T. *Polyolefins*, in *Solid State NMR of Polymers*, Ando, I.; Asakura, T., Editors. 1998, Elsevier Science B.V.: Amsterdam. p. 415-444.

Axelson, D.E.; Mandelkern, L.; Popli, R.; Mathieu, P. *Carbon-13 NMR of Polyethylenes: Correlation of the Crystalline Component T_1 with Structure*. Journal of Polymer Science: Polymer Physics Edition, 1983. **21**: p. 2319-2335.

Axelson, D.E. *Carbon-13 Solid-State NMR of Semicrystalline Polymers*, in *High Resolution NMR Spectroscopy of Synthetic Polymers in Bulk*, Komoroski, R.A., Editor. 1986, VCH Publishers, Inc.: Deerfield Beach, Florida, USA. p. 157-226.

Baker, A.M.E.; Windle, A.H. *Evidence for a partially ordered component in polyethylene from wide-angle X-ray diffraction*. Polymer, 2001. **42**: p. 667-680.

Bennett, A.E.; Rienstra, C.M.; Auger, M.; Lakshmi, K.V.; Griffin, R.G. *Heteronuclear decoupling in rotating solids*. Journal of Chemical Physics, 1995. **103**(16): p. 6951-6958.

Bovey, F.A.; Jelinski, L.; Mirau, P.A. *Nuclear Magnetic Resonance Spectroscopy*. 2nd ed. 1988, San Diego: Academic Press, Inc.

Bowden, P.B.; Young, R.J. *Review: Deformation mechanisms in crystalline polymers*. Journal of Materials Science, 1974. **9**: p. 2034-2051.

Boyd, R.H. *Relaxation Processes in Crystalline Polymers -- Experimental Behavior -- A Review*. Polymer, 1985. **26**(3): p. 323-347.

Boyd, R.H. *Relaxation Processes in Crystalline Polymers -- Molecular Interpretation -- A Review*. Polymer, 1985. **26**(8): p. 1123-1133.

Brooks, N.W.; Duckett, R.A.; Ward, I.M. *Investigation into double yield points in polyethylene*. Polymer, 1992. **33**(9): p. 1872-1880.

Brooks, N.W.J.; Duckett, R.A.; Ward, I.M. *Modeling of double yield points in polyethylene: Temperature and strain-rate dependence.* Journal of Rheology, 1995. **39**(2): p. 425-436.

Brooks, N.W.J.; Unwin, A.P.; Duckett, R.A.; Ward, I.M. *Double Yield Points in Polyethylene: Structural Changes Under Tensile Deformation.* Journal of Macromolecular Science -- Physics, 1995. **B34**(1&2): p. 29-54.

Brooks, N.W.J.; Duckett, R.A.; Ward, I.M. *Temperature and Strain-Rate Dependence of Yield Stress of Polyethylene.* Journal of Polymer Science: Part B: Polymer Physics, 1998. **36**: p. 2177-2189.

Bunn, C.W. *The Crystal Structure of Long-Chain Normal Paraffin Hydrocarbons. The "Shape" of the CH_2 Group.* Transactions of the Faraday Society, 1939. **35**: p. 482-491.

Butler, M.F.; Donald, A.M.; Bras, W.; Mant, G.R.; Derbyshire, G.E.; Ryan, A.J. *A Real-Time Simultaneous Small- and Wide-Angle X-ray Scattering Study of In-Situ Deformation of Isotropic Polyethylene.* Macromolecules, 1995. **28**(19): p. 6383-6393.

Cawood, M.J.; Channell, A.D.; Capaccio, G. *Crack initiation and fibre creep in polyethylene.* Polymer, 1993. **34**: p. 423-425.

Chen, W.; Fu, Y.; Wunderlich, B.; Cheng, J. *The Morphology of Gel-Spun Polyethylene Fibers, Investigated by Solid-State ^{13}C NMR.* Journal of Polymer Science: Part B: Polymer Physics, 1994. **32**: p. 2661-2666.

Cheng, J.; Fone, M.; Reddy, V.N.; Schwartz, K.B.; Fisher, H.B.; Wunderlich, B. *Identification and Quantitative Analysis of the Intermediate Phase in a Linear High-Density Polyethylene.* Journal of Polymer Science: Part B: Polymer Physics, 1994. **32**(2683-2693).

Cheng, J.; Fone, M.; Fu, Y.; Chen, W. *Variable-Temperature Study of a Gel-Spun Ultra-High Molecular-Mass Polyethylene Fiber by Solid State NMR.* Journal of Thermal Analysis, 1996. **47**: p. 673-683.

Clauss, J.; Schmidt-Rohr, K.; Spiess, H.W. *Determination of domain sizes in heterogeneous polymers by solid-state NMR.* Acta Polymerica, 1993. **44**: p. 1-17.

Darras, O.; Seguela, R. *Tensile Yield of Polyethylene in Relation to Crystal Thickness.* Journal of Polymer Science: Part B: Polymer Physics, 1993. **31**: p. 759-766.

Dieter, G.E. *Mechanical Metallurgy.* Third ed. 1986, New York: McGraw-Hill Book Company.

Earl, W.L.; VanderHart, D.L. *Observations in Solid Polyethylenes by Carbon-13 Nuclear Magnetic Resonance with Magic Angle Sample Spinning.* Macromolecules, 1979. **12**(4): p. 762-767.

Eckman, R.R.; Henrichs, P.M.; Peacock, A.J. *Study of Polyethylene by Solid State NMR Relaxation and Spin Diffusion.* Macromolecules, 1997. **30**(8): p. 2474-2481.

Egger, N.; Schmidt-Rohr, K.; Blümich, B.; Domke, W.-D.; Stapp, B. *Solid State NMR Investigation of Cationic Polymerized Epoxy Resins.* Journal of Applied Polymer Science, 1992. **44**: p. 289-295.

Ernst, R.R.; Bodenhausen, G.; Wokaun, A. *Principles of Nuclear Magnetic Resonance in One and Two Dimensions.* The International Series of Monographs on Chemistry. 1987, New York: Oxford University Press Inc.

Fischer, E.W. *Neutron Scattering Studies on the Crystallization of Polymers.* Polymer Journal, 1985. **17**(1): p. 307-320.

Flory, P.J. *Thermodynamics of Crystallization in High Polymers. IV. A Theory of Crystalline States and Fusion in Polymers, Copolymers, and Their Mixtures with Diluents.* Journal of Chemical Physics, 1949. **17**(3): p. 223-240.

Flory, P.J.; Yoon, D.Y. *Molecular morphology in semicrystalline polymers.* Nature, 1978. **272**: p. 226-229.

Fu, Y.; Chen, W.; Pyda, M.; Londono, D.; Annis, B.; Boller, A.; Habenschuss, A.; Cheng, J.; Wunderlich, B. *Structure-Property Analysis for Gel-Spun, Ultrahigh Molecular Mass Polyethylene Fibers.* Journal of Macromolecular Science -- Physics, 1996. **B35**(1): p. 37-87.

Gaucher-Miri, V.; Séguéla, R. *Tensile Yield of Polyethylene and Related Copolymers: Mechanical and Structural Evidences of Two Thermally Activated Processes.* Macromolecules, 1997. **30**(4): p. 1158-1167.

Gelfer, M.Y.; Schmidt-Rohr, K. *Investigation of Morphology and Molecular Mobility in Ethylene-Hexene Co-Polymers by Solid-State NMR.* Polymeric Materials: Science and Engineering, 1999. **80**: p. 380-381.

Gelfer, M.; Beyer, F.; Gido, S.P.; Alamo, R.; Schmidt-Rohr, K. *Polyethylene Crystallite Thickness Distribution from ^{1}H NMR Rotating-Frame Relaxation, Calibrated by Electron Microscopy and Raman LAM.* Macromolecules, submitted.

Gibson, A.G.; Davies, G.R.; Ward, I.M. *Dynamic mechanical behaviour and longitudinal crystal thickness measurements on ultra-high modulus linear polyethylene: a quantitative model for the elastic modulus.* Polymer, 1978. **19**: p. 683-693.

Glotin, M.; Mandelkern, L. *A Raman spectroscopic study of the morphological structure of the polyethylenes.* Colloid & Polymer Science, 1982. **260**(2): p. 182-192.

Goldman, M.; Shen, L. *Spin-Spin Relaxation in LaF_3.* Physical Review, 1966. **144**(1): p. 321-331.

Hartmann, S.R.; Hahn, E.L. *Nuclear Double Resonance in the Rotating Frame.* Physical Review, 1962. **128**(5): p. 2042-2053.

Hentschel, D.; Sillescu, H.; Spiess, H.W. *Molecular Motion in Solid Polyethylene as Studied by ^2D Wide Line NMR Spectroscopy.* Makromol. Chemie, 1979. **180**: p. 241-249.

Hiss, R.; Hobeika, S.; Lynn, C.; Strobl, G. *Network Stretching, Slip Processes, and Fragmentation of Crystallites during Uniaxial Drawing of Polyethylene and Related Copolymers. A Comparative Study.* Macromolecules, 1999. **32**(13): p. 4390-4403.

Hu, W.-G.; Schmidt-Rohr, K. *Polymer ultradrawability: the crucial role of α-relaxation chain mobility in the crystallites.* Acta Polymerica, 1999. **50**: p. 271-285.

Hu, W.-G.; Boeffel, C.; Schmidt-Rohr, K. *Chain Flips in Polyethylene Crystallites and Fibers Characterized by Dipolar ^{13}C NMR.* Macromolecules, 1999. **32**(5): p. 1611-1619.

Hu, W.-G.; Schmidt-Rohr, K. *Characterization of ultradrawn polyethylene fibers by NMR: crystallinity, domain sizes and a highly mobile second amorphous phase.* Polymer, 2000. **41**: p. 2979-2987.

Hughes, D.J.; Mahendrasingam, A.; Oatway, W.B.; Heeley, E.L.; Martin, C.; Fuller, W. *A simultaneous SAXS/WAXS and stress-strain study of polyethylene deformation at high strain rates.* Polymer, 1997. **38**(26): p. 6427-6430.

Juska, T.; Harrison, I.R. *A Proposed Plastic Deformation Mechanism for Semi-Crystalline Polymers.* Polymer Engineering Reviews, 1982. **2**(1): p. 13-28.

Kaji, A.; Ohta, Y.; Yasuda, H.; Murano, M. *Phase Structural Analysis of Ultra High-Molecular Weight Polyethylene Fibers by Solid State High Resolution NMR.* Polymer Journal, 1990. **22**(6): p. 455-462.

Kaji, A.; Yamanaka, A.; Murano, M. *Stuctural Analysis of Polyethylene Fibers by Solid State High Resolution NMR; the Distribution of ^{13}C Spin-Lattice Relaxation Times.* Polymer Journal, 1990. **22**(10): p. 893-900.

Keller, A.; Pope, D.P. *Identification of Structural Processes in Deformation of Oriented Polyethylene.* Journal of Materials Science, 1971. **6**: p. 453-478.

Kiho, H.; Peterlin, A.; Geil, P.H. *Polymer Deformation. VIII. Stability of the Monoclinic Phase of Polyethylene.* Journal of Polymer Science: Part B, 1965. **3**(2): p. 157-160.

Kip, B.J.; van Eijk, M.C.P.; Meier, R.J. *Molecular Deformation of High-Modulus Polyethylene Fibers Studied by Micro-Raman Spectroscopy.* Journal of Polymer Science: Part B: Polymer Physics, 1991. **29**: p. 99-108.

Kitamaru, R.; Horii, F. *NMR Approach to the Phase Structure of Linear Polyethylene.* Advances in Polymer Science, 1978. **26**: p. 138-178.

Kitamaru, R.; Horii, F.; Murayama, K. *Phase Structure of Lamellar Crystalline Polyethylene by Solid-State High-Resolution ^{13}C NMR: Detection of the Crystalline-Amorphous Interphase.* Macromolecules, 1986. **19**(3): p. 636-643.

Komoroski, R.A., ed. *High Resolution NMR Spectroscopy of Synthetic Polymers in Bulk.* Methods in Stereochemical Analysis, ed. Marchand, A.P. Vol. 7. 1986, VCH Publishers, Inc.: Deerfield Beach, Florida, USA.

Kuwabara, K.; Kaji, H.; Horii, F.; Bassett, D.C.; Olley, R.H. *Solid-State ^{13}C NMR Analyses of the Crystalline-Noncrystalline Structure for Metallocene-Catalyzed Linear Low-Density Polyethylene.* Macromolecules, 1997. **30**(24): p. 7516-7521.

Kwon, Y.K.; Boller, A.; Pyda, M.; Wunderlich, B. *Melting and heat capacity of gel-spun, ultra-high molar mass polyethylene fibers.* Polymer, 2000. **41**: p. 6237-6249.

Lagaron, J.M.; Dixon, N.M.; Reed, W.; Pastor, J.M.; Kip, B.J. *Morphological characterisation of the crystalline structure of cold-drawn HDPE used as a model material for the environmental stress cracking (ESC) phenomenon.* Polymer, 1999. **40**: p. 2569-2586.

Lagarón, J.M.; Dixon, N.M.; Gerrard, D.L.; Reed, W.; Kip, B.J. *Cold-Drawn Material As Model Material for the Environmental Stress Cracking (ESC) Phenomenon in Polyethylene. A Raman Spectroscopy Study of Molecular Stress Induced by Macroscopic Strain in Drawn Polyethylenes and Their Relation to Environmental Stress Cracking.* Macromolecules, 1998. **31**(17): p. 5845-5852.

Lagarón, J.M.; López-Quintana, S.; Rodriguez-Cabello, J.C.; Merino, J.C.; Pastor, J.M. *Comparative study of the crystalline morphology present in isotropic and uniaxially stretched "conventional" and metallocene polyethylenes.* Polymer, 2000. **41**: p. 2999-3010.

Lee, M.; Goldburg, W.I. *Nuclear-Magnetic-Resonance Line Narrowing by a Rotating rf Field.* Physical Review, 1965. **140**(4A): p. A1261-A1271.

Lin, L.; Argon, A.S. *Review: Structure and plastic deformation of polyethylene.* Journal of Materials Science, 1994. **29**: p. 294-323.

Mandelkern, L. *The Relation between Structure and Properties of Crystalline Polymers.* Polymer Journal, 1985. **17**(1): p. 337-350.

Mandelkern, L.; Peacock, A.J. *The Relation Between Structure and Mechanical Properties of Crystalline Polymers.* Studies in Physical and Theoretical Chemistry, 1988. **54**: p. 201-227.

Mandelkern, L. *The Structure of Crystalline Polymers.* Accounts of Chemical Research, 1990. **23**(11): p. 380-386.

Mandelkern, L.; Alamo, R.G. *Comments on Paper "Raman Spectroscopy Employed for the Determination of the Intermediate Phase in Polyethylene".* Macromolecules, 1995. **28**(8): p. 2988-2989.

McCrum, N.G.; Read, B.E.; Williams, G. *Anelastic and Dielectric Effects in Polymeric Solids.* 1967, New York: Dover Publications, Inc.

Meinel, G.; A., P. *Plastic Deformation of Polyethylene II. Change of Mechanical Properties during Drawing.* Journal of Polymer Science: Part A-2, 1971. **9**: p. 67-83.

Moonen, J.A.H.M.; Roovers, W.A.C.; Meier, R.J.; Kip, B.J. *Crystal and Molecular Deformation in Strained High-Performance Polyethylene Fibers Studied by Wide-Angle X-ray Scattering and Raman Spectroscopy.* Journal of Polymer Science: Part B: Polymer Physics, 1992. **30**: p. 361-372.

Mowery, D.; Schmidt-Rohr, K. *Major Intermediate Component in Cold-Drawn High-Density Polyethylene Identified by Solid-State NMR.* Polymeric Materials: Science and Engineering, 2001. **85**: p. 35-36.

Mutter, R.; Stille, W.; Strobl, G. *Transition Regions and Surface Melting in Partially Crystalline Polyethylene: A Raman Spectroscopic Study.* Journal of Polymer Science: Part B: Polymer Physics, 1993. **31**: p. 99-105.

Nakai, T.; Terao, T. *Measurements of Heteronuclear Dipolar Powder Patterns due only to Directly Bonded Couplings.* Magnetic Resonance in Chemistry, 1992. **30**(1): p. 42-44.

Naylor, C.C.; Meier, R.J.; Kip, B.J.; Williams, K.P.J.; Mason, S.M.; Conroy, N.; Gerrard, D.L. *Raman Spectroscopy Employed for the Determination of the Intermediate Phase in Polyethylene.* Macromolecules, 1995. **28**(8): p. 2969-2978.

O'Connell, P.A.; Bonner, M.J.; Duckett, R.A.; Ward, I.M. *The relationship between slow crack propagation and tensile creep behaviour in polyethylene.* Polymer, 1995. **36**(12): p. 2355.

Peterlin, A.; Corneliussen, R. *Small-Angle X-Ray Diffraction Studies of Plastically Deformed Polyethylene. II. Influence of Draw Temperature, Draw Ratio, Annealing Temperature, and Time.* Journal of Polymer Science: Part A-2, 1968. **6**: p. 1273-1282.

Peterlin, A. *Bond Rupture in Highly Oriented Crystalline Polymers.* Journal of Polymer Science: Part A-2, 1969. **7**: p. 1151-1163.

Peterlin, A. *Molecular Model of Drawing Polyethylene and Polypropylene.* Journal of Materials Science, 1971. **6**: p. 490-508.

Peterlin, A. *Plastic deformation of polymers with fibrous structure.* Colloid and Polymer Science, 1975. **253**(10): p. 809-823.

Peterlin, A. *Drawing and extrusion of semi-crystalline polymers.* Colloid & Polymer Science, 1987. **265**(5): p. 357-382.

Popli, R.; Mandelkern, L. *Influence of Structural and Morphological Factors on the Mechanical Properties of the Polyethylenes.* Journal of Polymer Science: Part B: Polymer Physics, 1987. **25**: p. 441-483.

Prasad, K.; Grubb, D.T. *Direct Observation of Taut Tie Molecules in High-Strength Polyethylene Fibers by Raman Spectroscopy.* Journal of Polymer Science: Part B: Polymer Physics, 1989. **27**: p. 381-403.

Rodríguez-Cabello, J.C.; Merino, J.C.; Jawhari, T.; Pastor, J.M. *Rheo-optical Raman study of chain deformation in uniaxially stretched bulk polyethylene.* Polymer, 1995. **36**(22): p. 4233-4238.

Rodríguez-Cabello, J.C.; Martín-Monge, J.; Lagarón, J.M.; Pastor, J.M. *Determination of the content of extended chain segments in isotropic and uniaxially stretched polyethylenes by Raman spectroscopy.* Macromolecular Chemistry and Physics, 1998. **199**(12): p. 2767-2776.

Rull, F.; Prieto, A.C.; Casado, J.M.; Sobron, F.; Edwards, H.G.M. *Estimation of Crystallinity in Polyethylene by Raman Spectroscopy.* Journal of Raman Spectroscopy, 1993. **24**: p. 545-550.

Sadler, D.M.; Barham, P.J. *Structure of drawn fibers: 1. Neutron scattering studies of necking in melt-crystallized polyethylene.* Polymer, 1990. **31**: p. 36-42.

Saraf, A.W.; Desai, P.; Abhiraman, A.S. *Morphology and Near T_m Behavior of High Performance Ultrahigh Molecular Weight Polyethylene Fibers.* Journal of Applied Polymer Science: Applied Polymer Symposium, 1991. **47**: p. 67-86.

Schaefer, J.; Stejskal, E.O.; Buchdahl, R. *High-Resolution Carbon-13 Nuclear Magnetic Resonance Study of Some Solid, Glassy Polymers.* Macromolecules, 1975. **8**(3): p. 291-296.

Schmidt-Rohr, K.; Spiess, H.W. *Chain Diffusion between Crystalline and Amorphous Regions in Polyethylene Detected by 2D Exchange ^{13}C NMR.* Macromolecules, 1991. **24**(19): p. 5288-5293.

Schmidt-Rohr, K.; Clauss, J.; Spiess, H.W. *Correlation of Structure, Mobility, and Morphological Information in Heterogeneous Polymer Materials by Two-Dimensional Wideline-Separation NMR Spectroscopy.* Macromolecules, 1992. **25**(12): p. 3273-3277.

Schmidt-Rohr, K.; Wilhelm, M.; Johansson, A.; Spiess, H.W. *Determination of Chemical-Shift Tensor Orientations in Methylene Groups by Separated-Local-Field NMR.* Magnetic Resonance in Chemistry, 1993. **31**: p. 352-356.

Schmidt-Rohr, K.; Spiess, H.W. *Multidimensional Solid-State NMR and Polymers.* 1994, San Diego: Academic Press, Inc.

Seto, T.; Hara, T.; Tanaka, K. *Phase Transformation and Deformation Processes in Oriented Polyethylene.* Japanese Journal of Applied Physics, 1968. **7**(1): p. 31-42.

Shen, C.; Peacock, A.J.; Alamo, R.G.; Vickers, T.J.; Mandelkern, L.; Mann, C.K. *Structural Studies of Crystalline Linear Polyethylenes as Revealed by Factor Analysis of Their Raman Spectra.* Applied Spectroscopy, 1992. **46**(8): p. 1226-1230.

Sinclair, K.B. *Future Trends in Polyolefin Materials.* Macromolecular Symposia, 2001. **173**: p. 237-261.

Smith, J.B.; Manuel, A.J.; Ward, I.M. *Broadline n.m.r. studies of ultra-high modulus polyethylenes.* Polymer, 1975. **16**: p. 57-65.

Steidl, J.; Pelzbauer, Z. *Structural Changes during Deformation of High Molecular Weight and Low Molecular Weight Polyethylene.* Journal of Polymer Science: Part C, 1972. **38**: p. 345-356.

Strobl, G.R.; Hagedorn, W. *Raman Spectroscopic Method for Determining the Crystallinity of Polyethylene.* Journal of Polymer Science: Polymer Physics Edition, 1978. **16**: p. 1181-1193.

Strobl, G. *The Physics of Polymers.* 2nd ed. 1997, Berlin: Springer-Verlag.

Takayanagi, M.; Imada, K.; Kajiyama, T. *Mechanical Properties and Fine Structure of Drawn Polymers.* Journal of Polymer Science: Part C, 1966. **15**: p. 263-281.

Tonelli, A.E.; Schilling, F.C. *^{13}C NMR Chemical Shifts and the Microstructure of Polymers.* Accounts of Chemical Research, 1981. **14**: p. 233-238.

Tonelli, A.E. *High resolution NMR as a local probe of structure, conformation, and mobility in solid polymers.* Journal of Molecular Structure, 1995. **355**: p. 105-119.

Torchia, D.A. *The Measurement of Proton-Enhanced Carbon-13 T_1 Values by a Method Which Suppresses Artifacts.* Journal of Magnetic Resonance, 1978. **30**: p. 613-616.

VanderHart, D.L. *Influence of Molecular Packing on Solid-State ^{13}C Chemical Shifts: The n-Alkanes.* Journal of Magnetic Resonance, 1981. **44**: p. 117-125.

VanderHart, D.L.; Khoury, F. *Quantitative determination of the monoclinic crystalline phase content in polyethylene by ^{13}C n.m.r.* Polymer, 1984. **25**: p. 1589-1599.

Veeman, W.S. *Carbon-13 Chemical Shift Anisotropy.* Progress in NMR Spectroscopy, 1984. **16**: p. 193-235.

Vickers, M.E.; Fischer, H. *Real-time in situ X-ray diffraction study of polyethylene deformation.* Polymer, 1995. **36**(13): p. 2667-2670.

Ward, I.M., ed. *Developments in oriented polymers -- 1.* Developments. 1982, Applied Science Publishers Ltd: Barking, Essex, England.

Ward, I.M., ed. *Developments in oriented polymers -- 2.* Developments. 1987, Elsevier Applied Science Publishers Ltd: Barking, Essex, England.

Ward, I.M.; Hadley, D.W. *An Introduction to the Mechanical Properties of Solid Polymers.* 1993, New York: John Wiley & Sons, Inc.

Wilson, C.W.; Pake, G.E. *Nuclear Magnetic Relaxation in Polytetrafluoroethylene and Polyethylene.* Journal of Chemical Physics, 1957. **27**(1): p. 115-122.

Wunderlich, B. *Macromolecular Physics.* Vol. 1. 1973, New York: Academic Press.

Xiao, C.; Huang, J.; Dafforn, A.; Yee, A. *When Does Plastic Yield Occur?* in *ANTEC*. 1999. New York.

Yamanobe, T. *Structure and Dynamics of Crystalline and Noncrystalline Phases in Polymers*, in *Solid State NMR of Polymers*, Ando, I.; Asakura, T., Editors. 1998, Elsevier Science B.V.: Amsterdam. p. 267-305.

Zhurkov, S.N.; Kuksenko, V.S. *The micromechanics of polymer fracture.* International Journal of Fracture, 1975. **11**(4): p. 629-639.